Ultrasound-CT Registration of Vertebrae for Image-Guided Spinal Fusion Surgeries

Charles Xiao Bo Yan

Doctor of Philosophy

Department of Biomedical Engineering

McGill University

Montréal, Québec

June 22, 2013

A thesis submitted to McGill University in partial fulfillment
of the requirements for the degree of Doctor of Philosophy

DEDICATION

To my parents,

Isabelle Rongqing Fu and Jia Liu Yan,

for their unconditional love and support

ACKNOWLEDGEMENTS

I would like to thank my supervisor, Dr. D. Louis Collins, for guiding me when I was lost, for supporting me when I found my path, and for always being there for me. I couldn't have done it without him.

Further thanks extends to my thesis committee members, Dr. Bruce Pike, Dr. Pierre Hellier and Dr. Rolando Del Maestro, for their valuable advice and support.

I would also like to thank to my co-authors, Dr. Benoît Goulet, Dr. Donatella Tampieri, Julie Pelletier and Sean Jy-Shyang Chen, for their insights, support and collaboration.

My gratitude to:

- Dr. Vladimir Fonov, for always having a solution to any technical problem;
- Dr. Laurence Mercier, for helping me with the image-guided surgery system;
- Dr. Heming Zhang, for helping me conduct the porcine cadaver registration experiments;
- Anka Kochanowska, for her excellent programming work;
- Simon Drouin, for the exceptional illustrations in the manuscripts;
- Dr. Mallar Chakravarty, for helping me with the image processing tools;
- Nicolas Guizard, for helping me with the batch processing tools;
- Pina Sorrini and Nancy Abate, for always being so helpful and supportive;

- Colleagues of the Image Processing Laboratory and Brain Imaging Centre, Dr. Andrew Janke, Dr Bérengère Broche, Dr. Jacqueline Chen, Jennifer Chew, Lara Bailey, Marta Kersten, Mishkin Debrakhshan, Dr. Pierrick Coupé, for their insights and collegiality.

ABSTRACT

Accurate surgical navigation for pedicle screw implantation significantly reduces the complication rate in spinal fusion surgeries. To achieve accurate navigation based on preoperative computed tomography (CT), accurate patient-to-image registration is necessary. However, current manual registration techniques are invasive and greatly prolong operative time. To resolve these shortcomings, automated patient-to-image registration through tracked intraoperative ultrasound has been proposed, but existing ultrasound-CT registration techniques are limited and not ready for clinical application in spine surgeries. This thesis presents the development of a technique for ultrasound-CT image registration of vertebrae that satisfies the practical requirements of being automated, accurate, robust, reasonably fast and appropriately validated.

The ultrasound-CT registration technique first extracts the vertebral bone surface from both the ultrasound and CT images through scan line tracing. The extracted surfaces are then registered by intensity cross-correlation. Preliminary registration results on a single vertebra of a plastic Sawbones phantom yielded target registration error (TRE) under 1 mm. Subsequently, the technique was extensively validated on 18 vertebrae of 3 porcine cadavers, with a total of 18,000 registrations. All validation was with respect to gold standard registrations generated with imaging fiducials. The results demonstrated good registration accuracy, with median TRE of 1.65 mm, and good robustness, with 82.7% of TREs < 2 mm. The generated gold standard registration had a median TRE of 0.718 mm.

The registration technique was further improved by eliminating the step of reconstructing ultrasound image slices into a volume. This was achieved by directly registering the ultrasound slices as a group to the target CT image volume. This improvement significantly reduced the total registration time from 8 min down to 4 min. The registration accuracy and robustness were also slightly improved, with a median TRE of 1.45 mm and 84.6% of TREs < 2 mm. In addition, a trade-off between registration accuracy and speed was established through the number of ultrasound image slices used in the registration.

The technique of ultrasound-CT registration of vertebrae developed in this thesis is automated, accurate, robust, quick and practical for intraoperative use. In the future, validation on human cadavers and patients will enable the technique to be applied in clinical settings.

ABRÉGÉ

La navigation chirurgicale précise du vissage pédiculaire réduit de façon significative le taux de complication des chirurgies de fusion spinale. La précision de la navigation basée sur la tomographie axiale (CT) préopératoire exige l'exactitude du recalage patient-image. Actuellement, les techniques de recalage manuelles sont invasives et prolongent le temps opératoire. Le recalage patient-image automatique par l'intermédiaire d'échographie peropératoire localisé a été proposé, mais les méthodes existantes de recalage d'échographie-CT sont limitées et ne sont pas prées pour l'usage clinique dans les chirurgies spinales. Cette thèse présente le dévelopement d'une technique pour le recalage échographie-CT vertébrale. Cette technique satisfait aux exigences pragmatiques d'être automatique, précise, robuste, avoir une vitesse raisonnable et d'être validée d'une manière adéquate.

La technique de recalage d'échographie-CT extrait tout d'abord la surface osseuse de vertèbre à partir des images échographiques et CT. Ensuite, les surfaces extraites sont recalée par la corrélation croisée d'intensité de voxels. Le recalage d'un seul vertèbre d'un fantôme Sawbones en plastique a donné comme résultat préliminaire une erreur de recalage de cible ("target registration error" ou TRE) au-dessous de 1 mm. Par la suite, la technique a été validée plus largement sur 18 vertèbre de 3 cadavres porcins, un total de 18,000 recalages. Les validations ont employé les recalages d'étalon d'or générés avec des points de repères d'imagerie.

Les résultats démontrent de bonnes précisions de recalage, ayant un TRE médian de 1.65 mm, et de bonne robustesse avec 82.7% des TREs < 2 mm. Le recalage d'étalon d'or avait un TRE médian de 0.718 mm.

La technique de recalage a été amélioré en eliminant l'étape de la reconstruction des secteurs d'image d'échographie en un volume. Ceci a été accompli en recalant directement les secteurs d'échographie comme un group au volume d'image cible CT. Cette amélioration a réduit le temps total de recalage de 8 min à 4 min. La précision et robustesse étaient aussi améliorés légèrement, avec un TRE médian de 1.45 mm et 84.6% de TREs < 2 mm. De plus, un compromis entre la précision et la vitesse de recalage a été établi par le nombre de secteurs d'échographie utilisés dans le recalage.

Cette thèse presente le developement d'une technique de recalage échographie-CT vertébrale automatique, précise, robuste, rapide et pratique pour l'usage peropératoire. Dans l'avenir, la validation sur les cadavres humains et les patients vont permettre l'adoption de cette technique à l'usage clinique.

TABLE OF CONTENTS

LIST OF TABLES

LIST OF FIGURES

CHAPTER 1
Introduction

1.1 Motivation

Advances in modern medical imaging are constantly changing the way medicine is practiced. New imaging techniques with higher specificity and increasing spatial and contrast resolution are empowering doctors to make diagnostic decisions never imagined before. At the same time, the advent of information technologies in the last few decades has found new applications for medical imaging in addition to making diagnoses. One such application is surgery performed under medical image guidance. Traditionally, surgeons have always relied on their experience, their knowledge of anatomy and their direct view of the patient's exposed organs and structures to guide their surgical procedures. However, there are situations where they need to operate on structures that cannot be exposed to the surgical field for direct viewing. In these circumstances, surgical precision may decrease and clinical outcomes may suffer. Image-guided surgery solves this problem by enabling surgeons to visualize the anatomical structures and the surgical tools that are hidden from direct viewing in computer rendered images, as if conferring the surgeons the ability to "see through" the patient's body. One type of surgery that benefits from image-guidance is spinal fusion surgery with pedicle screw implantation. In this surgery, because the concerned anatomy is hidden from the direct field of vision of the surgeon, the pedicle screws are inserted "blindly" into the patient's vertebrae in highly risky anatomical locations surrounded by important blood vessels and nerves, thus resulting in high rate of neurological and vascular complications. Image-guidance system enables surgeons to visualize the hidden anatomy, and instead of implanting the pedicle screws "blindly", they can choose insertion points, trajectories and depth with more confidence by visually following the computer-rendered images and surgical tools, thus increasing implantation precision and reducing errors. A critical step in such an image-guided surgery system is establishing a spatial transformation between the patient and the preoperatively acquired CT images. This step, termed patient-image registration, is the focus of this thesis. More specifically, this thesis describes the development of a patient-image registration technique based on intraoperative ultrasound images and preoperative CT images of vertebrae for the application of image-guidance to pedicle screw implantation. This registration technique is validated using images of a realistic plastic phantom and porcine cadavers. As will be made evident in the Background section and throughout the thesis, the goal is to develop an accurate and automated registration technique that will simplify and speed up the step of patient-image registration in spinal fusion surgeries.

1.2 Thesis Outline

This thesis is organized into six chapters. Chapter 2 provides the background material necessary to understand the following chapters. It includes an introduction to spinal fusion surgery with pedicle screw implantation, an overview of image-guided spine surgery, a brief review of the intraoperative imaging modalities applied to spinal fusion surgery, and a literature review of existing ultrasound-CT registration techniques for orthopedic surgeries. Chapter 3, 4 and 5 are individual manuscripts. Chapter 3 describes the registration algorithm and presents some preliminary results. Chapter 4 presents validation experiments using images acquired from porcine cadavers. Chapter 5 introduces an ultrasound slice to CT volume registration technique that does not require reconstruction of ultrasound image slices into a volume. The thesis ends with a discussion, conclusions and suggestions for future work in Chapter 6.

1.3 Original Contributions

The following are the main contributions of this work:

1 Development and implementation of a new intensity-based method for ultrasound-CT registration of vertebrae;

2 Design and implementation of a system of imaging fiducials that can be applied to both phantom and cadaver vertebrae to obtain gold standard registration;

3 Validation of the new registration technique using both phantom data and porcine cadaver data based on gold standard registration;

4 Development and implementation of a 2D ultrasound slices to 3D CT volume image registration method;

5 Quantitative comparison of slices-to-volume registration with volume-to-volume registration using both phantom and porcine cadaver data;

1.4 Author Contributions

I am the first author of all three manuscripts included in this thesis and have performed all of the methodological developments, experimental design, and the analysis of results. The contributions of all co-authors included supervision, data acquisition, and the review of manuscripts. The following list summarizes the contributions of each author by manuscript:

Chapter 3 Towards Accurate, Robust and Practical Ultrasound-CT Registration of Vertebrae for Image-Guided Spine Surgery

Authors: C. X. B. Yan, B. Goulet, J. Pelletier, S. Chen, D. Tampieri and D. L. Collins

Guarantors of integrity of entire study: all authors; study concepts and design: C.X.B.Y., B.G., J.P., D.L.C.; registration algorithm and implementation: C.X.B.Y.; phantom design and construction: C.X.B.Y., S.C., D.L.C.; data acquisition: C.X.B.Y., D.T.; experiments and analysis: C.X.B.Y.; guidance and supervision: D.L.C.; manuscript preparation: C.X.B.Y.; manuscript revision: all authors; editing and final version approval: C.X.B.Y., D.L.C.;

Chapter 4 Validation of Automated Ultrasound-CT Registration of Vertebrae

Authors: C. X. B. Yan, B. Goulet, S. Chen, D. Tampieri and D. L. Collins

Guarantors of integrity of entire study: all authors; study concepts and design: C.X.B.Y., D.L.C.; porcine cadaver experimental setup: C.X.B.Y., S.C., D.L.C.; data acquisition: C.X.B.Y., D.T.; experiments and analysis: C.X.B.Y.; guidance and supervision: D.L.C.; manuscript preparation: C.X.B.Y.; manuscript revision: all authors; editing and final version approval: C.X.B.Y., D.L.C.;

Chapter 5 Ultrasound-CT Registration of Vertebrae without Reconstruction

Authors: C. X. B. Yan, B. Goulet, D. Tampieri and D. L. Collins

Guarantors of integrity of entire study: all authors; study concepts and design: C.X.B.Y., D.L.C.; registration algorithm and implementation: C.X.B.Y.; data acquisition: C.X.B.Y., D.T.; experiments and analysis: C.X.B.Y.; guidance and supervision: D.L.C.; manuscript preparation: C.X.B.Y.; manuscript revision: all authors; editing and final version approval: C.X.B.Y., D.L.C.;

CHAPTER 2
Background

2.1 Spinal Fusion Surgery

The number of spinal fusion surgeries has doubled in the past decade in the United States to close to half a million spinal fusions performed annually [1]. A multitude of factors may have contributed to this increase, including the aging population, advances in spinal fixation devices and the increased availability of alternative bone grafting materials. Instrumentation with pedicle screws and rod fixation improves the rate of spinal fusion, especially in patients with complex deformities such as scoliosis or mechanical instability with severe spondylolisthesis [2–4]. The main indications for spinal fusion surgeries with fixation by instrumentation are spondylolisthesis, scoliosis, vertebral fractures, vertebral dislocations, spinal stenosis, spinal tumours and pseudarthrosis [5]. In addition, severe disc degenerative diseases that are refractory to medical management are currently the most important condition treated by spinal fusion surgeries with instrumentation, but the indication of spinal fusion for this condition is still being debated [5, 6]. This section provides an overview of pedicle screw placement for spinal fusion surgeries, its associated complications and its rates of misplacement, but it first starts with an introduction to the anatomy of the human vertebrae to familiarize the reader with some of the anatomical terms used throughout this thesis.

2.1.1 Anatomy of Human Vertebrae

The vertebral column extends from the skull to the pelvis (Fig. 2–1a). It consists of 7 cervical vertebrae in the neck, 12 thoracic vertebrae in the thorax, 5 lumbar vertebrae in the lower back, 1 sacrum and 1 coccyx in the pelvic region. It is a vital structure that supports and distributes the weight of the human upper body and also protects the spinal cord by encasing it medially inside the spinal canal within the vertebrae. The nerves branching from the spinal cord exit laterally through the intervertebral foramina (Fig. 2–1b) to innervate the rest of the body. There are also large and medium sized vessels that course longitudinally just anterior to the vertebral column (Fig. 2–1c). Therefore, the vertebral column is a high risk area to be operated on as it is surrounded by vital structures such as nerves and blood vessels.

The more detailed vertebral anatomy is illustrated with the example of lumbar vertebrae shown in Fig. 2–2. The two figures contain a phantom model of three lumbar vertebrae (L3, L4, L5) with labels mostly on the L4 vertebra for illustration. (The reader is advised to become familiar with the labeled structures before continuing further.) Fig. 2–2a illustrates the posterior surface of the vertebrae, which includes the anatomical structures typically exposed during spinal fusion surgery through a posterior approach, namely the spinous processes, the laminae, the superior and inferior facets and the transverse processes. The pedicles and the vertebral bodies are illustrated in Fig. 2–2b. Note that the pedicles and vertebral bodies are not visible from the posterior view. This spatial relationship is of clinical significance, because of this, surgeons do not have a direct view of the pedicles and the vertebral bodies during the pedicle screw implantation. Therefore, they must "blindly" drill the holes and implant the pedicle screws.

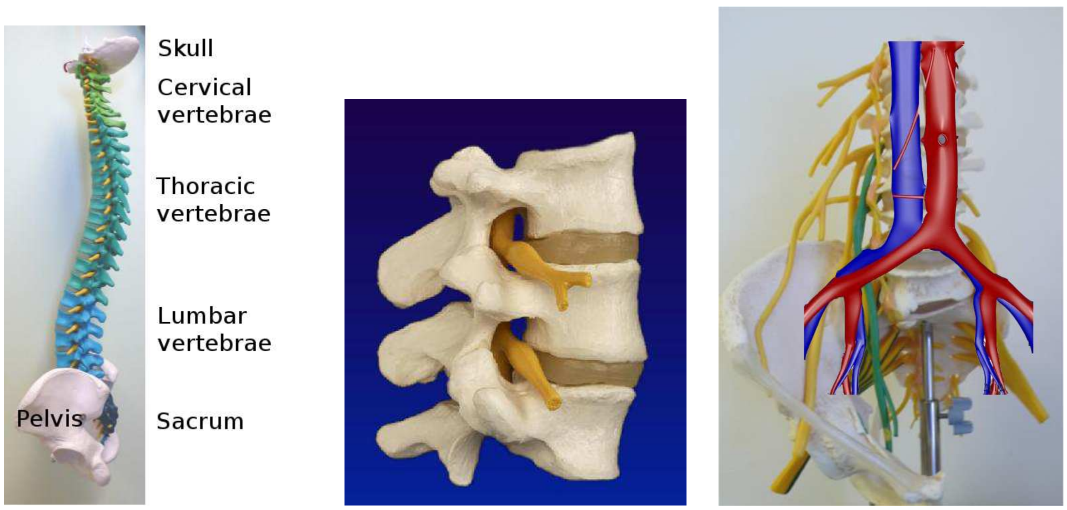

(a) (b) (c)

Figure 2–1: (a) Lateral view of a phantom model of the entire vertebral column including parts of skull and pelvis; (b) Lateral view of a phantom model of lumbar vertebrae with nerve roots branching from the spinal cord and exiting through the intervertebral foramina; (c) Anterior view of a phantom model of lumbar vertebrae showing blood vessels just anterior to the vertebral bodies. All figures are reproduced and modified with permission from Goulet [7].

2.1.2 Pedicle Screw Implantation and Rod Fixation

The surgical technique of traditional spinal fusion surgery with pedicle screw implantation and rod fixation has been previously presented in detail [8–11]. Here, we provide a brief overview using the posterior fixation of the lumbar vertebrae as an example. After general anesthesia, patients are placed in a prone position on the operating table. Following preoperative preparations, the surgeon makes a

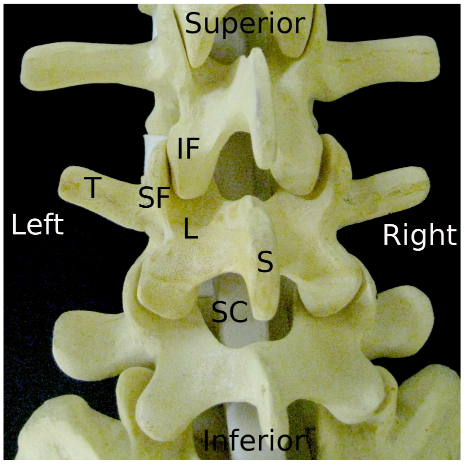

(a)

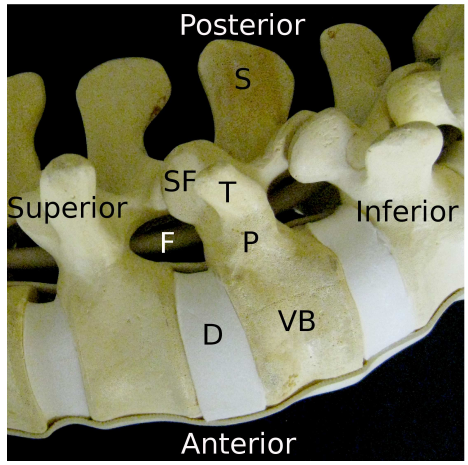

(b)

Figure 2–2: Lumbar vertebral anatomy from (a) posterior view and (b) sagittal view. T: transverse process, SF: superior facet, IF: inferior facet, L: lamina, S: spinous process, SC: spinal canal, P: pedicle, VB: vertebral body, D: intervertebral disc, F: intervertebral foramen

midline lumbar incision that spans the vertebral segments to be instrumented. The paraspinous muscles are retracted and the subperiosteal muscles at the segments to be fused are dissected to expose the transverse processes (Fig. 2–3a and 2–3b). The external landmarks above the pedicle, including the superior facets and the transverse processes, are identified and the exposure is facilitated by removing the soft tissue from the bone surface. The entry sites of the pedicle screws are between the superior facets and the transverse processes (Fig. 2–3c and 2–3d). Often, an anteroposterior fluoroscopic image is taken intraoperatively to help the surgeon identify the entry point. For each pedicle, a pin oriented along the axis of the pedicle is driven through the entry site with a twisting handle to create a hole that will guide the implantation of the screw. The screw size is preselected for each pedicle based on the anatomical characteristics of each seen on the preoperative CT image. Figure 2–4c shows examples of some pedicle screws used in spinal fusion surgeries. The pedicle screws are inserted into the prepared holes and threaded in by a screwdriver at the same trajectory as that of the holes (Fig. 2–4a and 2–4b). The screws are subsequently advanced to penetrate most of the vertebral body to provide sufficient mechanical stability but are stopped before reaching the anterior wall of the vertebral body so as to avoid penetrating the wall and causing injuries to the blood vessels just anterior to the vertebral column (Fig. 2–4d). The screw penetration is monitored using lateral fluoroscopic images. Once all the pedicle screws are implanted, the metallic rods are selected to match the curvature and length of the segments to be fused. The selected rods are connected to the pedicle screws longitudinally and small final adjustments are made in place (Fig. 2–5). After rod placement and wound irrigation, bone grafts are packed in between the vertebral bodies (interbody fusion) or between the facets and transverse processes (posterolateral fusion). Closed suctioning drainage system is placed to prevent fluid accumulation and a multi-layered closure of the surgical site is performed. Patients usually wear orthosis postoperatively for 3 to 6 months with rehabilitative therapy and follow-ups.

2.1.3 Potential Complications of Pedicle Screw Misplacement

Pedicle screw implantation for spinal fusion surgeries is prone to placement errors due to the anatomical variability of the vertebral pedicles and the lack of direct visualization of structures deep and medial to the pedicles. For example, perforation of the pedicle screw superiorly or inferiorly (Fig. 2–6a) may injure

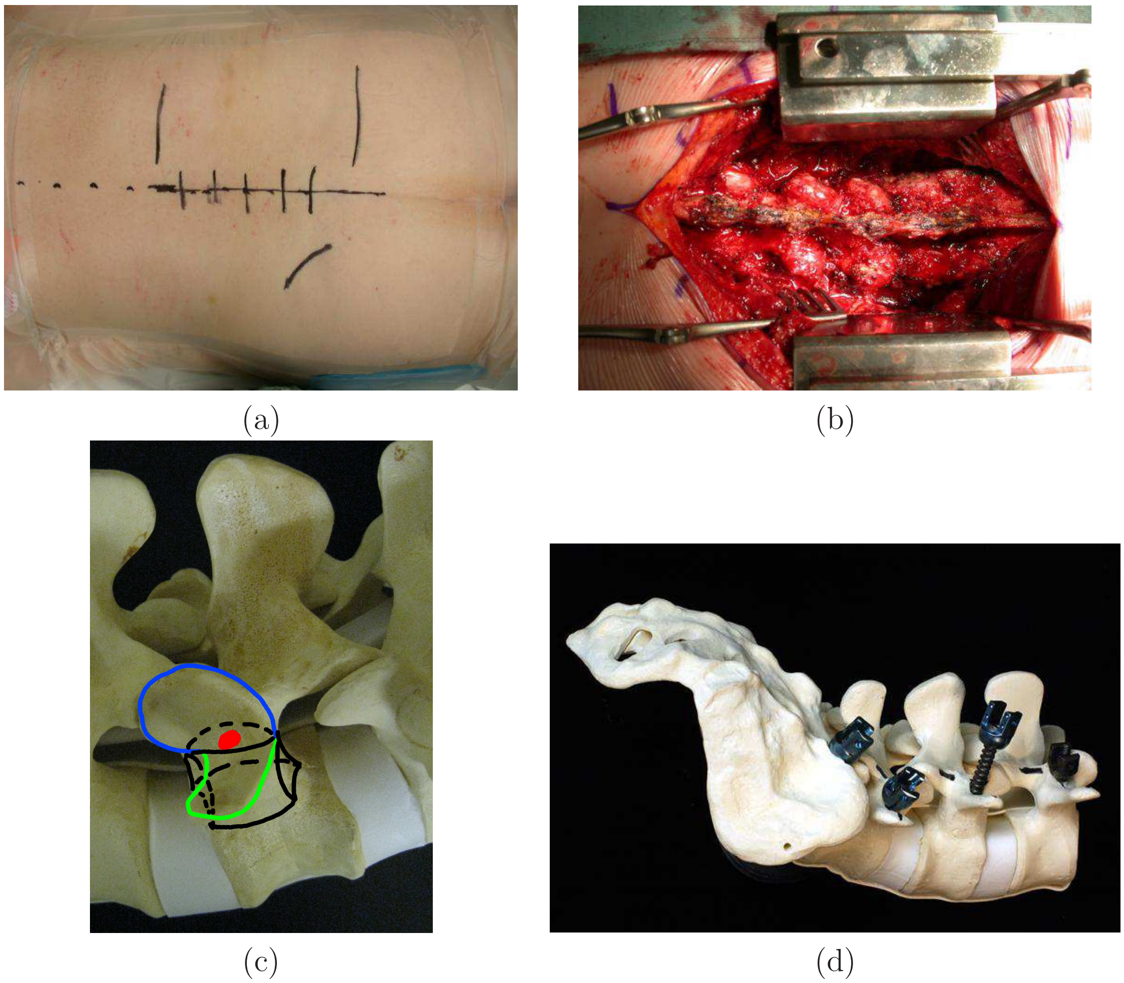

Figure 2–3: (a) Markings for the midline incision to be made in a posterior lumbar fusion surgery; (b) Paraspinous muscles are retracted to expose the vertebral anatomy; (c) The entry point of the pedicle (red point) is in between the superior facet (blue delineation) and the transverse process (green delineation); (d) Phantom model showing the entry points of the pedicle screws. All figures are reproduced and modified with permission from Goulet [7].

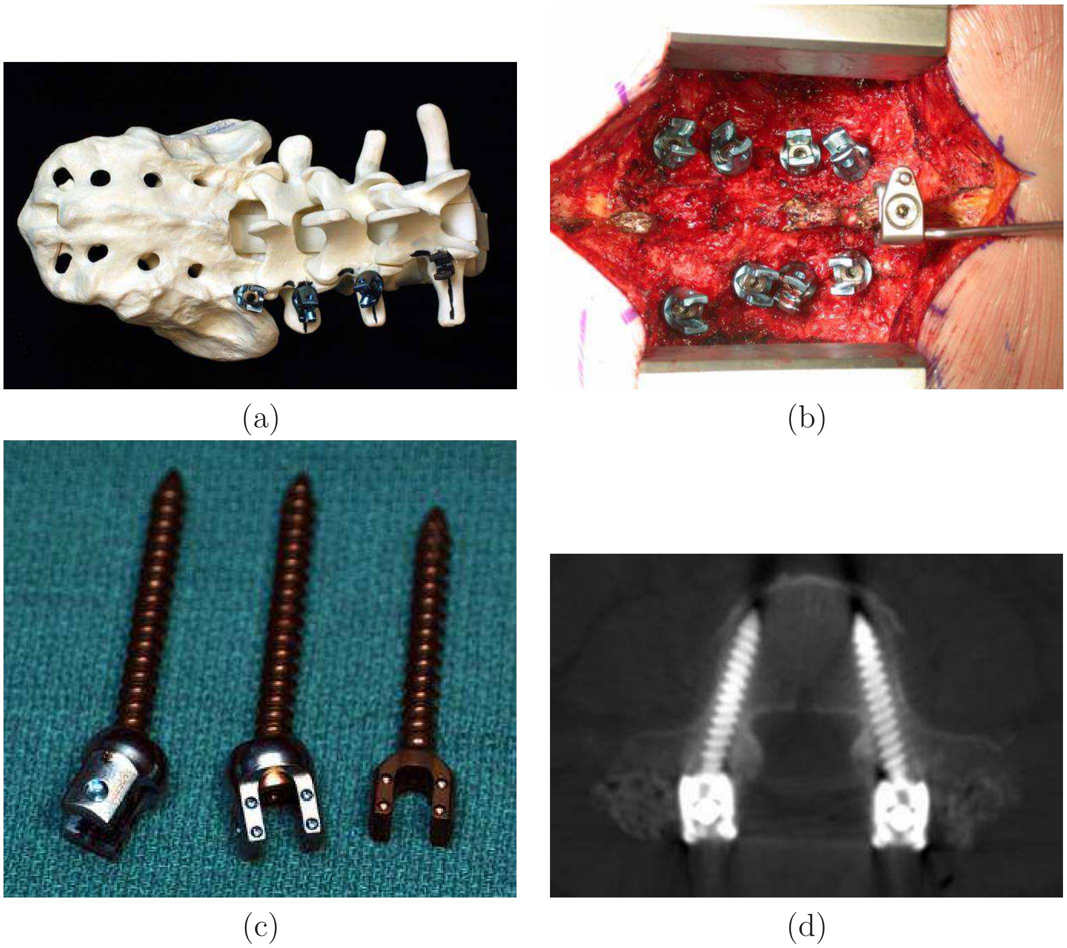

Figure 2–4: (a) Simulated pedicle screw insertion in a phantom model; (b) Pedicle screws implanted in the lumbar vertebrae of a patient; (c) Examples of pedicle screws used in spinal fusion; (d) To achieve maximal mechanical stability, the pedicle screws are advanced as anteriorly as possible without penetrating the anterior cortex of the vertebral body. All figures are reproduced and modified with permission from Goulet [7].

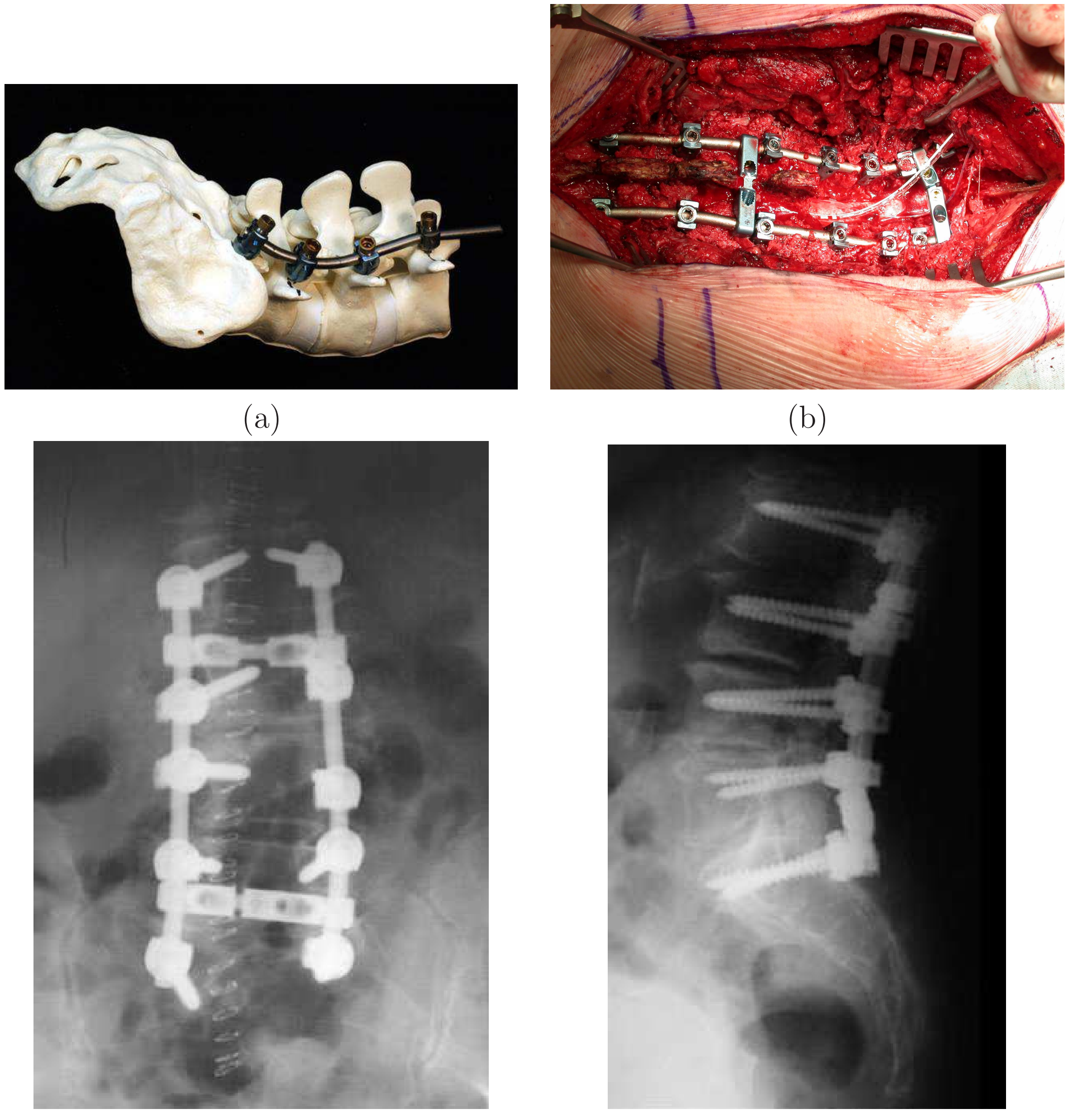

(a) (b) (c) (d)

Figure 2–5: The intervertebral fixation is achieved by connecting all pedicle screws to two parallel metallic rods longitudinally. The rods are selected to match the length and curvature of the segments to be fused. The figures show the fixated lumbar vertebrae in (a) a phantom model, (b) a patient during the surgery, (c) a posterior-anterior radiograph and (d) a lateral radiograph of a patient with lumbar fusion surgery. All figures are reproduced and modified with permission from Goulet [7].

the nerve roots that exit from the the intervertebral foramina shown in Fig. 2–2b. Perforation of the screw medially could impinge on the spinal cord, while anterior perforation of screw may injure the aorta in the thoracic and lumbar regions (Fig. 2–6b). Inaccurate pedicle screw implantation may cause neurological, vascular and mechanical complications [12, 13]. Neurological complication is the most common form and typically results from screws perforating the medial wall of the pedicle into the spinal canal[14]. Gertzbein and Robbins [15] has graded the perforation of pedicle screw based on increment of 2 mm. They noted that while 0 to 4 mm of medial perforation might still be considered safe, perforations beyond 4 mm are likely to lead to neurological complications. Vascular complications usually result from screws that perforate the vertebral body anteriorly, leading to injuries of blood vessels anterior to the vertebral bodies. Mechanical complications often result from perforations of the lateral wall of the pedicle, causing a weaker fixation due to rigidity failure [13]. The rate of pedicle perforation has been reported by many studies and it has been shown that conventional pedicle screw implantation based on anatomical landmarks or fluoroscopy causes misplaced screws in 10-50% of cases [14–19].

2.2 Image-Guidance for Spine Surgery

The high rates of pedicle screw placement errors and their associated complications have prompted the surgeons to search for better ways to guide the implantation of pedicle screws. In this section, we briefly describe the basics of image-guided surgery (also known as surgical navigation) and its application in pedicle screw implantation.

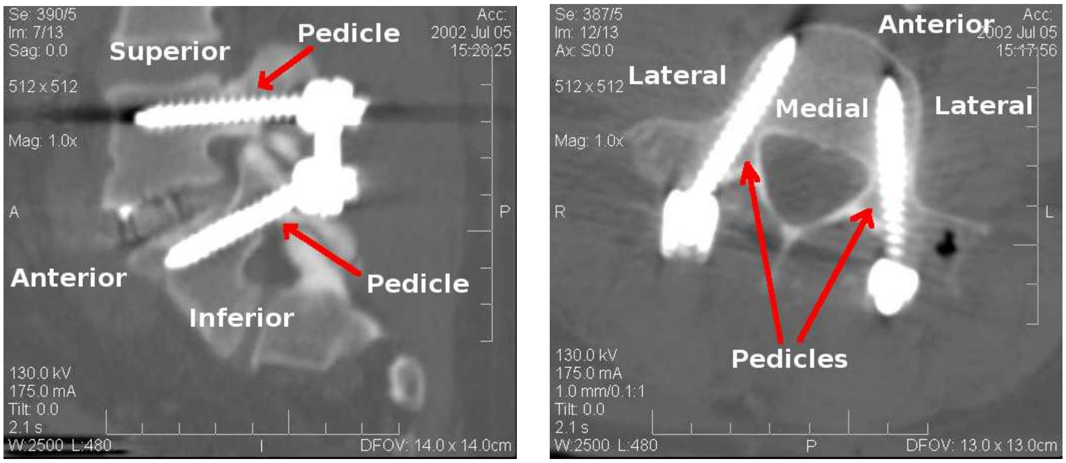

(a) (b)

Figure 2–6: The two figures show the directions of potential perforation of the pedicle cortex in (a) superior or inferior and (b) medial, lateral or anterior direction.

2.2.1 Image-Guided Surgery Systems

Image-guided surgery (IGS) systems assist surgeons mainly in two functions. Firstly, they enable the surgeons to visualize on the computer screen anatomical structures and surgical instruments that are not exposed to the direct field of vision. For example, even if the pedicles and part of the surgical instruments are hidden under the posterior vertebral structures, the IGS system is able to display the entire vertebral anatomy along with the surgical instruments on the computer screen while preserving accurately the spatial relationship among them. In a way, the IGS systems confer the surgeons with “X-ray vision” so that they can operate on structures that are hidden from view. Secondly, the IGS systems enable additional information to be overlaid on the patient anatomy. In the case of pedicle screw implantation, a surgical plan detailing the size, depth, orientation and entry point of the pedicle screw implants are overlaid on the preoperative CT image so that surgeons can follow these plans during the actual surgery. The resulting benefits are numerous, including lower surgical risk, increased possibility of performing more complex instrumentation, decreased postoperative complications, more confidence in the surgical procedures, and better postoperative function.

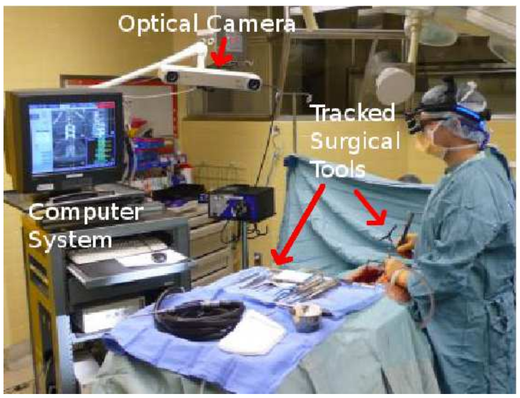

(a)

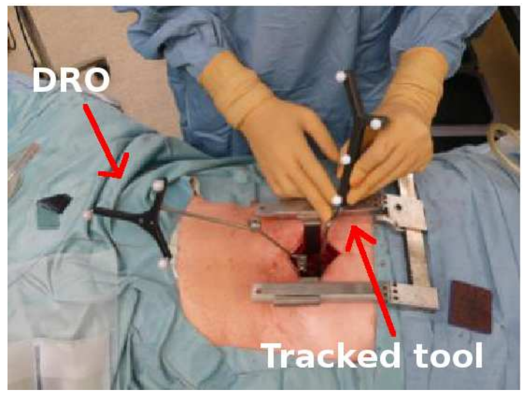

(b)

Figure 2–7: (a) The components of an image-guided surgery system consists of an optical camera, a computer system running a surgical navigation software, and the surgical tools with tracked target mounted on them. (b) The tracked surgical tools have reflective spheres mounted on them in uniquely identifiable configuration, known as tracked targets. All figures are reproduced and modified with permission from Goulet [7].

The two functions of IGS described above are achieved through a combination of hardware and software components (Fig. 2–7a). The hardware includes an optical camera, a computer system and multiple tracked surgical tools. The optical camera (Polaris, Northern Digital Inc., Ontario, Canada) continuously monitors and records the position and orientation of tracked targets. The tracked targets are reflective spheres mounted on the surgical tools in uniquely identifiable configurations (Fig. 2–7b). In this way, tracking is achieved when the optical camera emits infrared light on the targets and then receives back the infrared rays reflected by the reflective spheres. Among the targets, a unique one termed the dynamic reference object (DRO), serves as the reference point of all other tracked tools (Fig. 2–7b). During the surgery, the other tracked tools' position and orientation are represented in a coordinate system relative to the DRO termed the *world space* (sometimes also referred to as the *patient space*). In addition, all tracked positions and orientations are input into the computer system running a software such as the IBIS platform described in Mercier et al [20]. This software manages all functionalities of the IGS system, including the tracking of all surgical tools, the registration of preoperative images to the patient, and the visualization of the tracked surgical tools and the registered images. When the surgeon is operating, the surgical tools and images are rendered on the same screen to display to the surgeon the position and orientation of the surgical tools relative to the patient anatomy and the overlaid surgical plans (Fig. 2–8). Many such commercial and research surgical navigation platforms exist in the market. The most well-known commercial systems include Medtronic's StealthStation, Stryker's NavSuite, Brainlab's VectorVision, Norway's SonoWand System, Zimmer's OrthoSoft, Siemens' NaviVision, GE's Instatrak, etc. Two widely known research IGS platforms are the 3D Slicer and the IGSTK systems.

Figure 2–8: The surgical tools, CT image and the overlaid surgical plan are rendered on the same screen to display the position and orientation of the surgical tools relative to the patient anatomy. The figure is reproduced with permission from Goulet [7].

2.2.2 Pedicle Screw Implantation Guided by Preoperative CT

The earliest surgical navigation systems for pedicle screw implantation were based on preoperative CT images of the patient's vertebral column. This section provides an overview of the mechanism of preoperative CT image-guided pedicle screw implantation and a brief literature review of the field.

In pedicle screw implantation guided by preoperative CT image, a model of the vertebrae is created based on the vertebral bone surface segmented from the CT image before surgery. Using the vertebral model, a surgeon plans the entry points of each pedicle screw and selects the screw size and length, where the largest screw that will fit in the pedicle is selected for optimal mechanical stability [7, 13]. During the surgery, a manual registration of each vertebra to the preoperative CT image is performed after exposing the posterior vertebral surface with retraction and dissection. The manual registration consists of identifying bony anatomical landmarks on the vertebra using a tracked pointer tool and pairing them with the corresponding landmarks on the CT image. The pairs of corresponding landmarks enable the IGS system to generate a spatial transformation (i.e., registration) between the patient and the preoperative CT image. Using this registration transformation, the tracked surgical tools are displayed in the same space as the preoperative CT image, enabling the surgeon to visualize the spatial relationship between the surgical tools and the patient anatomy.

Subsequently, the accuracy of the registration is verified by touching the vertebral bone surface with the surgical tools and inspecting whether the same anatomy is touched by the surgical tools rendered on the computer screen. In general, this manual registration procedure described above takes from 5 to 10 minutes when it is based only on anatomical homologous landmarks [21, 22]. However, if the registration accuracy is not satisfactory, another surface-point-based manual registration (see Section 2.4.1) using 20 to 30 vertebral bone surface points is performed, lasting approximately 15 minutes [7, 23]. These manual registration procedures are repeated until an accurate registration is established. At our institution, the combination of manual registration and screw insertion takes 19.8 minutes per screw on average and the manual registration is repeated for each vertebral segment requiring pedicle screw implantation [7].

As was noted in Subsection 2.1.3, the rate of screw misplacement could range from 10 to 50% in conventional spinal fusion not guided by a navigation system [14–19]. The use of image-guidance in spinal fusion surgeries has greatly increased the accuracy of screw implantation and reduced the rate of screw misplacement. This improvement was first demonstrated in the 1990's by experiments on cadaver and animal subjects. Nolte et al [24] demonstrated the potential for image-guided pedicle screw implantation in 1995 through an experiment of pedicle screw insertion in two human cadaver lumbar spines guided by preoperative CT images. In the same year, Amiot et al [25] performed insertion of six pedicle screws in three lumbar vertebrae of a live sheep guided by preoperative CT image. Based on the surgeon's assessment during the operation, five of the six intrapedicular holes drilled were correctly represented. The following year, Glossop et al [26] published a study where Kirschner wires were inserted into eight intrapedicular holes of a human cadaver drilled by preoperative CT guidance to simulate pedicle screw insertion. Postoperative CT scan was used to assess placement accuracy and it was found that the average distance between the planned and actual wire entry point was 1.2 mm.

Soon after the first few cadaver and animal experiments, a number of case series involving human subjects were published. Kalfas et al [27] published in 1995 the results of performing 150 lumbar pedicle screw placement in 30 patients under surgical navigation with preoperative CT. The accuracy of screw placement was assessed by post-operative radiographs and CT images. They found that there were only 12 suboptimal and 1 unsatisfactory placements, totaling 13 misplaced screws (8.7% misplacement rate). Other similar case series studies also reported low rates (0 to 8.5%) of pedicle screw misplacement using surgical navigation [28–31]. These studies did not include a control group and thus could not compare the accuracy of screw placement under image-guidance with that of the conventional method.

Cohort studies were also conducted to compare the accuracy of pedicle screw placement using surgical navigation to that of the conventional methods. Between 1995 and 1997, Merloz et al [13] arbitrarily assigned 32 patients with thoracolumbar fractures or spondylolisthesis to pedicle screw implantation with preoperative CT guidance and 32 patients to conventional pedicle screw placement without navigation (the control group). In the control group, they found a screw misplacement rate of 44% on post-operative CT image assessment, whereas for the group with image-guidance, only 9% of the screws were incorrectly implanted. Similarly, in a cohort study with 100 patients in the control group (544 screws) and 50 patients in the navigation group (294 screws), Amiot et al [32] found 85% correct placement in the control group and 95% correct placement in the navigation group.

A notable randomized controlled trial by Laine et al [18] was published in 2000 comparing pedicle screw insertion guided by preoperative CT image in 41 patients (219 screws) to conventional non-navigated screw placement in 100 patients (277 screws). Patients were randomly assigned to either a control or a navigation group and the experiments were conducted in a double-blind fashion. Screw placements were evaluated by a radiologist (blinded evaluator) on postoperative CT images. The rate of pedicle perforation was found to be 13.4%

in the control group compared to 4.6% in the navigated group. However, the operative time taken by the navigated group (mean of 179 min) was longer than the conventional group (mean 160 min), even though the number of screws per patient in the two groups are statistically the same due to randomization.

Although preoperative-CT based navigation is able to significantly increase the accuracy of pedicle screw placement and reduce the rate of pedicle perforation, the time for manual registration may add important additional operative time when several vertebrae are being operated on during a spinal fusion surgery. Manual registration is also more invasive because additional soft tissue dissection is often needed to expose more of the vertebral bone (e.g., posterior surface of transverse processes) to obtain good landmarks for mapping the surface points. To eliminate these drawbacks and to make image-guided techniques more efficient, surgeons have turned to intraoperative imaging modalities for either direct visualization of patient anatomy during the surgery or for collecting anatomical information to speed up registration during surgery.

2.3 Intraoperative Imaging Modalities for Pedicle Screw Implantation

A number of intraoperative imaging modalities exist and have been implemented for surgical navigation of pedicle screw implantation. This section provides an overview of the intraoperative imaging modalities, including 2D and 3D fluoroscopy, CT, MRI and ultrasound.

2.3.1 2D-Fluoroscopy

Two-dimensional X-ray fluoroscopy is generated with an imaging device called the C-arm, which is essentially a portable X-ray imaging device whose rotating mechanical arm allows a great range of movement, thus enabling intraoperative X-ray imaging at many different angles and providing the surgeons with multiple X-ray views of the patient. In 2000, Nolte et al [33] published a proof-of-concept study demonstrating the use of spatially tracked intraoperative 2D-fluoroscopy in guiding pedicle screw placement. Before the screw placement, one lateral and two oblique views of the vertebra were obtained with the C-arm. The C-arm was tracked in space, as it had a target mounted on it that was tracked by an optical camera. The C-arm had been pre-calibrated with respect to the target so that the 2D-fluoroscopic images were also tracked in the world space along with the surgical tools. These tracked fluoroscopic images were used directly by the surgeons for guiding pedicle screw placement, therefore, no additional patient-to-image registration was needed as is the case in preoperative CT-based navigation. The authors first validated the technique on plastic phantoms and three human cadaveric lumbar spines, with a total of 40 screws implanted in plastic phantoms and 30 screws implanted in cadavers. On histological sections, they found the screws engaged the pedicle cortex in 3.2% of the cases, touched the cortex in 14% of the cases, and were placed ideally in 82.8% of cases. In a short series of clinical evaluation on three patients with a total of 11 screws, they found both acceptable entry point and screw trajectory in 9 out of 11 cases when compared with preoperative CT-based navigation.

In a case series including 12 patients and 66 pedicle screws, Fu et al [34] in 2004 evaluated the feasibility and accuracy of pedicle screw insertion guided by 2D-fluoroscopy navigation in the thoracolumbar region. They found 5 out of 66 screw placements (7.6%) showed cortical violation of the pedicle, four medially and one laterally. In another case series, Rampersaud et al [35] implanted 360 screws in the thoracolumbar regions of 45 patients using 2D-fluoroscopy navigation and found a pedicle wall breach rate of 15.3% (55/360 screws). However, almost half (49%) of the breaches were due to the use of a screw with diameter larger than the pedicle itself, indicating the importance of proper preoperative planning. In an retrospective chart review of 37 patients with a total of 277 screws, Lekovic et al [36] found no statistically significant difference in the cortical breach rate between 2D-fluoroscopy navigation (8.7%) and 3D-fluoroscopy navigation (5.3%). More recently, Ravi et al [37] published in 2011 the results of pedicle screw placement in a minimally-invasive fashion guided by 2D-fluoroscopy navigation in 41 patients with a total of 161 screws. They found a breach rate of 23%, with the majority of the breaches (83.8%) being minor (less than 2 mm of perforation). It was also noted that 90% of the breaches were in the axial plane (medially 30%, laterally 60%), demonstrating the vulnerability of 2D-fluoroscopy navigation to trajectory deviations in the axial plane.

2.3.2 3D-Fluoroscopy

Holly and Foley [38] demonstrated in 2003 the feasibility of using 3D-fluoroscopy navigation for pedicle screw implantation through the placement of 94 pedicle screws in three cadaver specimens. They obtained the 3D-fluoroscopic images using Siremobil's Iso-C (an C-arm with isocentric point), which was tracked by an optical camera through the target mounted on the C-arm. Pre-calibration was performed such that the images were also tracked in the world space. The

C-arm rotated 190° around the specimen to acquire 100 images in a 2-minute cycle. These images were subsequently reconstructed into axial, coronal and sagittal images for navigation. Patient-to-image registration was not necessary because the pedicle screw placement was directly guided by the reconstructed images, which were already tracked in space. The pedicle screws were then implanted using tracked surgical tools in a manner similar to that involved in preoperative-CT-based guidance. The authors found 89/94 (94.7%) pedicle screws to be correctly placed and the five incorrectly placed screws all had cortical violations less than 3 mm. Geerling et al [39] conducted a drilling experiment on a foam spine model to compare the accuracy of 3D-fluoroscopy navigation with that of preoperative-CT-based guidance. They found a statistically superior point and trajectory accuracy in 3D-fluoroscopy guided navigation (0.5 mm) compared to CT-based navigation (1 mm).

Subsequent to the experiments on plastic phantom models and cadavers, several case reports and case series demonstrated higher accuracy of pedicle screw placement when guided by 3D-fluoroscopy navigation, including both the cervical spine [40, 41] and the thoracolumbar spine [42]. More notably, Rajasekaran et al [43] published a randomized controlled trial in 2007 comparing the accuracy of pedicle screw placement between non-navigated conventional methods and 3D-fluoroscopy navigation. They randomly assigned 16 patients to the non-navigated control group and 17 patients to the 3D-fluoroscopy navigation group with double-blinding. They found a significant difference in pedicle perforation rate of 23% in the control group compared to 2% in the navigation group. More recently, two cohort studies compared pedicle screw placement in a minimally invasive fashion in the lumbar region. Nakashima et al [44] found a 15.3% pedicle perforation rate in non-navigated control group compared to 7.3% in 3D-fluoroscopy navigated group, whereas Fraser et al [45] found 26.3% perforation in control and 9.1% in navigation. A meta-analysis published by Tian et al [46] in 2011 found that compared to conventional non-navigated pedicle screw placement, the 3D-fluoroscopy navigated placement had much lower odds ratio of perforation (0.09-0.36).

2.3.3 Intraoperative CT

The first generation of intraoperative CT scanners mostly required specialized operating rooms in which tracks were prebuilt on the floor so that the CT scanner could slide to an area near the operative field and the moveable operating table could bring the patient into the scanner [17, 47–49]. The first application of intraoperative CT for navigated pedicle screw implantation was reported by Haberland et al [17] in 2000 in a case series where a total of 161 screws were implanted in the thoracolumbar regions of 35 patients. Only 3/161 screws (1.9%) caused lateral wall perforation of less than 2 mm. Other similar case series in the cervical [48], thoracic [47], and thoracolumbar sections [19, 49] all reported pedicle perforation rates between 1.2% to 11.5%. In addition to requiring specialized operating rooms, another drawback of these sliding intraoperative CT scanners compared to more modern ones (discussed next) was that many of them still required patient-to-image registration, likely because these scanners were not tracked by the navigation system. In fact, many of them [17, 47, 49] implanted imaging fiducials (e.g., titanium screws) on the patient vertebrae intraoperatively, before the CT scan, to achieve patient-to-image registration. Doing so not only lengthens operative time, but is also more invasive due to the physical implantation of fiducials on patients.

In the past five years, the advent of a newer generation of intraoperative CT scanners, termed the O-arm, has simplified intraoperative CT imaging. The O-arm is a cylindrical bore mounted on a freely movable base. The cylindrical bore can open laterally when the base is moved under the patient so as to position the patient within the bore. When the opened section of the bore closes again, the source and detector of the CT can rotate 360° around the patient just as a conventional CT. Because the base is freely movable, the O-arm does not require specialized operating room installations. In addition, a tracked target is typically integrated with the O-arm, so that all images acquired by it are tracked in world space, obviating the need for patient-to-image registration. The first published successful uses of O-arm for navigated pedicle screw implantation were presented in 2008 by case reports, including a spinal fusion surgery in a refractory adult scoliosis case [50] and a pars interarticularis fixation in an athlete with L5 spondylolysis [51]. Subsequently, case series of O-arm navigation demonstrated low pedicle perforation rates ranging from 1.8% to 6.6% [52–54]. Two cohort studies [55, 56] comparing O-arm navigated pedicle screw implantation with the conventional freehand (non-navigated) technique found significantly lower rates of severe pedicle perforation in the O-arm navigated groups (1% and 3% respectively) than the freehand groups (5.9% and 9% respectively). When O-arm navigation was compared to preoperative-CT-based navigation, no statistically significant difference in terms of pedicle screw accuracy was found by Costa et al [57], but the O-arm navigation required a shorter operative time (92 min) compared to the preoperative-CT-based navigation (128 min).

2.3.4 Intraoperative MRI

Surgical navigation with intraoperative MRI enables surgeons to directly navigate on MR images of the patient acquired intraoperatively. Similar to intraoperative CT, a tracked target on the MR scanner obviates the need for patient-to-image registration. The main application of intraoperative MRI since its introduction to clinical use has been in guiding brain tumour resections [58–63]. Navigation with the preoperative MRI had an important navigation error known as the brain shift, which was caused by the relatively displacement of the brain to the skull when the cerebral spinal fluid supporting the brain was drained during craniotomy. This issue is eliminated with intraoperative imaging, since intraoperative MR acquires patient brain anatomy after the craniotomy. In addition, performing intraoperative MRI at different steps of the tumour resection enables better tracking of the tumour remnant, thus resulting in more optimal resection of the tumour [58–63]. However, to the author's best knowledge, intraoperative MRI has not yet been applied to spine surgery to date. There are likely multiple reasons for which intraoperative MRI has not been used in spine surgery, such as the fact that bony structures are better visualized on CT than MRI, the prohibitive cost of intraoperative MRI [64] and its limited image quality compared to conventional MRI, the requirement for using magnetic field compatible surgical instruments, the limitation on patient positioning and the limited access to the surgical field.

2.3.5 Intraoperative Ultrasound

Ultrasound imaging has many advantages compared to the above-mentioned imaging modalities. Ultrasound is inexpensive, highly mobile, real-time, has easily changeable imaging plane, and does not expose patients or healthcare professionals to ionizing radiation. Intraoperative ultrasound has been employed during tumour resections to augment the detection of tumours and to help improve the completeness of tumour removal in the brain [65–69], liver [70, 71], breast [72, 73], pancreas [74] and kidney [75]. In procedures involving the spine, intraoperative ultrasound has been used to help localize intramedullary tumours [76] and intradural tumours [77] for resection, to monitor fracture repositioning [78] and spinal cord decompression [79], to guide biopsy aspiration of spinal lesions [80], to guide syrinx removal [81], to guide epidural blocks [82] and facet joint injections [83]. Weber et al [84] have also experimented with intraoperative ultrasound on a dissected pig vertebra to assess its potential application to navigation in robotic surgery. To date, intraoperative ultrasound has not been used clinically to guide pedicle screw insertion, likely due to the low image quality of bony structures beyond the bone surface. However, intraoperative ultrasound has been used more and more in combination with preoperative imaging such as MRI and CT images to improve the accuracy and the speed of surgical navigation techniques, such as in the detection and correction of brain-shift [20, 85–87], the guidance of screw implantation in the pelvis [88, 89], the guidance of biopsy and therapy for prostate cancer [90], and the guidance of the ablation of lesions in livers and kidneys [91]. The next section describes the architecture and the mechanism of an ultrasound-based navigation system that combines the use of intraoperative ultrasound with preoperative images.

2.3.6 Ultrasound-Based Image-Guided Surgery System

In ultrasound-based IGS systems for pedicle screw implantation, the intraoperative ultrasound acquires patient anatomy during the surgery (Fig. 2–9a). The ultrasound probe is tracked in space by a target mounted on the probe (a target consists of reflective spheres arranged in a unique configuration) (Fig. 2–9b). Therefore, the ultrasound images acquired by the probe are also localized in space by the tracking system. The relationship between the ultrasound images and the target on the probe is established by a process known as ultrasound calibration [92]. The combination of the tracking and the ultrasound calibration confers each ultrasound image pixel at position (i,j) a set of coordinates (x,y,z) in world space. This correspondence in turn means that the patient anatomy (e.g., vertebral bone surface) acquired by the intraoperative ultrasound is also tracked in world space. In this way, the tracked intraoperative ultrasound effectively replaces the function of the tracked pointer tool in the manual registration technique. Instead of localizing the patient anatomy with a few landmarks or a series of surface points acquired with the pointer tool, the entire vertebral surface can be acquired faster and more accurately with the sweeps of an ultrasound probe.

Similar to the landmark-based manual registration where corresponding landmarks on both patient and the CT image are needed to achieve registration,

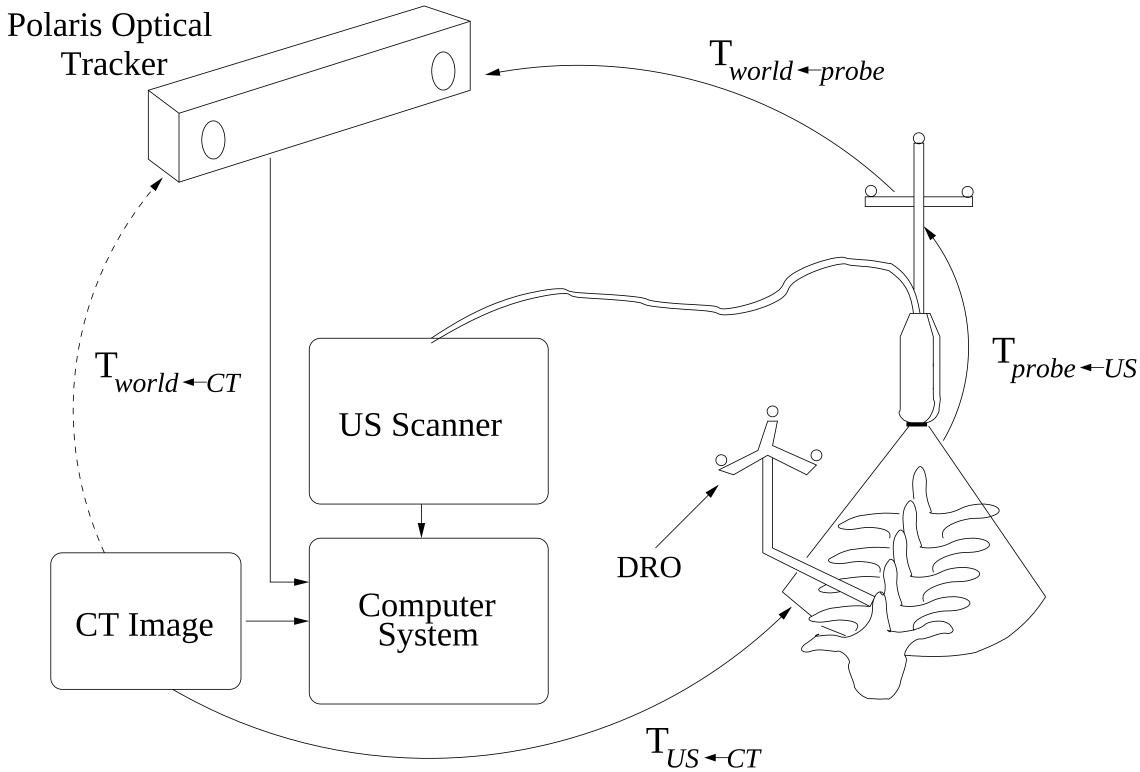

(a)

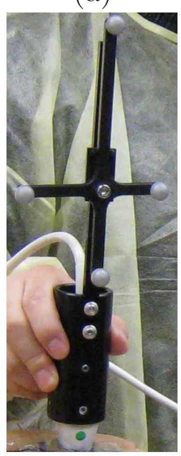

(b)

Figure 2–9: (a) Overview of ultrasound-based IGS system; (b) Ultrasound probe with tracking target mounted on the probe; tracking target consists of reflective spheres organized in a unique configuration.

patient anatomy acquired by ultrasound needs to be registered to the CT image so that a spatial relationship can be established between the CT image and the tracked surgical tools. More specifically, the spatial transformation resulting from ultrasound-CT registration can be concatenated to ultrasound calibration and tracking transformation to yield a CT-to-world space transformation as in:

$$\mathbf{T}_{world \leftarrow CT} = \mathbf{T}_{world \leftarrow probe} \mathbf{T}_{probe \leftarrow US} \mathbf{T}_{US \leftarrow CT} \tag{2.1}$$

where $\mathbf{T}_{world \leftarrow probe}$ is the tracking of the ultrasound probe, $\mathbf{T}_{probe \leftarrow US}$ is the ultrasound calibration done preoperatively, and $\mathbf{T}_{US \leftarrow CT}$ is the ultrasound-CT registration obtained by the method described in this thesis. These three transformations are concatenated in the order shown in equation (2.1) to obtain the desired transformation($\mathbf{T}_{world \leftarrow CT}$) for the registration between the patient vertebrae and the preoperative CT. In these three transformations, the tracking of the ultrasound probe is performed by the Polaris optical camera system and the tracking accuracy depends on the hardware itself. Ultrasound calibration has been studied extensively and a good review of the field can be found in Mercier et al [92]. This thesis focuses on the third component of this transformation, the registration between the ultrasound and CT images of the vertebrae. The following is a review of the ultrasound-CT registration techniques developed for image-guided orthopedic surgeries.

2.4 Ultrasound-CT Registration for Orthopedic Surgery

The techniques of ultrasound-CT registration of bone structures can be divided into two main categories, point-based registration (also known as feature-based registration) and intensity-based registration. Point-based registration involves the extraction of bone surfaces from both ultrasound and CT images, converting the surfaces to clouds of points, and registering the clouds of points. Intensity-based registration may involve preprocessing of ultrasound and CT images, but typically does not require precise segmentation of bone surface from ultrasound images. The registration is computed between the intensity values of the pixels and voxels in the processed images. Both categories of registration techniques have their own merits and drawbacks. While point-based registrations excel at faster runtime, they are susceptible to local minima and require segmentation, which makes the methods impractical intraoperatively. On the other hand, while intensity-based registration techniques obviate the need for precise ultrasound segmentation, the preprocessing steps and the computation of cost-functions based on intensity values often significantly lengthen the runtime. In this section, we outline some of the representative work in both categories of ultrasound-CT registration of bone structures.

2.4.1 Point-Based Registration

Ault and Siegel [93, 94] were one of the first to attempt ultrasound-CT registration for application to orthopedic surgery. In 1994, they published a study in which they built a femur phantom by immersing a clean femur in a plastic tube filled with water. They then imaged the phantom with ultrasound, reconstructed the ultrasound images into a volume, and subsequently segmented and triangulated the partial surface of the femur from the image volume they obtained. The segmentation involved a series of image processing techniques including thresholding, morphologic filtering and polynomial fitting. The same segmentation and surface reconstruction was applied to the CT image of the phantom. Finally, they manually aligned the two reconstructed surfaces from US and CT and showed a 5 mm displacement error after several repeated manual alignments. In doing so, they demonstrated the potential of using ultrasound to achieve patient registration for frameless stereotactic orthopedic surgery.

A group of French researchers, Lavallée et al [95], presented an experiment in 1996 in which they performed ultrasound imaging on an isolated vertebra. They then manually segmented the vertebral surface in ultrasound into a cloud of points and registered the points to the corresponding surface segmented from CT images. The registration was performed automatically using a least-squares formulation. Using this registration method, Carrat et al [88] and Tonetti et al [89] performed percutaneous placement of screws guided by preoperative CT images on pelvises of cadavers and patients. The pelvic bone surface in the intraoperative ultrasound was manually segmented and converted to a cloud of points and registered to the bone surface of the CT image, which is also extracted semi-manually using an interactive software. These experiments were not validated with fiducial-based gold standard registration. However, postoperative CT scans were performed to verify the screw placements by measuring the distances from the sides and tip of screw to its closest cortical surfaces. No screw breached the cortical bone surface in any of the experiments.

Around the same time, Herring et al [96] from Vanderbilt University presented preliminary works on the registration of automatically segmented vertebral surface from both ultrasound and CT images. The vertebral surface from the ultrasound images was automatically extracted through a series of operations including denoising, morphological opening, linear thresholding and ray-tracing. The bone surface from CT was extracted by a modified Marching Cubes algorithm [97]. The surfaces extracted from ultrasound and CT were converted to two groups of points and registered using the Besl-McKay iterative closest point (ICP) algorithm [98]. Because the ultrasound transducer was not tracked in space, they were only able to make qualitative interpretation of the registration results by visually inspecting the ultrasound points overlaid on the CT image. However, Muratore et al [99] from the same group published four years later a quantitative validation of their proposed registration method by obtaining tracked ultrasound images of a plastic spine phantom. The accuracy of the registration was assessed by computing the target registration error (TRE) with respect to the gold standard registrations generated from imaging fiducials implanted on the spine phantom. The best mean TRE achieved was 1.33 mm and the worst TRE was 5.43 mm. Unfortunately, the studies were not continued further with validation using cadaver or patient images that would give more clinically realistic results.

Automated segmentation was integrated with registration in Amin et al [100] to enhance the quality of the automated extraction of bone surface from ultrasound. In this technique, the extracted ultrasound bone surface was updated at each iteration of the registration. At each update, the proximity of a pixel to the estimated bone surface (spatial prior) was used to assist the segmentation algorithm to determine whether the pixel belonged to the bone surface. In addition, the segmentation also factored in the intensity of the pixel (intensity prior) and whether shadow region was present beyond the pixel (edge prior). The registration technique was applied to images from a plastic pelvic phantom and a patient pelvis. The phantom experiment was validated with respect to fiducial-based gold standard registration and the patient experiment was compared to a surface-point-based registration. Both experiments yielded good accuracy with fiducial registration error (FRE) less than 2 mm in each axis. The main drawback of this technique was that it required good initial estimate of the registration in order to be effective, as the bone surface segmentation depended on the spatial prior of the pixels in the ultrasound images.

Barratt et al [101] presented a technique in which both ultrasound calibration and ultrasound-CT registration were optimized concurrently. It had the advantage of reducing the ultrasound calibration inaccuracy due to the variation of speed of sound in the different tissues of human body. The registration experiments were performed on images acquired from human cadaver femurs and pelvises. The point clouds obtained from manually segmented ultrasound bone surface were registered by iterative Gauss-Newton optimization to the semi-automatically segmented CT bone surface, along with the ultrasound calibration parameters. The final mean TRE computed with respect to fiducial-based registration was 1.6 mm, with a success rate (TRE < 5 mm) of 94.7%. However, further work might be needed to eliminate the step of manual segmentation to make the technique more suitable for intraoperative use.

Although the iterative closest point optimization can provide fast and relatively accurate registration, it is easily trapped into local minima, causing decreased robustness. Moghari and Abolmaesumi [102] replaced ICP with another iterative point-based registration technique using unscented Kalman filter (UKF). Because registration based on UKF is more resistant to local minima than ICP, it is less sensitive to initial misalignment and outliers. This method was employed by Rasoulian et al [103, 104] to perform ultrasound-CT registration of vertebrae in five plastic phantoms and a sheep cadaver. They employed an automated ultrasound bone surface segmentation technique by Foroughi et al [105] and used the ITK-snap software [106] to semi-manually segment the CT bone surface. Point-based registration of extracted surfaces using UKF was performed on multiple vertebrae simultaneously, with an added biomechanical constraint to limit the allowable range of curvature among the vertebrae. The technique yielded good registration accuracy with mean final TRE of 2.2 mm and success rate (TRE < 3 mm) of 82% for the sheep cadaver. However, the lengthy registration time of 29 minutes makes the technique not yet applicable for intraoperative use.

Brounstein et al [107] proposed a point-based ultrasound-CT registration technique using Gaussian mixture models (GMM) to represent point clouds. In this technique, they first segmented the bone surface from the ultrasound images using 3D local phase features, a segmentation technique previously developed by Hacihaliloglu et al [108]. Then, both the ultrasound and CT bone surfaces were converted to point clouds. The point clouds were subsampled using GMM, which is a statistical model that represents an entire population of point clouds using multi-dimensional Gaussian distributions. The subsampling of point clouds enabled faster registration compared to using all points. The two GMMs were registered iteratively by minimizing the L2 metric distance between them. The registration experiments were performed on images from a pelvic phantom and a patient pelvis. The accuracy of registration was not assessed using TRE, but instead using a surface registration error (SRE), which was the root-mean-square distance between the two registered surfaces. The registration experiments resulted in a median SRE of 0.42 mm for the pelvic phantom and a median SRE of 0.63 mm for the patient pelvis.

2.4.2 Intensity-Based Registration

Brendel et al [109] were the first to present an intensity-based ultrasound-CT registration technique to register lumbar vertebrae without requiring ultrasound segmentation. In this technique, the CT image was processed by a ray-tracing technique that aimed to extract the same amount of vertebral bone surface as that seen in the ultrasound image. This was achieved by eliminating the CT voxels occluded by the tissue-bone interface to simulate the shadow regions in ultrasound and by eliminating bone surfaces that were not orthogonal to the direction of incident rays. The extracted bone surface from CT was directly registered to the unprocessed ultrasound image by maximizing the total intensity of the part of ultrasound image that overlaps with the extracted surface from CT. The ray-tracing technique required that the scanning pathway of the ultrasound be known a priori. In this study, the pathway was assumed to be directly posterior to the spinous process and moving in an inferior to superior direction.

This intensity-based technique was tested on an ex-vivo preparation of a human lumbar spine. However, because no ground truth was generated, only qualitative assessment by visual inspection of the registered images could be conducted. Quantitative validation experiments of this registration technique was presented a few years later through a plastic lumbosacral phantom [110]. More than 90% of the final TREs of the phantom registration experiments were under 1.5 mm. Using the same intensity-based registration technique, Winter et al [111, 112] acquired ultrasound and CT images from patients to compare gradient and evolutionary-based optimization algorithms and to develop an ultrasound acquisition protocol that improved the registration accuracy. The validation experiments were performed using patient images under clinically realistic conditions and showed good robustness. However, the accuracy was assessed by comparing the registration results to a bronze standard reference registration. This bronze reference registration was generated by the same algorithm that was under study and was visually checked by the authors themselves. Therefore, the reported final mean deviation of 0.03 mm from the bronze reference registration was more of a measure of the convergence and reproducibility of their optimization algorithms than the actual registration accuracy.

Penney et al [113, 114] developed an intensity-based registration technique through the use of probability images. The probability images represented the probability of a pixel or voxel containing bone surface. The ultrasound and CT images were converted to probability images through probability density functions (PDF), which were obtained by combining a large amount of a priori images segmented manually. For ultrasound images, the bone surface was manually extracted and for each pixel on the surface, two features were associated with it: the pixel intensity and the length of the shadow region below it. Similarly, for CT images, for each voxel on the manually extracted bone surface, two features were associated with it: the magnitude of the intensity gradient and the likelihood of bone surface versus skin surface. Ultrasound and CT images acquired from three human cadaver pelvises and six cadaver femurs were used to obtain the PDFs. During the registration of each individual pelvis or femur, both ultrasound and CT images were converted to probability images by computing the features at each pixel or voxel and by comparing them with those in the PDFs. The probability images of ultrasound and CT were registered by cross correlation and hill-climbing optimization, and yielded mean TRE of 1.6 mm. However, the long registration runtime of up to 10.5 minutes and the need for a large number of a priori images made this registration technique less ideal for intraoperative use.

More recently, ultrasound simulation derived from CT images has been applied to registration. This was exemplified by the work of Wein et al [91, 115], in which simulated ultrasound images were created based on acoustic impedance properties derived from the tissue density (Hounsfeld Unit) in CT images. The simulated ultrasound images were then registered to the real ultrasound images using a similarity measure that the authors created, termed Linear Correlation of Linear Combination metric (LC^2), which was essentially a correlation of real ultrasound intensities with a linear combination of simulation measures from CT. The registration technique was applied for radiotherapy planning of livers, kidneys and neck tumours. Gill et al [116, 117, 118] adapted this technique to the ultrasound-CT registration of vertebrae. The ultrasound simulation was modified so that there was total reflection at the bone surface and that all areas occluded by the bone surface were not simulated. A groupwise registration of vertebrae was performed, where a simultaneous registration of multiple vertebrae consists of a combination of several individually rigid registrations. In addition, a biomechanical model similar to that in Rasoulian et al [103, 104] was used to constrain the allowable range of lumbar curvature. The technique was validated using a lumbar spine phantom and the lumbosacral section of a sheep cadaver, where three vertebrae (L3-L5) were registered. The final mean TRE ranged from 0.8 to 2.7 mm for the plastic spine phantom with a registration success rate of 98.5% (TRE $<$ 3 mm), and 0.6 to 2.26 mm for the sheep cadaver with a success rate of 87% (TRE $<$ 3 mm). Due to the heavy computational requirement of this simulation-based registration technique, registration runtime averaged 43 minutes on a central processing unit (CPU) and 4 minutes on a graphics processing unit (GPU). This registration method was adopted by the same group for the registration of a statistical shape model (SSM) of vertebrae to ultrasound images in Khallaghi et al [119] and for the registration of SSM of pelvis to ultrasound images in Ghanavati et al [120, 121]. The simulation of ultrasound from the SSMs yielded registration accuracy near 2.5 mm. However, in both cases, the validation experiments consisted only of registration using ultrasound images of plastic phantoms, which were not as clinically realistic as the images of cadavers or patients.

2.5 Ultrasound Slices to Preoperative Volume Registration

Many existing techniques of multimodal ultrasound registration align a volume of ultrasound to a volume of CT or MR image. The ultrasound image volume is obtained by reconstructing a 3D volume from the 2D ultrasound image slices using a method such as one of those described in Solberg et al [122]. However, volumetric reconstruction of ultrasound is a challenging problem as it imposes additional runtime on top of the registration algorithm and may entail data loss due to pixel interpolation. On the other hand, by directly registering ultrasound slices to an image volume, the reconstruction step is circumvented. Doing so not only reduces the runtime and the potential data loss, but also makes the registration algorithm more flexible in selecting the number of slices for registration and enabling parallel computation.

Blackall et al [123] employed registration of ultrasound slices to MRI volume of a gelatin phantom to calibrate the ultrasound images with respect to the tracked ultrasound probe. Each 2D ultrasound image were traversed pixel by pixel to find the corresponding interpolated voxel in the MRI volume. The intensities of the corresponding pixels and voxels were combined to compute a joint histogram to derive the normalized mutual information (NMI). The NMI was maximized by a simple iterative optimization algorithm similar to hill-climbing. This registration technique achieved an ultrasound calibration with a mean point reconstruction accuracy of 1.16 mm, which was similar to the accuracy achieved with conventional point-based calibration methods. However, registration accuracy was not reported in the results.

In Penney et al [113, 114] described above, a slices-to-volume registration was performed. The ultrasound slices and the CT volume were first converted to bone surface probability images. For each ultrasound slice, the CT probability image volume was resliced to provide the CT slice corresponding to the ultrasound. The cross correlation between all corresponding slices of probability images was computed and maximized by hill-climbing to achieve registration. The direct slices-to-volume registration helped to speed up the registration runtime. However, in this case, the registration runtime was as long as 10.5 minutes, likely due to the need to convert all images to probability maps before optimization.

Brooks et al [124] developed a deformable slices-to-volume registration between ultrasound and MR images of a phantom with an inflatable balloon. The mutual information of gradient magnitudes was used as a similarity measure between each ultrasound slice and the corresponding voxels in the MR volume. Individual similarity measures were combined into a weighted average group similarity, which was maximized by a Quasi-Newton optimization to achieve registration. Registration was performed between ultrasound slices and MR volumes with the balloon inflated at various degrees, and were compared to the corresponding ultrasound volume to MR volume registration. It was found that the slices-to-volume registration achieved higher accuracy than the volume-to-volume registration and that the runtime of slices-to-volume registration was only one third of the time for volume-to-volume registration.

2.6 Summary and Moving Forward

Cleary et al [125] presented in 2000 a report detailing the technical requirements for image-guided spine surgery. The report was based on the consensus from about 70 experts in the field. In this report, emphasis was placed on the need for registration techniques that are automated, robust, appropriately validated and have a sufficient speed. More specifically, they recommended that the registration should have an accuracy of 1-2 mm, that the validation should be conducted by comparing results with respect to fiducial-based gold standard registrations, and that the recommended execution time for registration for pedicle screw implantation be under 5 minutes. While many of the ultrasound-CT registration techniques reviewed above demonstrated good performance, it was difficult to find one that satisfied all these requirements. Therefore, the goal of this thesis is to develop and validate an ultrasound-CT registration technique for vertebrae that satisfies all these requirements. Most of the existing work mentioned above either require manual intervention to segment the ultrasound images, fail to demonstrate clinical relevance by only using data from simple plastic phantoms, fail to demonstrate true accuracy by not using fiducial-based gold standard for accuracy assessment, or require an unreasonably long execution time of more than 5 minutes per vertebra. The work that is most closely related to ours is from Brendel et al [109, 110], Winter et al [111, 112] and Gill et al [116, 117, 118]. While the technique by

Brendel et al [109, 110] and Winter et al [111, 112] demonstrated good speed and robustness, their accuracy assessment was performed by comparing registration results with a ground truth that was itself generated by the registration algorithm being assessed. In other words, instead of assessing registration accuracy, they assessed registration convergence and reproducibility. On the other hand, Gill et al [116, 117, 118] presented a technique that demonstrated good accuracy on a sheep cadaver, but the validation was limited as it was only on a single animal subject and the algorithm took 43 minutes to register three vertebrae. This thesis presents a new technique for registering ultrasound and CT images of vertebrae. The technique was validated with images from both plastic phantoms and porcine cadavers and with respect to fiducial-based gold standard registration. In addition, it was adapted to a 2D slices to 3D volume registration technique. The thesis will demonstrate that the technique satisfies Cleary et al [125]'s requirements with the goal of moving the research a step closer towards practical application of ultrasound-based intraoperative registration for image-guided spinal fusion surgery.

CHAPTER 3
Ultrasound-CT Registration of Vertebrae

Foreword

In this chapter, we present a new intensity-based registration technique for registering ultrasound and CT images of vertebrae in the context of image-guidance for spinal fusion surgery. As was discussed previously in Chapter 2, we developed our own registration technique instead of using an existing one because we wanted to develop a technique that is practical for intraoperative use. In this chapter, we first describe in detail the registration technique, including the pre-processing of the images and the optimization algorithm. Then, we present the registration experiments that used images from a plastic phantom and a single vertebra of a porcine cadaver. In addition, we present the process of generation of the gold standard registration to serve as a ground truth for assessing accuracy. Finally, we show the preliminary results of the registration accuracy and robustness of the technique based on the registration experiments.

Further extensive validations are presented in Chapter 4 and the issue of registration speed is addressed in Chapter 5. The Introduction (Section 3.1) and the description of ultrasound-based IGS system (Section 3.2.1) have already been presented in Chapter 2 and the reader may choose to skip these sections without missing information. This chapter has been published in the *International Journal of Computer Assisted Radiology and Surgery* [126].

Towards Accurate, Robust and Practical Ultrasound-CT Registration of Vertebrae for Image-Guided Spine Surgery

C. X. B. Yan, B. Goulet, J. Pelletier, S. J.-S. Chen,

D. Tampieri, D. L. Collins

Int J Comput Assist Radiol Surg, 6(4):523-37, 2011

Reprinted with permission from Springer

Abstract

Purpose: Accurate registration of patient anatomy and preoperative computed tomography (CT) images is key to successful image-guided spine surgery. Current manual landmark and surface-based techniques are time consuming and not always accurate. Intraoperative ultrasound imaging of the vertebrae, combined with automated registration, could improve surgery by improving accuracy, reducing operative time, and decreasing invasiveness.

Methods: We present a simple ultrasound-CT registration technique that is automated, accurate, and robust. Registration is achieved by aligning the posterior vertebral surface, extracted from both CT and ultrasound images, using a forward and a backward scan line tracing method, respectively. The registration technique is validated using a simple plastic phantom in a water bath and a more realistic porcine cadaver in a simulation of open back surgery.

Results: Clinically relevant accuracy was estimated by comparing automated registrations with gold standard imaging fiducial-based reference transformations, which yielded target registration errors of under 1 mm for the plastic phantom and under 1.6 mm for the porcine cadaver.

Conclusions: Our registration technique demonstrates good accuracy and robustness under clinically realistic conditions and thus warrants further studies on its surgical application.

3.1 Introduction

Over a quarter of a million spinal fusion surgeries are performed annually in the United States to treat degenerative disc disease, scoliosis, vertebral instability, fractures, and spinal stenosis, and the use of these surgeries is increasing rapidly [5]. Spinal fusion surgeries require the implantation of pedicle screws in the vertebrae to help stabilize the fusion of neighbouring segments. However, due to the complexity and variability of the anatomy and the incomplete exposure of the vertebral surface, pedicle screw insertion failure rates are as high as 20-30% when using traditional anatomy-guided techniques [14, 16–18].

To achieve higher accuracy and to reduce the rate of failure, image-guided surgery (IGS) systems are now used to guide many surgeons in spine surgeries [127]. The use of IGS systems in spine surgeries has greatly increased the accuracy of screw implantations and reduced their rate of failure [26–29, 128, 129]. The resulting benefits are numerous, including lower surgical risk, increased possibility of performing more complex instrumentation, decreased postoperative complications, more confidence in the surgical procedures, and better postoperative function.

A critical step in spine IGS navigation systems is registering patient anatomy to preoperative images. The standard clinical registration method is performed manually by identifying fiducial or anatomical landmarks on both the preoperative computed tomography (CT) image and the patient, or by identifying points on the vertebral surface [e.g. , 26, 130]. However, manual registration is time consuming and invasive. Based on our and others' experience, manual registration by mapping vertebral surface points could take 10 to 15 minutes per vertebra [131]. We also found that the combination of manual registration and screw insertion takes 19.8 minutes per screw on average [7]. The time for manual registration could add up to important additional operative time when several vertebrae are being operated on during a spinal fusion surgery. Manual registration is also more invasive because more soft tissue dissection are often needed to expose more of the vertebral bone (e.g., posterior surface of transverse processes) to obtain good landmarks for mapping the surface points. To eliminate these drawbacks and to make image-guided techniques more efficient, intraoperative imaging modalities are preferred for collecting anatomical information from the patient for registration during surgery.

A number of intraoperative imaging modalities exist and have been implemented for IGS application [132], such as C-arm fluoroscopy [38, 129, 133], intraoperative CT [17], and intraoperative magnetic resonance imaging [134]. However, these systems are limited due to either occupational radiation exposure [135], prohibitive cost, or stringent requirements for operating conditions and access to the patient. In light of these limitations, intraoperative ultrasound offers a safe, flexible, and inexpensive method of intraoperative acquisition.

In ultrasound-based spine IGS systems, the ultrasound probe (or transducer) is tracked in space so that the patient anatomy acquired is localized in space, that is, each pixel at position (i,j) in the ultrasound image has known (x,y,z) coordinates in real-world space. The ultrasound images are subsequently registered to the CT images so that the patient anatomies in the ultrasound can be matched to those in the CT image. Several groups have investigated ultrasound-CT registration of bone structures at different anatomical regions, such as the femurs [93, 101, 113, 136, 137], the pelvis [88, 100–102, 114, 120, 136, 138–141], or the vertebrae [95, 96, 99, 103, 109–112, 117, 139, 142].

We were motivated to develop our own vertebral registration technique instead of using an existing method for three reasons: (1) we want to integrate the procedure into our image-guided surgical platform; (2) we need a technique that is reasonably quick compared to the manual registration so that it can be used in the operating room without disrupting the surgical workflow; and (3) while many of the existing ultrasound-CT registration techniques yield accuracy within the acceptable range (i.e., under 2 mm), to our knowledge, none have been quantitatively evaluated on realistic vertebral data with respect to gold standard ground truth in a surgical setting, except in [118, 143].

Many of the earlier techniques require manual or semi-automated segmentation of ultrasound images of vertebrae [e.g. , 95, 138]. Because ultrasound is acquired intraoperatively, any manual processing after the ultrasound acquisition will lengthen the operating time. For example, Carrat et al [88] reported that using a manual segmentation technique increased the regular operating time for iliosacral instrumentation by 25 minutes. Therefore, our technique is designed to not require human intervention in processing ultrasound data.

Other vertebral registration techniques have employed either computer simulation models [e.g., 142] or plastic phantoms [e.g., 99, 103, 110] for validation. Although such models and phantoms provide a preliminary means to evaluate the feasibility of a registration technique, they are a necessary but insufficient means of validation. Results derived from these simulations cannot be readily linked to potential clinical applications because the data are still too simplistic when compared with the more clinically relevant images derived from cadavers or patients. We will demonstrate the difference in accuracy and robustness between results obtained from a plastic phantom and those from an animal cadaver.

One drawback of using cadaver or patient images to validate vertebral registration techniques is the lack of a reliable ground truth. This drawback results in the phenomenon that many registration techniques are not validated reliably when using clinically realistic data. In most of the previous studies of ultrasound-CT vertebral registration using cadavers, no gold standard registrations were generated to quantitatively validate the registration techniques with reliable ground truth. For example, Brendel et al [109] used an ex vivo human lumbar spine, yet they performed only a qualitative evaluation based on the visual inspection of images. For live human subjects, given that the vertebral column is a region of the utmost importance, it would be unethical to implant fiducials in patient vertebrae purely for research purposes. In a more recent study, Winter et al [112] developed an ultrasound acquisition protocol using actual patient images. The proposed ground truth employed for validation was generated by running through 50 cycles of the same registration technique being validated, effectively generating quantitative results that demonstrate the precision of the registration technique instead of its accuracy. In this paper, we address this problem by implanting imaging fiducials on an animal cadaver to generate a gold standard registration to serve as the ground truth.

Finally, because the majority of spinal fusion surgeries are performed as open back surgeries, we designed our experiments to better simulate the real surgical situation. Therefore, instead of acquiring ultrasound of the vertebrae through layers of skin and fatty tissues before surgical incision, we perform the acquisition after the incision has been made. The vertebrae are imaged by ultrasound through a saline-filled surgical cavity. In addition, acquisition through the surgical cavity greatly reduces the errors caused by variation in the speed of sound in different layers of tissue (see [101]) because the sound waves need not travel through a deep and variable layer of fatty tissue.

In this article, we first present an ultrasound-CT registration technique based on forward and backward scan line tracing. The registration technique is quantitatively validated using a gold standard (ground truth). The ground truth is generated from imaging fiducials that are implanted in the actual anatomy (vertebra) being registered. The validation is performed on both a plastic phantom in a water bath and on a porcine cadaver under conditions that simulate open back surgery, allowing clinically relevant results to be obtained.

3.2 Methods

3.2.1 Ultrasound-Based Image-Guided Surgery System

The ultrasound-based IGS system described in this paper consists of several components, including an optical camera, a dynamic reference object (DRO), an ultrasound scanner with a tracked probe, and a computer system (Fig. 3–1). The optical camera (Polaris, Northern Digital Inc., Ontario, Canada) continuously monitors and records the position and orientation of tracked targets (e.g., DRO, ultrasound probe, pointer, surgical tools, etc.). Tracking is achieved when the optical camera emits infrared light on the targets and then receives back the infrared rays reflected by the reflective spheres mounted on the targets. The targets' position and orientation are stored in a coordinate system relative to the DRO called the *world space* (sometimes also called the *patient space* during surgery). The computer system displays the tracked targets relative to a preoperative CT image to convey to the surgeon information about the position and orientation of the surgical tools with respect to patient anatomy and surgical plans.

To achieve proper surgical guidance, the preoperative CT image needs to be brought to the same world space position and orientation as the corresponding patient anatomy. This spatial alignment of image to anatomy requires a spatial transformation from the CT image space to the world space. In the case of ultrasound-based IGS systems, intraoperative ultrasound images are acquired

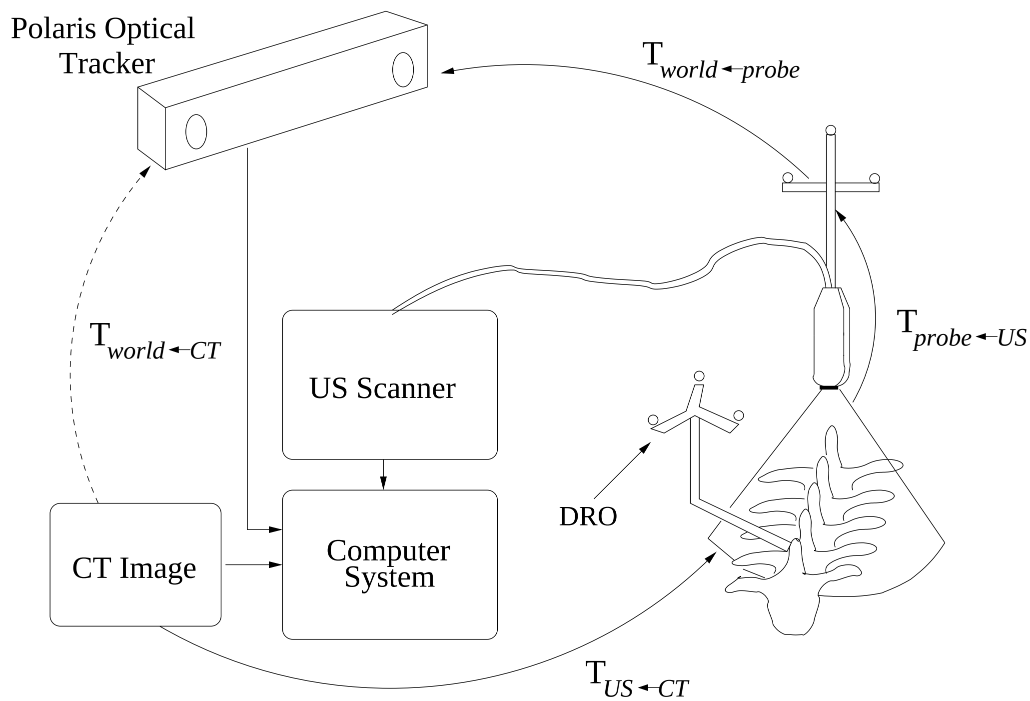

Figure 3–1: Overview of ultrasound-based IGS system.

to locate patient anatomy. The subsequent registration of the preoperative CT images to these ultrasound images can yield the CT-to-world-space transformation as in:

$$\mathbf{T}_{world \leftarrow CT} = \mathbf{T}_{world \leftarrow probe} \mathbf{T}_{probe \leftarrow US} \mathbf{T}_{US \leftarrow CT} \tag{3.1}$$

where $\mathbf{T}_{world \leftarrow probe}$ is the tracking of the ultrasound probe, $\mathbf{T}_{probe \leftarrow US}$ is the ultrasound calibration done preoperatively, and $\mathbf{T}_{US \leftarrow CT}$ is the CT-ultrasound registration obtained by the method described below. These three transformations are concatenated in the order shown in equation (3.1) to obtain the desired transformation($\mathbf{T}_{world \leftarrow CT}$) for the registration between the patient vertebrae and the preoperative CT. Note that this registration is a rigid transformation (only 3D translations and 3D rotations) because the vertebrae are rigid bodies.

Although multiple vertebrae are instrumented in one spinal fusion surgery, the rigid ultrasound-CT registration is performed on a single vertebra at a time. This is because the intervertebral discs and ligaments connecting neighbouring vertebrae are deformable and hence the relative positions between neighbouring vertebrae are not rigidly preserved from the patient position at preoperative CT imaging (supine) to the patient position during surgery (prone). The DRO is also moved every time the vertebra being operated on is changed. In practice, the DRO is always installed on the neighbouring vertebra, immediately next to the current vertebra that is being operated (Fig. 3–1). This practice offsets any other global motions (e.g., breathing) because Glossop and Hu [144] showed that in a global displacement such as that due to breathing motion, the displacement of one vertebra tracks very closely the displacement of its neighbouring vertebra (within

0.2 mm). Therefore, global motions affecting the current vertebra are effectively offset by installing the origin of the world space (DRO) on the neighbouring vertebra.

3.2.2 Image Processing of CT and Ultrasound

Imaging the same anatomy with both CT and ultrasound yields different results because the two modalities are based on different physical properties. However, vertebral bones in both CT and ultrasound images possess a common feature, namely, their intensities are much higher compared with neighbouring soft tissues. This feature is illustrated in Fig. 3–2. The vertebral bones have a higher intensity in the CT images because the X-ray attenuation coefficient of bones is much higher than that of soft tissues (Fig. 3–2a). As for ultrasound imaging, the majority of sound wave energy is reflected by the bone surface because high variations in acoustic impedance exist across the bone-tissue interface. These reflected ultrasound waves create a band of high-intensity voxels at the bone surface and shadow regions below the bone surface (Fig. 3–2b). Therefore, although the two modalities have different imaging physics, they both result in high-intensity bone surfaces. Our method aims to exploit this common feature to achieve the registration of vertebral bones in both CT and ultrasound images.

Some image processing steps are applied to both the CT and ultrasound images before registration optimization to exploit their common feature of high-intensity bone surfaces because soft tissues such as muscle, fascia, and fatty tissue have little in common in the two modalities. Therefore, the image processing mainly consists of extracting the bone surfaces in both the CT and ultrasound

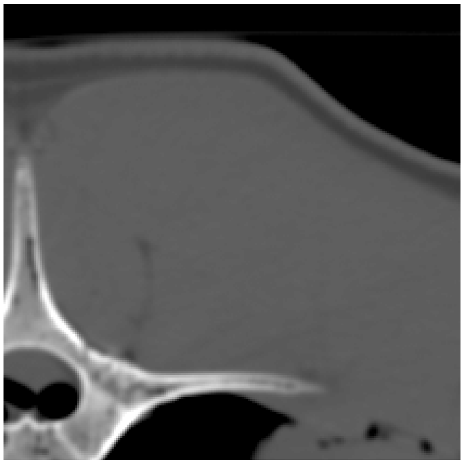

(a)

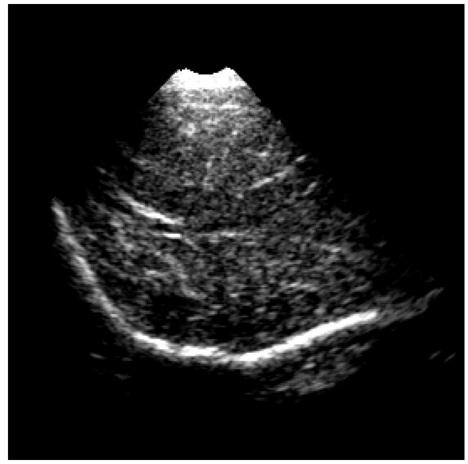

(b)

Figure 3–2: (a) Sample axial (transverse) image of the anterior aspect of a vertebra in CT. (b) Sample axial image of vertebral ultrasound, where the bone surface reflects the majority of acoustic energy, creating a band of high intensity at the location of the bone surface.

images. To achieve this extraction, we developed a scan line tracing method similar to that of Brendel et al [109, 110] and Winter et al [111, 112]. However, unlike their forward tracing method, we also apply a backward tracing on the ultrasound to take advantage of the shadow regions directly beneath the bone surfaces, inspired by Amin et al [100], Foroughi et al [105] and Hellier et al [145]. The scan line tracing methods are explained below.

The forward scan line tracing method approximates the imaging principle of B-mode ultrasound using a phased array probe (Fig. 3–3a). In this method, scan lines emanate from an imaginary probe and form a fan-shaped sector. Along each line, the first voxel above a fixed threshold of 150 Hounsfield units is used to roughly locate the bone surface. Following the first voxel above the threshold, additional voxels along the scan line within a penetration depth of 1 mm of the first voxel are kept as the extracted bone surface. Beyond the penetration depth for the extraction, voxels are considered to be shadowed by the bone surface and hence discarded (Fig. 3–3c). When extracting the posterior surface of the vertebrae, the imaginary probe is positioned 3 cm posterior to the spinous process and directed anteriorly, orthogonal to the length of the spine. The probe then travels in a superior-to-inferior direction to cover the vertebra of interest. After the probe makes its sweep through the CT volume, the posterior surface of the vertebra of interest is extracted from the image and this CT surface is cropped to the vertebral level being registered. Note that both the imaginary probe and the scan lines are not generated based on the real ultrasound probe's configuration. They only roughly approximate the geometry of the fan-shaped sector, because the goal of this scan line tracing technique is not to simulate realistically the imaging physics of ultrasound, but to extract the vertebral bone surface so as to achieve good registration.

The backward scan line tracing method also generates a fan-shaped sector from an imaginary probe just as in the forward method. However, unlike the forward method, the backward tracing method is applied to the ultrasound images instead of the CT images, and the traversal of the scan line starts at the far edge of the sector and moves back towards the imaginary probe, as shown in Fig. 3–4a. The backward tracing method makes use of the ultrasound shadow regions directly under the bone surface to help determine the position of the surface. The scan line traverses the shadow regions until it reaches the bone surface, where the high-intensity voxels at the surface are extracted. An intensity threshold of 20%

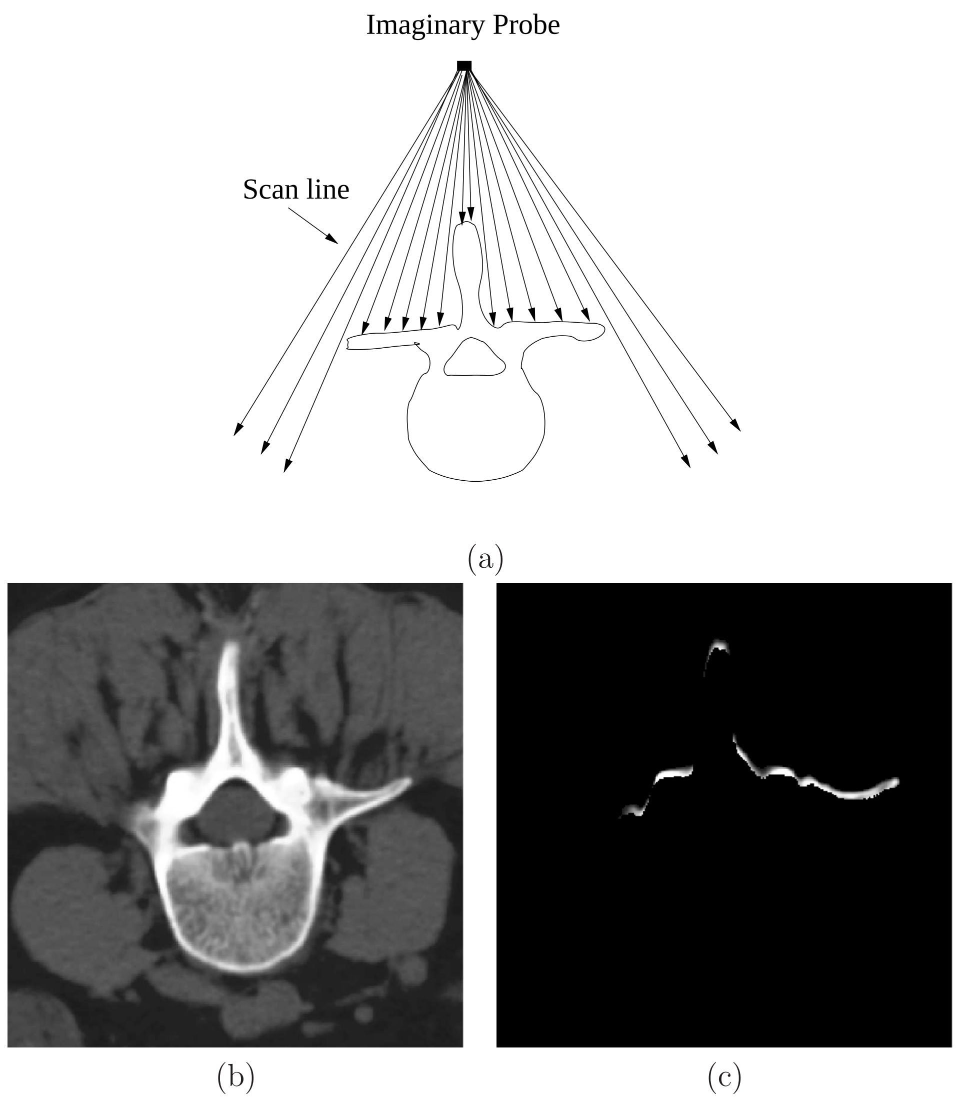

Figure 3–3: Surface extraction by forward scan line tracing: (a) Illustration of forward scan line tracing: scan lines from the imaginary probe form a fan-shaped sector and stop at the bone surface. (b) A sample vertebral CT image (axial slice). (c) Posterior vertebral surface extracted by forward tracing the CT image in (b).

of the maximum value and a penetration depth of 4 mm are used. Figure 3–4b and 3–4c show a sample ultrasound image and the resulting image after backward tracing. This backward tracing method is similar to Amin et al [100]'s directional edge detector, but the algorithm has been adapted to the fan-shaped sector of our phased array probe. Unlike Jain and Taylor [146] who identified the outer surface of the bone using combined probabilistic estimates, our technique identifies the bone surface from the inside and extracts the peak intensities in the ultrasound bone response.

3.2.3 Registration Optimization

Once the CT and ultrasound images are processed, an optimization function is executed to register the extracted surfaces. The extracted surfaces are in fact intensity peaks in the images, as illustrated by Fig. 3–5. The goal of registration is to align the highest-intensity voxels in both extracted surfaces through a rigid transformation. To achieve this, a normalized cross correlation is used as the objective function to align the two extracted surfaces, as in

$$C = \frac{\sum(US \cdot CT)}{\sqrt{\sum US^2} \cdot \sqrt{\sum CT^2}} \tag{3.2}$$

where C is the cross correlation value, CT is the intensity value of a voxel in the surface extracted from the CT image, and US is the interpolated intensity value at a point in the surface extracted from the ultrasound image that corresponds to the CT voxel by the rigid transformation being optimized. The cross correlation is maximized when the highest-intensity voxels in both extracted surfaces overlap.

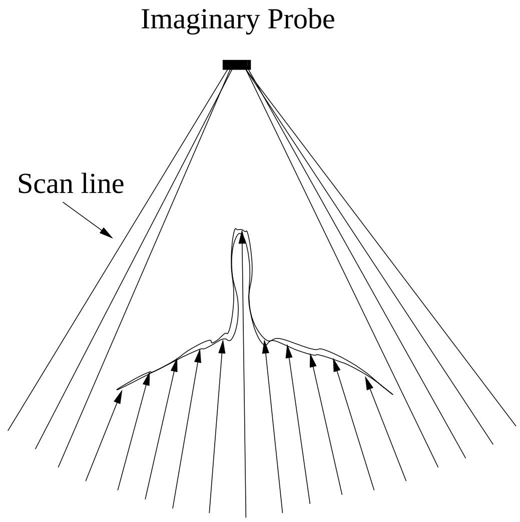

(a)

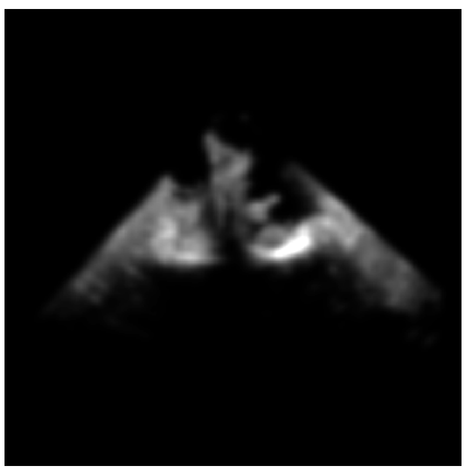

(b)

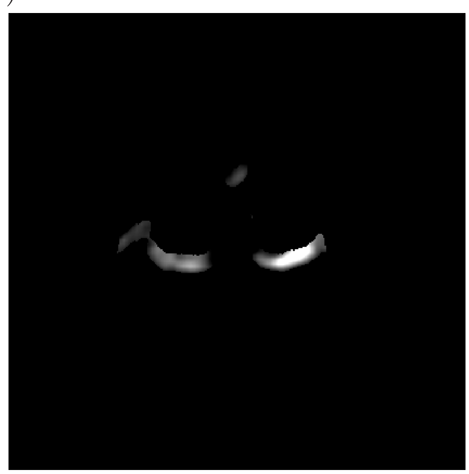

(c)

Figure 3–4: Surface extraction by backward scan line tracing: (a) Illustration of backward scan line tracing: the scan lines traverse from the far edge of the sector back towards the imaginary probe and stop at the bone surface. (b) A sample vertebral ultrasound image (MPR axial slicing). (c) Posterior vertebral surface extracted by backward tracing the ultrasound image in (b).

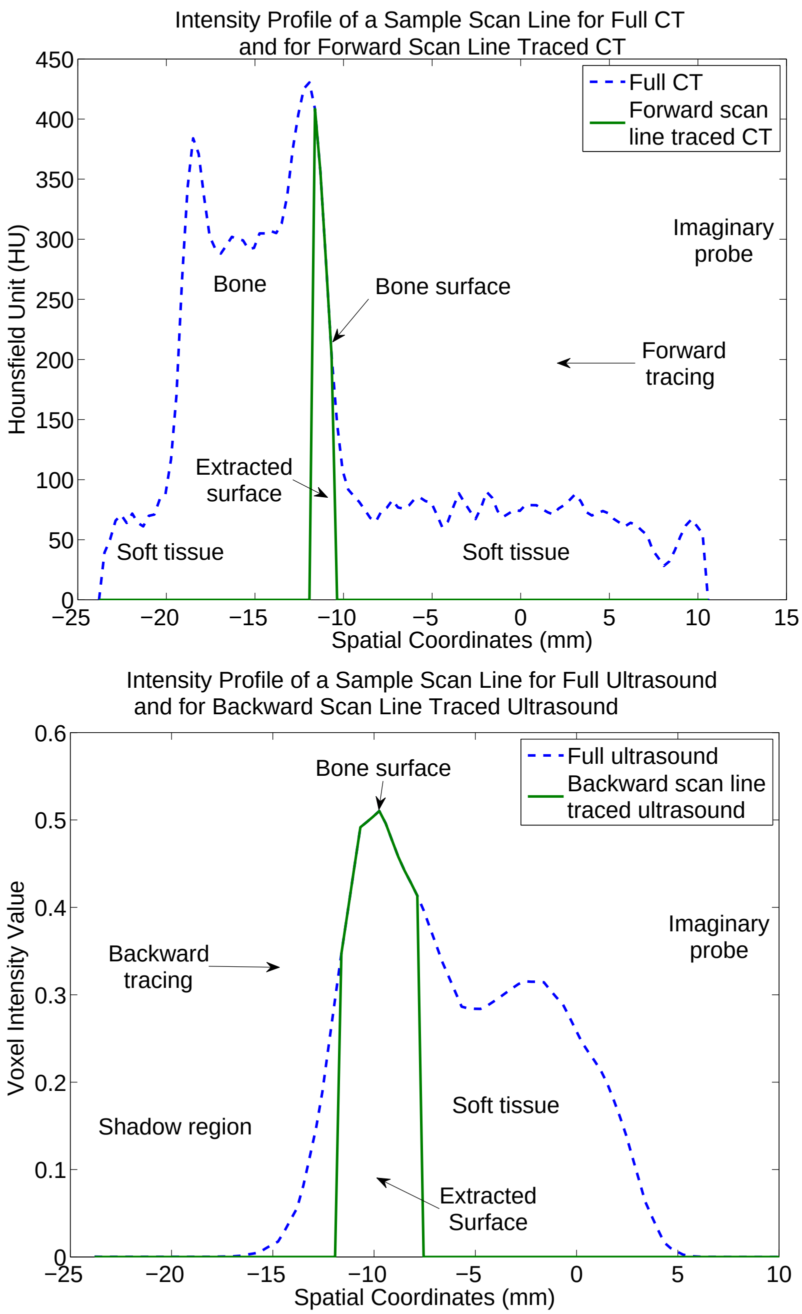

Figure 3–5: Intensity profiles of a sample scan line through a CT (top) and an ultrasound image (bottom). For both plots, the imaginary probe is at the right of the plot (i.e., anatomical posterior). The vertebral bone surface is extracted by forward tracing in CT and by backward tracing in ultrasound.

A multidimensional simplex optimization function is used to maximize the cross correlation between the two extracted surfaces. This optimization strategy can be thought of intuitively as an amoeba that crawls towards the objective function minimum or maximum while contracting and expanding as necessary [147], [148, Ch. 10.4]. The simplex method has been proven to perform very well when the number of parameters to optimize is relatively small (around half a dozen) [149]. Thus, it is a very suitable optimization method for rigid transformation, in which only three translation and three rotation parameters are optimized. Note that, although some images are illustrated in 2D in this article by their sample slices, all registration optimizations are performed in 3D coordinates.

3.3 Validation Experiments

3.3.1 Sawbones Phantom

The accuracy and robustness of the registration technique presented were first assessed through phantom experiments. The lumbosacral phantom (Sawbones Radiopaque Lumbar Phantom 1352-39) has a radiopaque coating that simulates bone response in CT images and a foam cortical shell that simulates bone surfaces (Fig. 3–6a). The L4 vertebral segment was used to assess registration accuracy and robustness. The phantom was imaged using the preoperative CT scanner (Picker International PQ6000) at the Montreal Neurological Institute and Hospital using the spine neurosurgery protocol. Axial slices 2.0 mm in thickness were acquired from anatomical superior to inferior, with an in-slice resolution of 0.35×0.35 mm^2.

The ultrasound acquisition was conducted using a Philips-ATL HDI 5000 system with a multi-frequency phased array probe (4-7 MHz). The probe has an

(a) (b) (c)

Figure 3–6: (a) Lumbosacral phantom used in the experiments (Sawbones Radiopaque Lumbar Phantom 1352-39). (b) Ultrasound imaging of the Sawbones phantom submerged in water. The probe was positioned posterior to the spinous process. (c) Sample axial ultrasound slice of the Sawbones phantom. P: posterior, A: anterior, L: left, R: right.

axial resolution of 0.5 mm, and approximate lateral and elevational resolution (slice thickness) of 1-2 mm (depending on the depth). The probe was tracked in space through four reflective spheres mounted on it. In addition, the probe was calibrated beforehand in water using the Z-bar phantom described in Comeau et al [150]. During the ultrasound imaging experiments, the lumbosacral phantom was fixed on a base and submerged in a container filled with water. For each registration, only the ultrasound images of the current vertebra of interest were acquired intraoperatively, because only a single vertebra were registered at a time. The ultrasound images were acquired with the probe positioned posterior to the spinous process in three different orientations (Fig. 3–6b) to study the registration accuracy of each. In the first set, axial slices of the spine were acquired from anatomical superior to inferior. In the second set, sagittal slices were acquired from one lateral side to the other. The third set had the same orientation as the first set except the probe was positioned to the left of the spinous process so that only one side of the posterior vertebral surface (laminae, articular processes, and spinous process) was imaged. Figure 3–6c shows a sample axial ultrasound slice of the phantom.

3.3.2 Porcine Cadaver

The cadaver validation experiments were performed with the lumbosacral section of a 60-kg porcine cadaver (Fig. 3–7a). Porcine spines are anatomically and functionally similar to human specimens and are frequently used as an alternate model for experiments involving spinal fusion and instrumentation techniques [151]. The porcine cadaver was imaged with CT using the same protocol as for the Sawbones phantom described above. The ultrasound imaging of the porcine cadaver was performed under conditions that simulate open spine surgery using a dorsal approach (equivalent to a posterior approach in humans). A dorsal midline incision was performed, and the soft tissues were retracted laterally to create a surgical cavity (Fig. 3–7b). Surgical irrigation saline (0.9% NaCl) was poured into the cavity to provide a medium for ultrasound imaging (Fig. 3–7c). The ultrasound probe was calibrated beforehand in surgical irrigation saline also using the Z-bar phantom [150]. The same three imaging orientations as in the phantom experiment were acquired, and the different imaging orientations of ultrasound resulted in different bone surfaces being acquired. Figure 3–7d shows a sample sagittal slice of the cadaver vertebra through the saline in the dorsal cavity. Figure 3–7e shows a sample axial slice also through the cavity, but the probe is oriented such that only the left side of the posterior vertebral surface is acquired (the right side is occluded by the shadow caused by the spinous process). Note that, compared with the images of the Sawbones phantom, the images of the surgical cavity contain more signals above the bone surfaces and shadow regions due to the presence of soft tissues (muscle, fascia, and fat) in the cadaver.

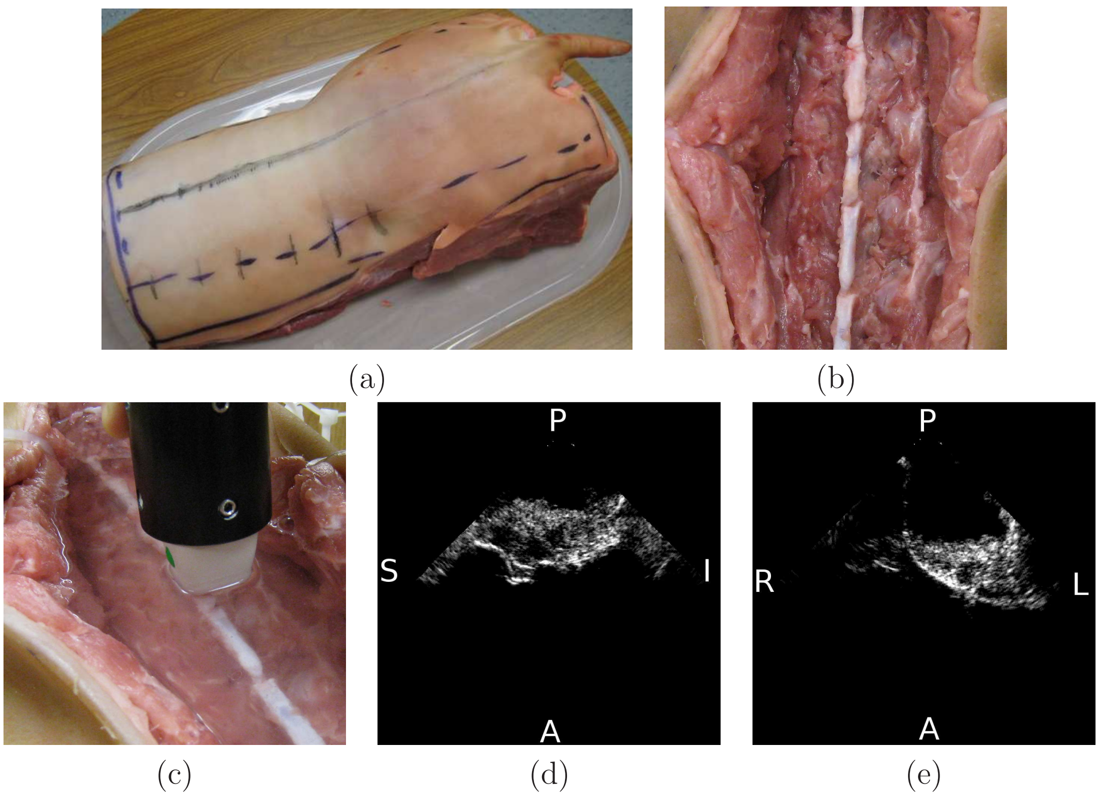

Figure 3–7: (a) The lumbosacral section of the porcine cadaver used for validation experiments. (b) Surgical cavity in the porcine cadaver created by a dorsal midline incision and the retraction of soft tissues. (c) The cavity is filled with surgical saline for ultrasound imaging. (d) Sample sagittal ultrasound slice of porcine dorsal cavity. (e) Sample axial ultrasound slice of porcine dorsal cavity; only the left side was acquired. Soft tissues on the bone surfaces can be seen in the ultrasound images. S: superior, I: inferior, P: posterior, A: anterior, L: left, R: right.

3.3.3 Generation of Gold Standard

Imaging fiducials were installed on both the phantom and the cadaver to enable the computation of gold standard reference registrations to serve as a ground truth. The imaging marker fiducials consisted of steel ball bearings 4 mm in diameter mounted on plastic posts made from pipette tips (Fig. 3–8a). The corresponding reference fiducials are designed such that, when installed on the same fiducial base as an imaging marker, the center of the outward-facing surface of the reference fiducial corresponds to the centroids of the ball bearings of the imaging marker. Four fiducial bases were implanted in the vertebral bodies of the phantom and the cadaver in different orientations (Fig. 3–8c). This configuration allows both the imaging markers and the reference fiducials to be rigidly installed on the vertebrae. In practice, the imaging markers provide the fiducial position in CT image space coordinates (ball bearing centroids), and the reference fiducials provide the fiducial position in world space coordinates (center of outward-facing surface). The imaging fiducials were implanted on the anteriorly located vertebral body so that they do not interfere with ultrasound acquisition, since ultrasound imaging in this experiment is only concerned with the posterior vertebral surfaces (Fig. 3–8c).

The imaging markers were installed on the fiducial bases when the CT images were acquired. The steel ball bearings of the imaging markers showed up as bright spheres on the CT images (Fig. 3–8b), and the centroids of the ball bearings were subsequently computed to obtain the fiducial positions in CT image space coordinates. Prior to imaging the phantom or cadaver with ultrasound, a dynamic

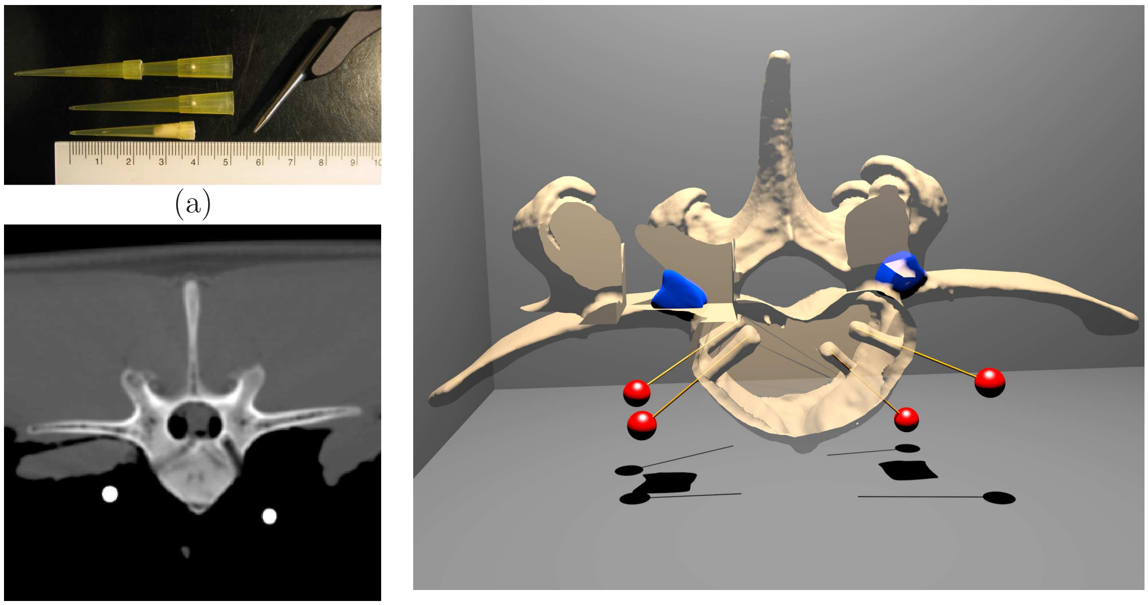

(a) (b) (c)

Figure 3–8: (a) Imaging markers made of steel ball bearings mounted on plastic posts. In the picture, the imaging markers are shown in comparison with a ruler (cm) and the tip of a tracked pointer. The topmost imaging marker is shown to be inserted into a fiducial base, the middle is an imaging marker by itself, and the bottom is a reference fiducial. In practice, the bases are implanted inside the phantom or cadaver, and the imaging markers or reference fiducials are inserted into the bases. (b) The implanted imaging markers appear as bright spheres in CT images. (c) A 3D rendering to show the positions of the imaging fiducials (red) and the surgical volumes of interest (blue) containing the target samples with respect to the vertebra. The vertebra is cut at a cross-section to show the surgical volumes of interest (blue) embedded inside the pedicles. In addition, because the fiducials were implanted on the anteriorly located (image bottom) vertebral body, they do not interfere with ultrasound acquisition of the posterior (image top) vertebral surface.

reference object (DRO) was rigidly attached to the vertebrae to establish a world space coordinate system. Because the DRO is attached to the experimental subjects, they can be moved freely without affecting tracking. The imaging markers were replaced with reference fiducials so that the fiducial positions in world coordinates can be obtained by pointing at the reference fiducials with the tip of a tracked pointer. The corresponding fiducial positions in both CT image coordinates and in world coordinates were paired up to compute the gold standard reference registration using the closed-form solution described in Horn [152]. Over multiple trials, the fiducial registration errors of the gold standard references were determined to be between 0.3 mm and 0.6 mm.

3.4 Registration Results

After the ultrasound acquisitions were completed, the 2D ultrasound slices were reconstructed into 3D volumes with a voxel size of $1 \times 1 \times 1$ mm^3 using a pixel-based method with a 3D kernel around the input pixels [122]. This voxel size was roughly comparable to that of CT volume and at the same time required a reasonable reconstruction time while still allowing good registration accuracy. Each ultrasound volume was then registered to its corresponding CT image using the registration technique described in Methods (Section 3.2). That is, the posterior vertebral bone surfaces were extracted from both the CT and the ultrasound volumes using the forward and backward scan line tracing techniques, respectively (described in Subsection 3.2.2). The extracted surfaces were then registered using the multidimensional simplex optimization (described in Subsection 3.2.3).

3.4.1 Qualitative Assessment of Registration

Some sample images in Fig. 3–9 and 3–10 display the registered surfaces and images (after the corresponding registration transformation was applied to the unprocessed CT and ultrasound images). Visual inspection of the registered images shown below (and many others not shown) gives qualitative confirmation of the accurate registration of the CT and ultrasound vertebral bone images.

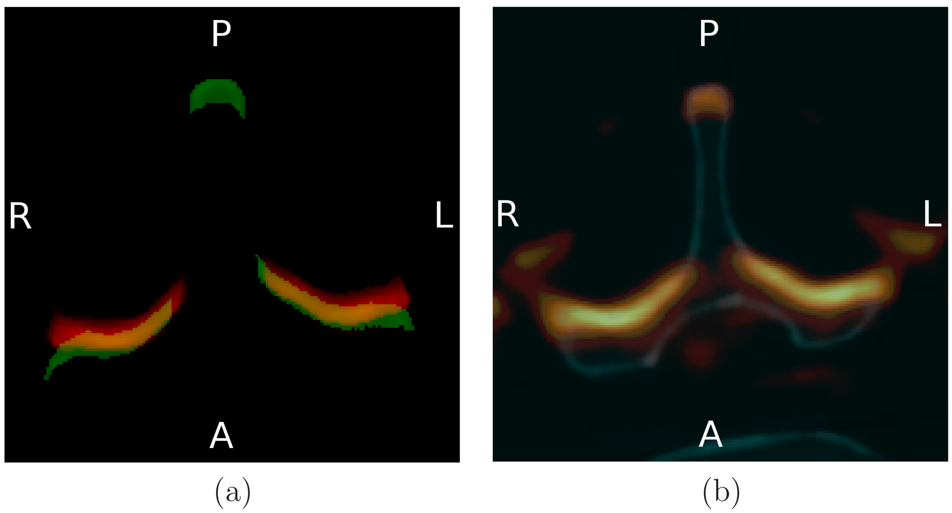

Figure 3–9: A pair of registered phantom images, where the ultrasound is acquired axially, with a superior-to-inferior sweep. (a) The surface extracted from the CT image is in green, and the surface extracted from the ultrasound is in hot metal. (b) The unprocessed CT image is displayed in grayscale, and the ultrasound is overlaid in hot metal. These two images were registered using the transformation obtained from surface registration in (a). P: posterior, A: anterior, L: left, R: right.

3.4.2 Quantitative Assessment of Registration

In addition to a qualitative assessment of the registration results by visual inspection, quantitative evaluations of the registration technique were also performed. To achieve this, the registrations generated by our technique were

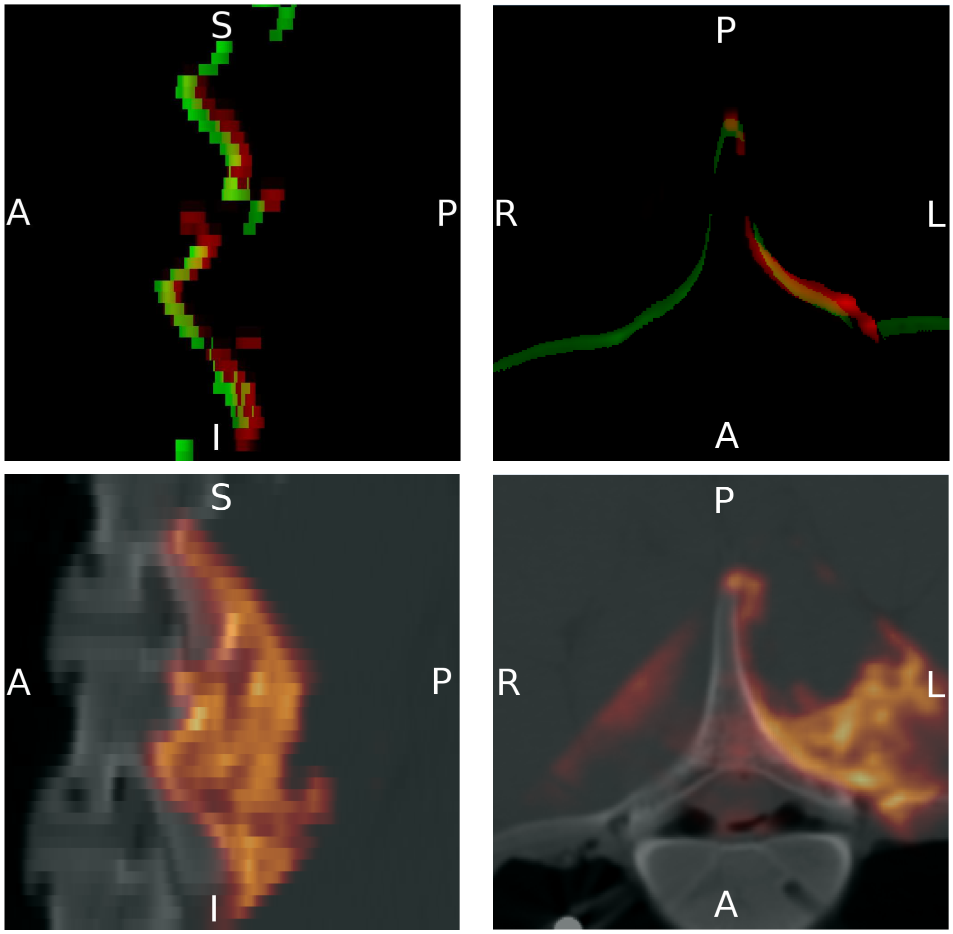

(a) (b)

Figure 3–10: Two pairs of registered cadaver images. In the top row, the surface extracted from the CT image is in green, and the surface extracted from ultrasound is in red. In the bottom row, the unprocessed CT image is displayed in grayscale, and the ultrasound is overlaid in hot metal. (a) The ultrasound was acquired sagittally from one lateral side to the other in the dorsal surgical cavity of the porcine cadaver. (b) The ultrasound was acquired from superior to inferior in the dorsal surgical cavity, but only the left side of posterior vertebral surface was acquired because the probe was positioned to the left of the spinous process, which blocks ultrasound transmission to the right side. S: superior, I: inferior, P: posterior, A: anterior, L: left, R: right.

compared with the gold standard registrations obtained previously through the use of imaging fiducials. The comparison was made by applying registration transformations to a set of sample points, also known as targets because they were sampled within surgical volumes of interest. In our case, these volumes are at the entry points of the pedicle screws, between the superior articular processes and the transverse processes (Fig. 3–8c), and contain approximately 5,000 targets. Each target underwent two transformations, one from the registration generated by our technique and one from the gold standard registration. The error is the distance between the two points transformed from the same target. The root mean square (RMS) value of such distances computed for all targets is defined as the target registration error (TRE) and is used here to describe the registration accuracy quantitatively.

For each dataset in the phantom and cadaver experiments, 1,000 registrations were performed with simulated initial misalignments to reliably determine the accuracy and robustness of our registration technique. Each registration started with a computer generated random initial position that was misaligned from the gold standard registration. The overall random misalignment was derived from three translational misalignments (x, y, and z directions) and three rotational misalignments (x, y, and z axes). Each random translational misalignment was limited to be within 10 mm, and each random rotational misalignment was limited to be within 10°. The overall misalignment was combined from all six component misalignments and its TRE was limited to be less than 20 mm.

3.4.3 Accuracy

The quantitative registration results for both the phantom and the porcine cadaver are shown in Table 3–1. Registration accuracy is determined by the final TRE after the ultrasound and CT images are registered. Registration results are listed for each of the three ultrasound probe orientations in both the phantom and the cadaver experiments (the three orientations were described in Subsection 3.3.1). When evaluated over the 1,000 trials, the median TRE was always under 1 mm for the Sawbones phantom and varied from 0.86 mm to 1.59 mm for the porcine cadaver. Each registration takes two minutes on average to execute.

Comparison of the results revealed that, for all orientations, the porcine cadaver experiments yielded larger final TRE values than the phantom experiments. This result is to be expected, as the ultrasound images of the porcine cadaver are less ideal (but more realistic) than the phantom images. In addition, for both the phantom and cadaver experiments, the registration was more accurate when the ultrasound probe was oriented to include both sides of the vertebra (second row in the table) rather than just the left side (third row in the table). The distribution of registration accuracy results for the porcine cadaver is represented more clearly in the histogram of final TRE values in Fig. 3–11, where the TRE values are tightly clustered under 2 mm for both sagittal and axial orientations, except for single-sided axial acquisition where the TRE distribution extends to higher values.

Table 3–1: Accuracy and robustness assessment of ultrasound-CT registration of both phantom and porcine cadaver vertebrae

Exp. subject	Ultrasound orientation	Ultrasound pathway[a]	Final TRE (RMS, mm) Median	Std	Percent success[b]
Phantom	Sagittal	Lat. to lat.	0.60	0.11	100.0%
	Axial	Sup. to inf.	0.63	0.10	100.0%
	Axial	Sup. to inf. (Left side)	0.94	0.33	99.5%
Porcine cadaver	Sagittal	Lat. to lat.	0.86	0.83	97.3%
	Axial	Sup. to inf.	1.42	0.89	92.6%
	Axial	Sup. to inf. (Left side)	1.59	1.09	66.4%

The data in each row are computed from 1,000 registrations with random starting positions. The random initial misalignments are limited to be less than 20 mm and have a mean of 10.4 mm.

[a] The path followed by the ultrasound probe are superior to inferior, one lateral side to the other, and superior to inferior but left side of the vertebra only.

[b] The percentage of registrations with final TRE below 2.0 mm is the percent success rate.

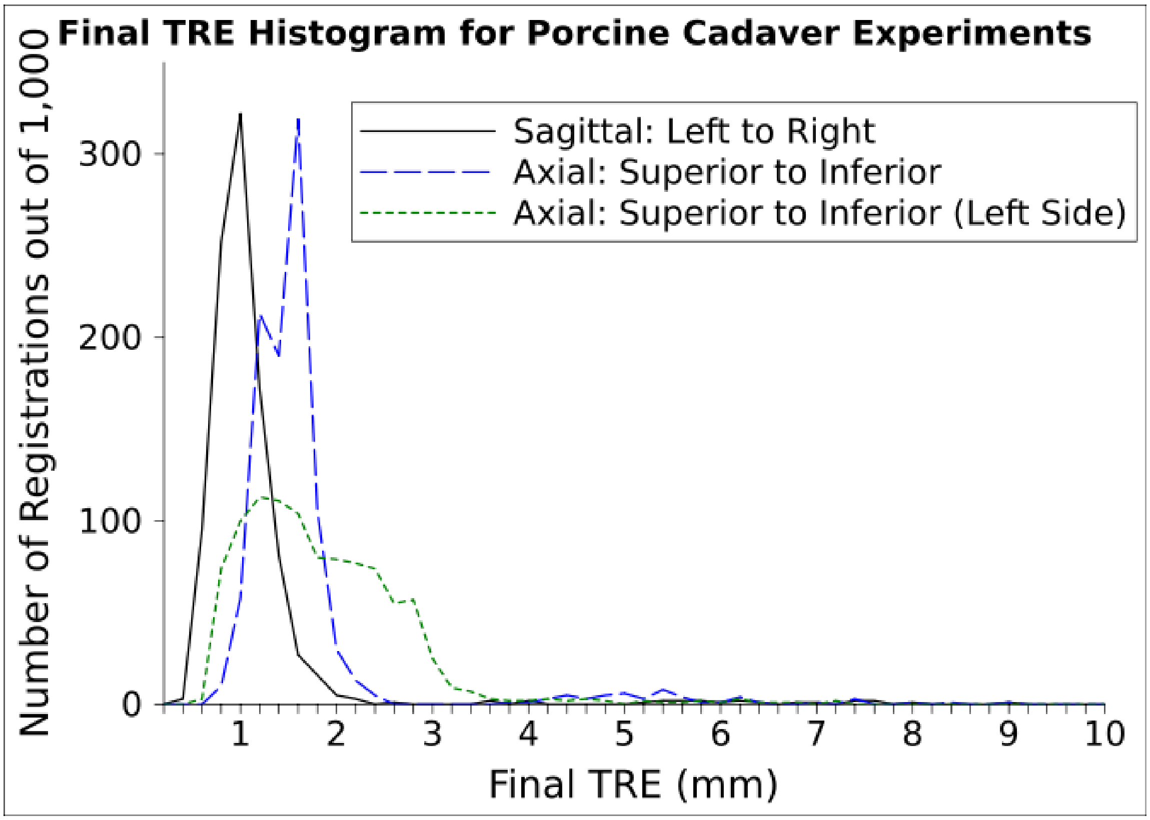

Figure 3–11: Histogram of final TRE values for all porcine cadaver registration experiments.

3.4.4 Robustness

To determine the robustness of the algorithm, a percentage registration success rate was derived. A consensus among experts in the field is that the registration accuracy requirement for spine surgery is 1-2 mm, as Cleary et al [125] stated in the "Final Report of the Technical Requirements for Image-Guided Spine Procedures Workshop." Therefore, any registration that results in a TRE larger than 2 mm is considered a failure when deriving the registration success rate. When evaluated over the 1,000 trials, the success rate on the Sawbones phantom was always greater than 99.5%, indicating near total successful recovery of the gold standard registration (see Table 3–1). For the porcine cadaver, the success rate varied from 92.6% to 97.3% when both sides of the vertebra were imaged. The success rate dropped to 66.4% when only one side of the vertebra was imaged.

3.4.5 Capture Range

Another set of porcine cadaver registration experiments was performed to assess the capture range of the registration technique (see Fig. 3–12). In these experiments, the overall random misalignment was again a combination of three translational misalignment components (x, y, and z directions) and three rotational misalignment components (x, y, and z axes). However, this time, the randomization parameters were chosen such that the TRE of the initial misalignments fell into six 5 mm intervals from 0-5 mm to 25-30 mm. For these intervals, the limits for the translational misalignment components in each direction were respectively (in ascending order) 3 mm, 6 mm, 10 mm, 13 mm, 15 mm, and 20 mm. However, all the random rotational misalignment components were still limited to be within 10° for each axis. Two hundred registrations were performed for each of the six 5 mm intervals and all three orientations, for a total of 3,600 registrations. The percentage registration success rate was evaluated at each interval. The success rate (defined in Subsection 3.4.4) was maintained above 90% for up to 20 mm of initial misalignments for ultrasound acquired in the sagittal orientation and for up to 15 mm for the axial orientation. In both cases, the capture range is wider than any realistic initial misalignments that can be expected in the operating room. However, the success rate is relatively low for single-sided acquisition (left side), as can be expected from its extended final TRE distribution in the histogram shown in Fig. 3–11.

3.5 Discussion

We have presented a technique for registering vertebral ultrasound and CT images for image-guided spine surgeries. The technique does not require manual processing of images during surgery and has been validated using realistic porcine cadaver images with respect to a ground truth established using imaging fiducials. The final target registration errors (TREs) are clustered under 2 mm for registration using ultrasound acquisitions that include both the left and right sides of the vertebra. This accuracy satisfies the accuracy requirement for spine surgery agreed upon by experts in the field [125]. In addition, the registration technique is robust, as it is able to maintain a high registration success rate of above 90% for initial misalignments up to 20 mm and better than 95% for misalignments up to 15 mm.

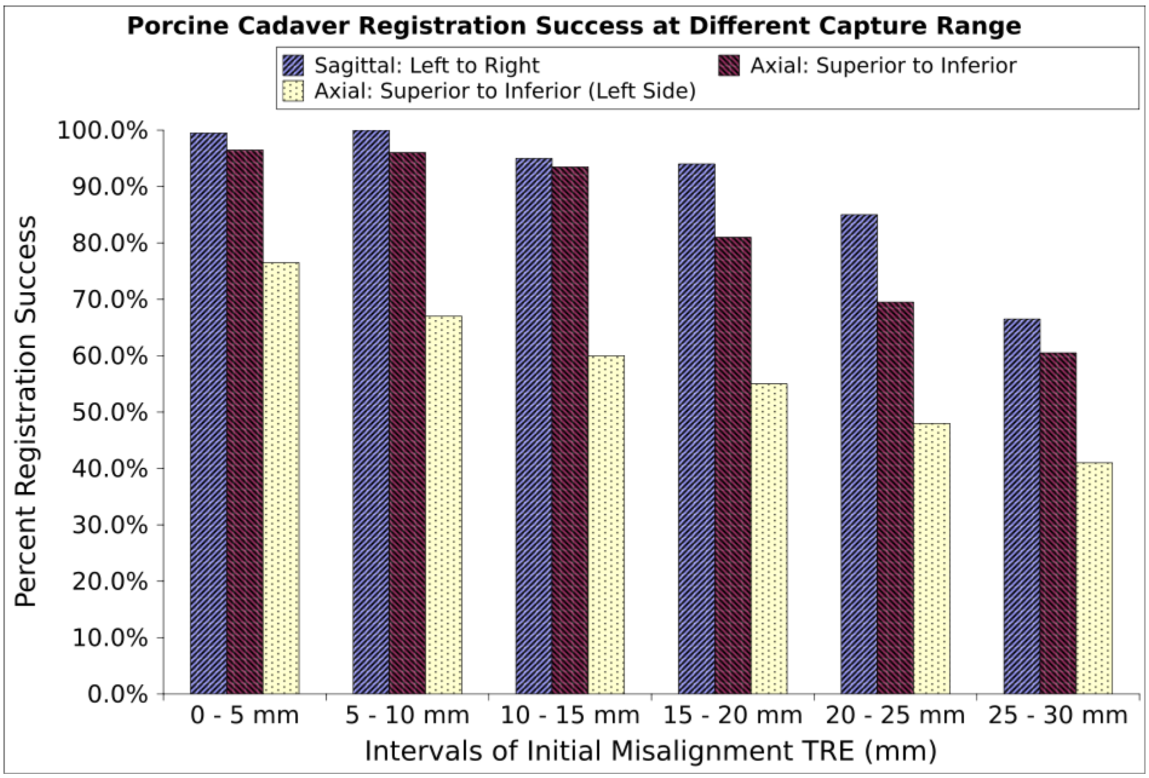

Figure 3–12: The percent registration success rate is plotted for six intervals of initial misalignment TRE for all three ultrasound acquisition orientations.

Not surprisingly, the technique does not perform as well when the ultrasound acquisition only includes one side of the vertebra, in which case it results in higher TREs and a lower registration success rate. Moreover, the registration results are also slightly more robust for ultrasound acquired in the sagittal orientation than in the axial orientation. Both of these observations may be explained by the fact that more of the vertebral surface is acquired in the sagittal orientation than in the other two orientations because of the nature of the phased array probe. This probe has a fan-shaped field of view that cannot cover transverse processes on both sides of the vertebra when imaged in the axial orientation. However, the advantages of using a phased array probe are its higher spatial resolution, which enables the acquisition of high-resolution ultrasound images, and its smaller footprint, which allows it to fit easily through the incision and enables intraoperative acquisition. Therefore, these results indicate that the sagittal orientation would be the preferred acquisition orientation in ultrasound scanning protocols using phased array probes.

Our registration technique using backward scan line tracing can achieve accurate and robust registration by exploiting the shadow regions beneath the bone surface. A drawback of our technique is that a specific intensity threshold needs to be manually determined for each new ultrasound scanning protocol. However, this limitation does not appreciably affect the clinical application because, once determined, the same threshold can be used for all surgeries using the same protocol. Our technique can also be improved by automating the determination of the threshold through an algorithm that analyzes the scan line profiles during the backward trace (e.g., see Hellier et al [145]).

We observed significant differences ($p < 0.001$; non-parametric Kruskal-Wallis ANOVA) when comparing the accuracy and robustness results of the Sawbones phantom experiments with those of the porcine cadaver experiments (Table 3–1). However, this observation does not come as a surprise, as the ultrasound images of the Sawbones phantom are less clinically realistic than those of the porcine cadaver. In fact, because the Sawbones phantom contains no soft tissue on the vertebrae and there is no variation in the speed of sound due to different tissue types, the ultrasound images of the phantom have an intrinsically segmented posterior vertebral surface (see Fig. 3–6c). Using these phantom images, our registration technique was able to achieve submillimeter accuracy and a perfect success rate. (Note however that these phantom images only contained the current vertebra of interest and did not contain any part of neighbouring vertebra, thus preventing the backward scan line tracing from mis-segmenting the posterior vertebral surface.) The registration accuracy and robustness achieved with these good quality phantom images are better or comparable to the results for many other techniques that have been validated using an artificial phantom [e.g., 96, 99, 103, 110, 142, etc.]. Nevertheless, because of their simplistic nature, validation using the phantom data alone is not sufficient to be linked to potential clinical applications.

Winter et al [111, 112] attempted to quantify registration results using clinically relevant patient data, but as described earlier, they did not measure errors with respect to a gold standard reference. Their reference registration is the optimal registration obtained after running through 50 cycles of their registration technique. This means that their obtained error of <1 mm only indicates how consistently their registration technique can arrive at the same optimum rather than how far their optimum is from the actual true position of the vertebrae. However, what really matters to the surgeon, and ultimately to the patient, is not how consistent the algorithm is, but how accurately the navigation system can represent the true position of the instruments with respect to patient anatomy. The advantage of using a porcine cadaver for validation is that it enables the implantation of imaging fiducials in the subject (without ethical issues) while still allowing the acquisition of clinically realistic images. The target registration errors we measured not only include the variability of the registration technique itself, but also other errors in the pipeline of the system, including optical tracking errors, ultrasound calibration errors (which include the errors caused by variation in the speed of sound), and errors in generating the fiducial-based gold standard itself. Therefore, our validation experiments reflect the true accuracy that can be expected in the operating room using our tracking system and our registration technique.

In Cleary et al [125], experts in the field of image-guided spine surgery recommended that for open back spinal fusion surgeries, the execution time of the image registration algorithm should be 5 minutes or less. In our case, our mean execution time is 2 minutes, which meets this recommendation. It should be noted that there are currently other ultrasound-CT registration techniques that have faster execution time than ours. However, our registration time is reasonable for our intended application, because it is only performed once before operating on each vertebra and not intended to be performed continuously during the intervention as for procedures performed under endoscopic guidance.

3.6 Conclusions

We have developed a registration technique for vertebrae that satisfies many practical considerations for application to actual surgeries. The technique is automated, accurate, and robust. It has been thoroughly validated using a fiducial-based gold standard and clinically realistic porcine cadaver images, and the results reflect the true accuracy and robustness that can be expected in surgical conditions. However, this development is only a first step towards an accurate, robust, and practical registration technique that can be used to guide spine surgeries in the operating room. Questions regarding the surgical outcome of our registration technique still need to be answered through more experiments on cadavers. These experiments would consist of performing spinal fusion surgeries on cadavers using our registration technique and analyzing the surgical outcome by performing postoperative imaging and dissection. Once the registration technique is proven safe through surgical outcome studies on cadavers, it can be moved to real patients for extensive clinical testing.

3.7 Addendum

This section has been added to this chapter following the oral defense to clarify certain issues raised during the defense. These clarifications were not incorporated into the main sections of this chapter to preserve its original published form.

Ultrasound reconstruction

In this chapter, a registration technique has been described for registering a three-dimensional (3D) ultrasound image volume to a 3D CT image volume. It was mentioned that a pixel-based method has been used to reconstruct the 2D ultrasound image slices into a 3D image volume. However, the details of the reconstruction were not presented. The following is a more detailed description of the reconstruction algorithm used for this thesis. For a more thorough review of the different techniques of reconstruction, the interested readers are referred to Solberg et al [122].

A 3D ultrasound volume can be obtained either directly with a 3D volumetric ultrasound scanner or indirectly through the reconstruction of 2D ultrasound image slices. In this thesis, the focus was on the use of 2D ultrasound images for registration. For reconstruction, the relative spatial positions of the ultrasound image slices were used to accurately position the slices with respect to each other. These positions could be obtained without any additional procedure because the ultrasound images were already tracked in space for the purpose of surgical navigation.

A pixel-based method was used for the reconstruction of ultrasound images into a volume. The method used was unique in that it performed the reconstruction in one step, as opposed to the more traditional two-step techniques (a distribution step and a hole-filling step). The method first assigned the value of each input pixel of the 2D ultrasound image to its corresponding 3D voxel. Then, it determined a 3D neighbourhood around each pixel within a certain radius (in this case, a radius of 2 mm). All voxels within this neighbourhood were assigned a weighted-value of the pixel, where the weight was calculated using a distance-dependent 3D Gaussian distribution. The end result of this reconstruction method is a 3D ultrasound image volume that is a weighted average of the ultrasound pixels and their neighbouring voxels.

Predefined parameters

There were several predefined parameters used in the registration experiments, namely, the threshold values for the forward tracing of CT images and the backward tracing of ultrasound images, and the trajectory of the imaginary probe in the extraction of the bone surfaces. Although the threshold for backward tracing was briefly discussed in this chapter, a more comprehensive discussion of these parameters is provided below.

The threshold value of 150 Hounsfield unit (HU) was used for the forward scan line tracing of CT images. The choice for this value, although arbitrary, does have a rationale related to the density of the tissues. As was shown by the voxel intensity profile of CT images in Fig. 3–5a, the soft tissues have density below 100 HU, whereas the bone tissues have density well above 250 HU. Therefore, the threshold value of 150 HU was able to effectively capture the tissue-bone interface when the scan-line was traced forward from the soft-tissue to the bone. Similarly, the threshold of 20% of maximum intensity value was chosen for backward scan line tracing based on the manual analysis of the intensity profile near the bone-tissue interface in the ultrasound images.

The manual determination of these threshold values does represent a drawback of the current technique, because it requires more frequent analysis and recalculation of threshold values by the surgical navigation engineer. Since the determination of these threshold values depends on the manual analysis of images acquired at particular image settings, the values would need to be recalculated when the navigation imaging protocol changes. Therefore, the current registration technique would benefit from the automation of threshold value determination in the future.

Another predefined parameter was that the bone surface extraction algorithm assumed a fixed trajectory of the imaginary ultrasound probe. The assumed trajectory consisted of the probe traversing from the superior end of the vertebra to its inferior end, directly posterior to the spinous process. For the axial sweep pattern, the real probe trajectory conforms to this assumed trajectory. However, for other sweep patterns, the real probe trajectories would be different from the assumed trajectory. Nevertheless, as will be shown in Chapter 4, the other sweep patterns result in registration accuracies that are similar to the axial sweep patterns, thus demonstrating that the registration technique was in general unaffected when the real probe trajectory deviates from the assumed trajectory.

In addition, the orthogonal sweep pattern was found to yield the best registration result. Therefore, a future improvement to the technique could be to consistently use the orthogonal sweep pattern for both the real ultrasound sweeps and the imaginary sweeps.

CHAPTER 4
Validation of Ultrasound-CT Registration of Vertebrae

Foreword

We presented in the previous chapter a new technique for registering ultrasound and CT images of vertebrae and demonstrated the technique's feasibility through preliminary experiments on a plastic phantom and a single vertebra of a porcine cadaver. However, the images of the plastic phantom cannot realistically represent the imaging subject in the clinical settings. Furthermore, images of a single vertebral level are unable to provide convincing evidence that the technique can be extended to other levels of the vertebral column. Therefore, the main focus of this chapter is to provide a more extensive cadaveric validation of the registration technique. We imaged and registered 18 thoracic and lumbar vertebrae of 3 porcine cadavers. Each vertebra was imaged by ultrasound in 10 different sweep patterns. We found that the registration technique could accurately register all vertebrae, with varying accuracies across sweep patterns and vertebral levels. The orthogonal-sweep pattern performed the best and yielded a median registration error of 1.65 mm for all vertebrae. The previously described method for generating the gold standard registrations has also been validated and was found to have an accuracy of 0.718 mm.

The Introduction (Section 4.1) has already been described in Chapter 2 and the reader may choose to skip this section without missing information. This chapter has been published in the *International Journal of Computer Assisted Radiology and Surgery* [153].

Validation of Automated Ultrasound-CT Registration of Vertebrae

C. X. B. Yan, B. Goulet, S. J.-S. Chen, D. Tampieri, D. L. Collins

Int J Comput Assist Radiol Surg, 7(4):601-610, 2012

Abstract

Purpose: Image-guided spine surgery requires registration of the patient anatomy and preoperative computed tomography (CT) images. A technique for intraoperative ultrasound image registration to preoperative CT scans was developed and tested. Validation of the ultrasound-CT registration technique was performed using porcine cadavers.

Methods: An ultrasound-CT registration technique was evaluated using 18 thoracic and lumbar vertebrae of 3 porcine cadavers with 10 different sweep patterns for ultrasound acquisition. For each sweep pattern at each vertebra, 100 randomly simulated initial misalignments were introduced. Each misalignment was registered. The resulting registration transformations were compared to gold standard registrations based on implanted fiducials to assess accuracy and robustness of the technique.

Results: The orthogonal sweep acquisition was found to perform best and yielded a registration accuracy of 1.65 mm across all vertebrae on all porcine cadavers, where 82.5% of the registrations resulted in target registration errors below the 2 mm threshold recommended by a joint report from the experts in the field. In addition, we found that registration accuracy varies by the sweep pattern

and vertebral level, but neighboring vertebrae tend to result in statistically similar accuracy. Ultrasound-CT registration took an average of 2.5 min to run and the total registration time per vertebra (also including time for ultrasound acquisition and reconstruction) is approximately 8 min.

Conclusions: A previously described ultrasound-CT registration technique yields clinically acceptable accuracy and robustness on multiple vertebrae across multiple porcine cadavers. The total registration time is shorter than that of surface-point-based manual registration.

4.1 Introduction

Spinal fusion surgeries are commonly performed to treat vertebral instabilities resulting from disc degeneration, trauma, and congential deformities [5]. One critical step of these surgeries is to implant screws into the pedicles of the vertebrae as part of the entire instrumentation. Because this step requires high accuracy, image-guided surgery (IGS) system can now be used to help guide this procedure. The virtual IGS images enable the surgeon to accurately visualize the spatial relationships between surgical tools and the surgical targets that are not directly visible due to occlusion by other structures of the patient's anatomy. This "X-ray"-like vision helps to significantly lower surgical risks and postoperative complications [127]. However, for the preoperative image-based IGS systems to achieve these improved clinical outcomes, an accurate registration between the patient anatomy and the preoperative images is crucial. Unfortunately, this step currently relies on a time-consuming manual landmark identification procedure in most IGS systems that leaves many surgeons wondering if the benefit is worth the added surgical time.

Intraoperative ultrasound has been considered a flexible and safe method of acquiring patient anatomy during surgery in a non-invasive manner. The patient anatomy acquired by a tracked ultrasound can be aligned to the preoperative CT image to achieve the registration between the patient and the image. Many have investigated the use of ultrasound-CT registration for orthopedic IGS applications, such as for femurs [93, 101, 113, 136, 137], pelvis [88, 100–102, 114, 120, 136, 138–141], or vertebrae [95, 96, 99, 103, 109–112, 117, 118, 139, 142, 143]. We have previously developed an ultrasound-CT registration technique for spine IGS systems (see Yan et al [126] or Chapter 3). This technique achieves registration by aligning the posterior vertebral surfaces extracted from both ultrasound and CT images. The technique was validated on a single vertebra (L4) of both a plastic phantom and a porcine cadaver and demonstrated good accuracy and robustness.

Although the preliminary results of our registration technique were promising, we wanted to extend the validation beyond a single vertebral level and a single subject. In this article, we present the results of applying our registration technique to all lumbar vertebrae and one thoracic vertebra of three porcine cadavers. The main goal is to find out whether the technique can be applied on vertebral levels beyond L4 and beyond a single porcine cadaver, as was done previously in our preliminary validation in Chapter 3. In addition, we also try to address three minor questions. They are: (1) whether the registration accuracy is affected by the different ultrasound sweep patterns; (2) whether the accuracy is different from one vertebral level to another; and (3) how reliable are the gold standard registrations and the simulated initial misalignments in our validation process.

4.2 Methods

4.2.1 Preparation of Porcine Cadavers

The lumbosacral sections of three 60-kg porcine cadavers were used in the registration experiments. Porcine cadavers were chosen for validation because their thoracolumbar vertebrae are anatomically similar to those of humans. They differ from human vertebrae in that they have larger transverse processes, shorter spinous processes, taller and narrower vertebral bodies, and larger pedicles. By matching the implant size to adapt to these differences, porcine cadavers are frequently used as alternatives to human specimens for experiments involving spinal fusion surgeries and instrumentation techniques [151]. They also have the additional benefit of involving fewer ethical issues than experimenting on patients when extensive instrumentation on the vertebrae is required. In addition, as it is relatively easy to procure fresh porcine cadavers, the porcine cadavers used in this study did not undergo any preservative fixation or freezing. Each fresh porcine cadaver was maintained in good condition by refrigeration at 4 °C between experiments for a total duration of three to four days, and brought to room temperature during both CT and ultrasound imaging. In the first porcine cadaver, lumbar vertebrae L3 to L6 were present in the specimen, in the second and third porcine cadavers, vertebrae T15 and L1 to L6 were present.

4.2.2 Coordinate Systems

The end goal of our technique is to register two coordinate spaces together, namely, the world space of the patient and the CT image space. These two spatial terms are used throughout this article and are described here for clarity. A more complete description of the system is in Chapter 3. The *world space* (also known as the *patient space*) is defined as the camera-tracked coordinate system relative to a dynamic reference object (DRO) mounted on the patient. The world space is the coordinate system for the patient anatomy. On the other hand, the *CT image space* is the local coordinate system within the preoperative CT image.

4.2.3 CT Imaging

Imaging fiducial markers were implanted on each vertebra before the experiments started to help generate the gold standard registration (more details are presented in Subsection 4.2.6). All three porcine cadavers were imaged using a CT scanner (Picker International PQ6000) at the Montreal Neurological Institute and Hospital using the preoperative spine neurosurgery protocol. The cadavers were placed in supine position and the field of view included the entire lumbosacral section. Axial slices were acquired from anatomical superior to inferior and had an in-slice resolution of 0.35×0.35 mm^2 with a slice thickness of 2.0 mm. Figure 4–1 shows part of a sample axial CT slice of the porcine cadaver.

4.2.4 Setup for Ultrasound Imaging

Each porcine cadaver was rigidly fixated to an aluminum frame before ultrasound imaging began (Fig. 4–2a). This allows the dynamic reference object (DRO) to be rigidly fixed with respect to all vertebrae, so that a world space

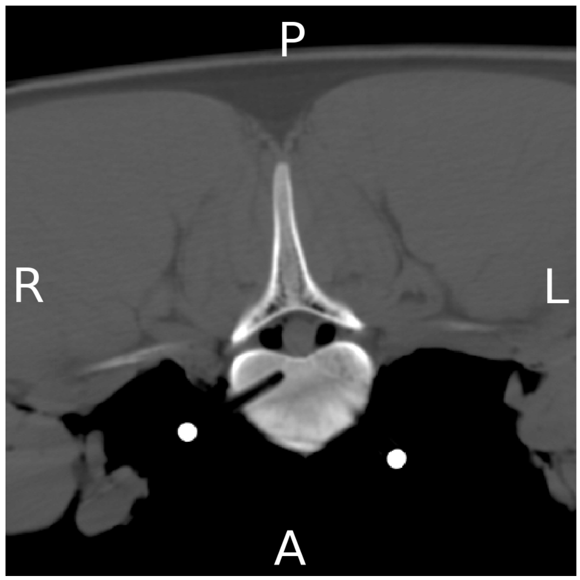

Figure 4–1: Part of a sample axial CT slice of a porcine cadaver at the level of L2. (The CT slice was cropped to the center to better illustrate the vertebra and the imaging fiducials.) The two bright spheres ventral to the vertebra are imaging fiducial markers fixed to the vertebra (note the fiducials are shown in Fig. 4–5). *P* posterior/dorsal, *A* anterior/ventral, *L* left, *R* right.

coordinate system can be established for all vertebrae. A surgical cavity similar to those in open back surgery with posterior approach was created through a dorsal midline incision and lateral retraction of soft tissues. Surgical irrigation saline (0.9% NaCl) was poured into the surgical cavity to provide a medium for ultrasound imaging (Fig. 4–2b). The ultrasound probe was calibrated beforehand in surgical saline using the Z-bar phantom described in Comeau et al [150]. In addition, the world space coordinates of all imaging fiducials on each vertebra were acquired before the ultrasound imaging of the vertebra (more detail in Subsection 4.2.6).

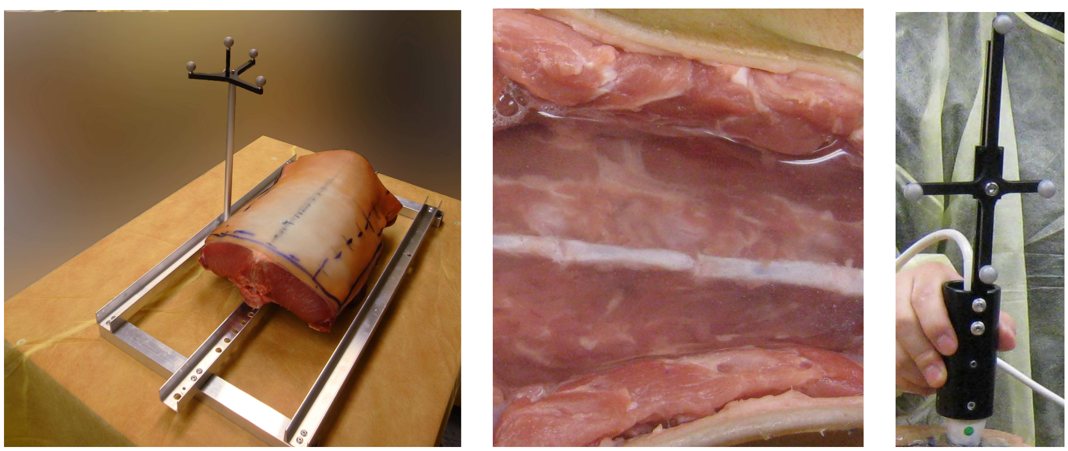

(a) (b) (c)

Figure 4–2: (a) Porcine cadaver is rigidly fixated to the dynamic reference object through an alumninum frame. (b) The surgical cavity of the porcine cadaver is filled with 0.9% NaCl irrigation saline to provide a medium for ultrasound imaging. (c) Four reflective spheres are mounted rigidly on the ultrasound probe to enable the probe to be tracked in the world space.

4.2.5 Ultrasound Imaging

The ultrasound images of the vertebrae were acquired through the irrigation saline inside the surgical cavity when the porcine cadavers were placed in a prone position. The ultrasound scanner was a Philips-ATL HDI 5000 system with a multi-frequency phased array probe (4-7 MHz) and it was part of the IGS system developed at the Image Processing Laboratory (IPL) of Montreal Neurological Institute [20]. The IGS system also included a Polaris infrared camera for tracking, a Linux-based computer, and the IBIS software system for managing all image-guidance related tasks (see Mercier et al [20]). The ultrasound probe was tracked in space through four reflective spheres mounted rigidly on the probe (see Fig. 4–2c). Each ultrasound sweep was limited to only the current vertebra being registered. The tracking and acquisition of ultrasound slices are managed by the IBIS software system.

For each of the three porcine cadavers, nine different single-sweep ultrasound acquisitions and one double orthogonal-sweep acquisition were performed. The details of all ultrasound sweep patterns are listed in Table 4–1 and the single sweeps are shown in Fig. 4–3 using human anatomical conventions. The orthogonal-sweep acquisition includes two sweeps that are perpendicular to each other. It consists of both a centered axial sweep from the superior to the inferior side of the vertebra (same as sweep 1) and a sagittal sweep from the left to the right side of the vertebra (same as sweep 4). Figure 4–4 shows a sample ultrasound slice from a sagittal sweep at the level of L4.

Table 4–1: Ultrasound sweep patterns of the registration experiments

Ultrasound sweeps	Slice orientation[a]	Probe position[a]	Probe orientation[a]	Sweep direction[a]
1	Axial	$\sim$ 3 cm P to ASP	Parallel to N	S to I
2	Axial	$\sim$ 3 cm P and $\sim$ 1 cm L to ASP	Parallel to N	S to I
3	Axial	$\sim$ 3 cm P and $\sim$ 1 cm R to ASP	Parallel to N	S to I
4	Sagittal	$\sim$ 3 cm P to ASP	Parallel to N	L to R
5	Sagittal	$\sim$ 3 cm P to ASP	Parallel to N	R to L
6	Diagonal (I,L to S,R)	$\sim$ 3 cm P to ASP	Parallel to N	L to R
7	Diagonal (I,R to S,L)	$\sim$ 3 cm P to ASP	Parallel to N	L to R
8	Axial	$\sim$ 3 cm P and $\sim$ 1 cm L to ASP	30° L to N	S to I
9	Axial	$\sim$ 3 cm P and $\sim$ 1 cm R to ASP	30° R to N	S to I
Orthogonal-sweep	Axial and sagittal	$\sim$ 3 cm P to ASP	Parallel to N	S to I & L to R

[a] Abbreviations: ASP = apex of spinous process, P = posterior, L = left, R = right, S = superior, I = inferior, N = normal vector of the coronal plane

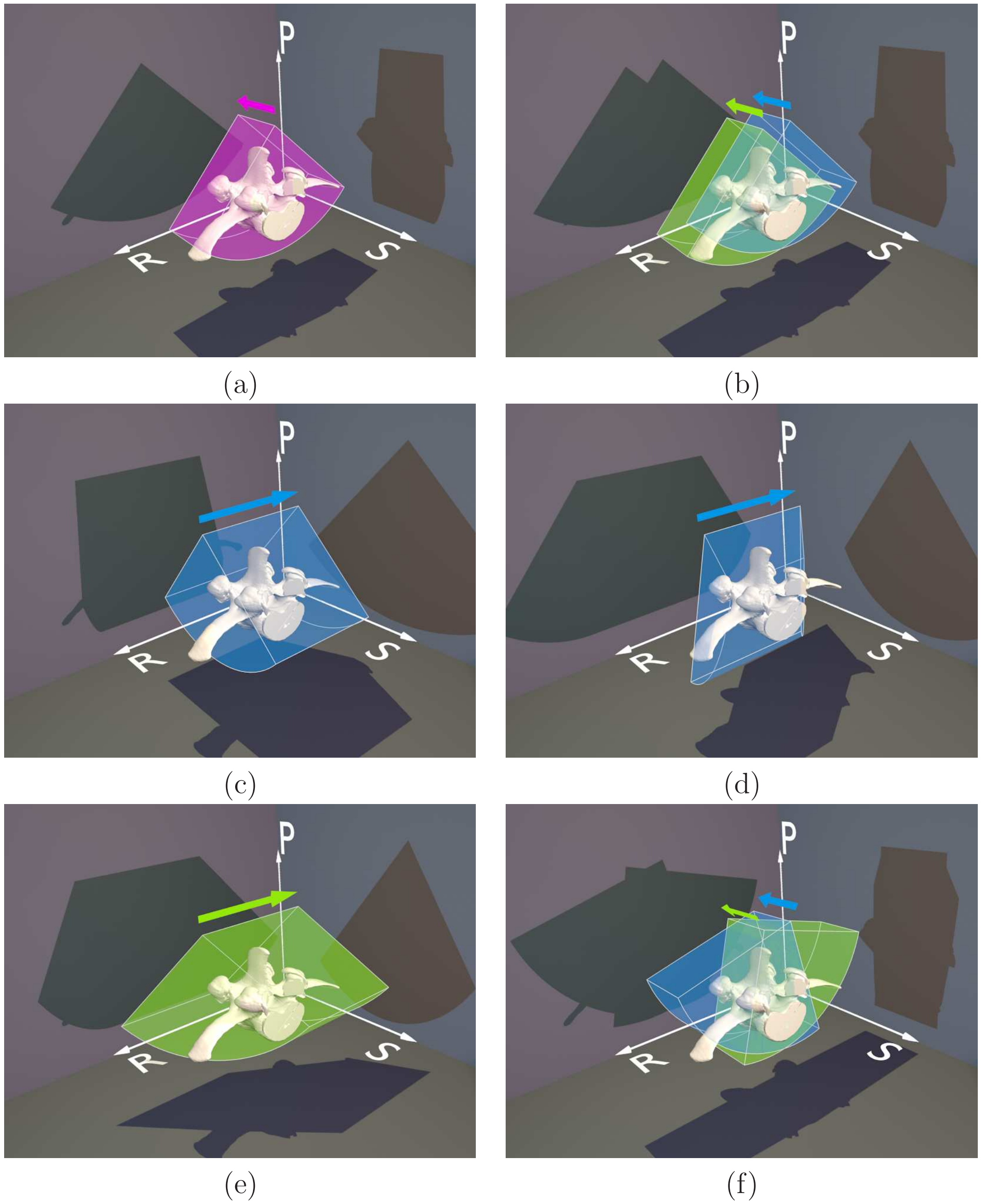

Figure 4–3: Illustrations of the ultrasound single sweep patterns: (a) sweep 1; (b) sweep 2 (blue) and sweep 3 (green); (c) sweep 4 (note sweep 5 is the same as 4 except in opposite sweep direction); (d) sweep 6; (e) sweep 7; (f) sweep 8 (blue) and sweep 9 (green). P = posterior, R = right, S = superior.

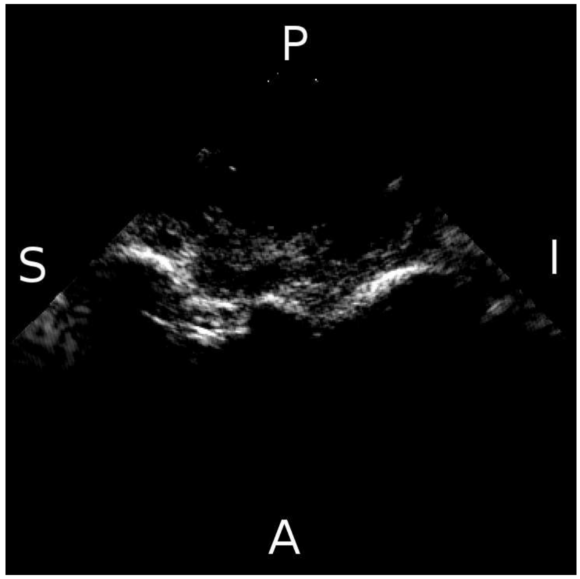

Figure 4–4: Sample ultrasound slice from a sagittal sweep at the level of L4. P posterior/dorsal, A anterior/ventral, S superior, I inferior.

4.2.6 Generation of Gold Standard

A set of four imaging fiducials were installed on each vertebra to generate the gold standard registration. Note that these fiducials are only installed for the sole purpose of generating gold standard registration and are thus not part of the clinical practice of spine IGS. The elements of imaging fiducials are made from pipette tips. Each fiducial consists of three elements: a fiducial base, an imaging marker, and a reference fiducial (Fig. 4–5a). Four fiducial bases were rigidly implanted inside the vertebral body of each vertebra, so that the imaging markers and reference posts could be inserted firmly into the base when needed. The bases are oriented anteriorly/ventrally so as to not interfere with the ultrasound acquisition posteriorly. The imaging markers contain steel ball bearings that show up as bright spheres on CT images (Fig. 4–1). The centroids of these ball bearings are the actual fiducial position. The markers are installed on the porcine cadaver before CT imaging. Finally, the reference fiducials are designed such that the center of their outward facing surface corresponds to the actual fiducial position when installed on the same base as the imaging marker providing the fiducial position. Therefore, before the ultrasound imaging of each vertebra, the reference fiducials are installed on the vertebra being imaged, and the fiducial positions are acquired in world space coordinates by pointing a tracked pointer's tip to the fiducial positions on the reference posts (Fig. 4–5b).

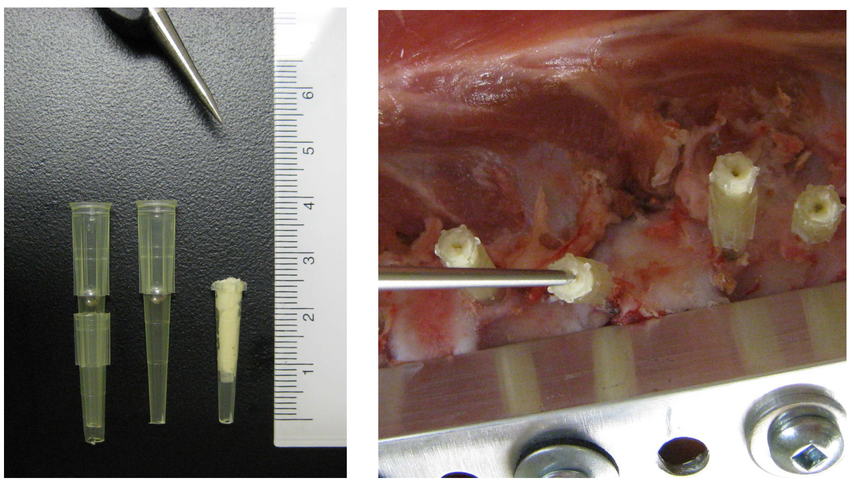

(a) (b)

Figure 4–5: (a) The imaging fiducial marker has three elements: an imaging marker (middle), a reference fiducial (right) and a fiducial base (left, imaging marker inserted into the base). (b) The tracked pointer's tip touches the fiducial position on the reference fiducial to acquire the world space coordinates of the fiducial position.

The registration obtained from our ultrasound-CT registration technique is a transformation from the world space (i.e., patient anatomy space) to the CT image space. Therefore, the gold standard registration that serves as the ground truth for assessing our technique's registration results also need to be a transformation from world space to CT image space. Such a gold standard registration is generated by pairing up the world space coordinates of each imaging fiducial to its corresponding CT image space coordinates. In this way, four pairs of corresponding point coordinates are obtained, one for each imaging fiducial installed on the vertebra. These pairs of point coordinates are input into Horn's algorithm [152], which is a closed-form solution (instead of iterative) that generates the best-fit transformation between the two coordinate systems to which the pairs of points belong to. This method computes one world space to CT image space transformation per vertebra, generated solely from the imaging fiducials installed on that vertebra. Such a gold standard registration is completely independent from our image registration technique, and hence serves as good ground truth to which registration results can be assessed.

4.2.7 Ultrasound-CT Registration Technique

The ultrasound-CT registration of vertebrae is accomplished by using our previously published ultrasound-CT registration technique (see Yan et al [126] or Chapter 3). In this technique, the ultrasound and CT images undergo a preprocessing step before the actual registration optimization. The preprocessing for the CT image is forward scan line tracing. In this step, an imaginary probe projects scan lines, which form a fan-shaped sector that approximates the cross-section in a phased-array probe. When the imaginary scan lines travel away from the imaginary probe to arrive at the vertebral bone surface in the CT image, the surface is extracted from the image. In this way, the forward scan line tracing technique exploits the large intensity difference between the soft tissues and the bone. On the other hand, the preprocessing of the ultrasound image is backward scan line tracing. This method is similar to forward scan line tracing, but instead of projecting away from the imaginary probe, the scan lines travel toward the imaginary probe. When these backward-traveling scan lines reach the vertebral bone surface in the ultrasound image, the surface is extracted. The backward scan line tracing technique exploits both the acoustic shadow created by the bone and the large intensity difference between soft tissues and bone. After preprocessing, these two extracted vertebral surfaces (one from CT, one from ultrasound) are aligned together by optimizing the cross-correlation between the intensity of the corresponding voxels in both surfaces. This technique has been validated on the L4 vertebra of both a plastic Sawbones phantom and a porcine cadaver. It achieved a registration accuracy with TRE below 1 mm on the phantom and below 2 mm on the porcine cadaver. (For more details, see Yan et al [126] or Chapter 3.) In this article, we present more extensive validation experiments that applies this registration technique with different ultrasound sweep patterns on multiple levels of the lumbar vertebrae and across three different porcine cadavers.

4.3 Registration Results

4.3.1 Validation of Gold Standard Registration

An experiment was performed to measure the precision and accuracy of the gold standard registrations so as to assess their reliability as ground truth. In this experiment, the process of generating gold standard registration was repeated 50 times using the imaging fiducials installed on a vertebra. More specifically, the world space coordinates of the imaging fiducials were acquired 50 times. Every time, the world coordinates of the set of four imaging fiducials were paired to their corresponding CT image coordinates, input into Horn's algorithm [152], and a gold standard registration was generated. Each gold standard registration has an associated fiducial registration error (FRE), which is the root mean square of the distances between the paired points after the best-fit transformation has been applied. By describing statistically the FREs of all 50 gold standard registrations, we can assess the precision of the process of generating gold standard registrations. In this experiment, the 50 FREs have a median of 0.452 mm and an interquartile range (IQR) of 0.122 mm. To assess the accuracy of each gold standard registration, we also measure its associated target registration error (TRE) instead of its FRE. The TRE also computes a root mean square of error distances between paired points after the registration transformation has been applied, but instead of using the imaging fiducials, the TRE uses sample targets that are independent of the fiducials that were used to generate the gold standard registration in the first place. In this case, 20 anatomical landmarks of the vertebra were selected as the independent target samples. The 50 TREs have a median of 0.718 mm and an IQR of 0.462 mm.

4.3.2 Registration Experiments

For every ultrasound sweep (n=10) at each vertebral level (n=18), the registration robustness was assessed with 100 runs, using a simulated new misalignment as the starting position of each run, for a total of 18,000 registration runs. The initial misalignments were simulated by generating randomly (with Gaussian distribution) three translationnal misalignments (x, y, and z directions) and three rotational misalignments (x, y, and z axes), and then applying these misalignments to the gold standard registration. Each resulting overall initial misalignment served as the starting transformation for each run of registration. The translational misalignments were limited to be within 10 mm in each direction, and the rotational misalignments were limited to be within 10° with respect to each axis. The overall target registration error (TRE) of the initial misalignment was limited to be less than 20 mm.

The accuracy of the registration results are assessed by computing the target registration error (TRE). The TRE is obtained by first transforming a set of sample points at the surgical target of interest (the pedicle screw entry points) by both the gold standard registration and by the automated registration and then computing the root mean square distance between the corresponding transformed sample points. This is the same assessement protocol as that used previously in Yan et al [126].

4.3.3 Effect of Ultrasound Sweep Pattern on Registration

The registration results are listed by ultrasound sweep pattern number in Table 4–2. In this case, because the distribution of TRE data is non-parametric, the multi-sample test used is the Kruskal-Wallis test (non-parametric equivalent of ANOVA) and the two sample test used is the Mann-Whitney U-test (a.k.a. Wilcoxon rank-sum test, the non-parametric equivalent of T-test). Application of the Kruskal-Wallis test reveals that the registration accuracy is different for different ultrasound sweeps ($p < 0.001$). The paired Mann-Whitney U-test confirms this finding for different sweep patterns. In addition, the U-test reveals that the orthogonal-sweep acquisition yields more accurate registration than any of the single-sweep acquisitions ($p < 0.001$, see Table 4–2).

Table 4–2: Final TRE (mm) of registration experiments for all vertebrae and all three porcine cadavers by sweep patterns

Ultrasound sweeps	axial 1	axial 2	axial 3	sagittal 4	sagittal 5	diagonal 6	diagonal 7	axial 8	axial 9	ortho
Median (mm)	1.93	2.31	1.93	2.13	2.00	2.10	2.20	2.20	1.90	1.65
IQR[a] (mm)	0.72	1.17	1.38	0.88	0.90	1.31	0.72	1.60	1.02	0.47
Diff. from ortho-sweep[b]	*	*	*	*	*	*	*	*	*	N/A

[a] IQR: interquartile range

[b] This shows the statistical significance of the difference between the TRE median of each single-sweep acquisition and that of the orthogonal-sweep acquisition. * = $p < 0.001$

4.3.4 Effect of Vertebral Level on Registration

The final TREs of the single-sweep and the orthogonal-sweep acquisitions are also examined per vertebral level in Table 4–3. Again, at each vertebral level, the orthogonal-sweep acquisitions still result in more accurate registration than the single-sweep ones. In addition, the difference of the final TREs between the vertebral levels was investigated using the orthogonal-sweep acquisitions. First, the Kruskal-Wallis test showed significant difference of the final TREs at different vertebral levels. However, detailed analysis by performing the Mann-Whitney U-test on pairs of vertebral levels reveals similarity between the TREs of several levels. The following pairs showed statistically insignificant difference in TRE (using the threshold of 0.001 for p value): (T15, L1), (T15, L2), (T15, L5), (L2, L4), (L2, L5), (L4, L5), (L5, L6). Finally, the final TREs of the orthogonal-sweep acquisition are plotted by vertebral level in Fig. 4–6. It can be seen that the registration accuracy tends to be similar for neighbouring vertebral levels (with L3 being the exception possibly due to variation of gold standard registration).

Table 4–3: Final TRE (mm) of registration experiments on all three porcine cadavers by vertebral level

Level	All single-sweeps		Orthogonal-sweep		P value
	median	IQR[a]	median	IQR[a]	
T15	2.18	1.28	1.52	0.39	< 0.001
L1	2.04	1.25	1.39	0.30	< 0.001
L2	2.06	0.62	1.60	0.26	< 0.001
L3	2.36	0.97	1.86	0.34	< 0.001
L4	1.90	0.65	1.63	0.25	< 0.001
L5	1.83	1.16	1.55	0.69	< 0.001
L6	2.31	1.50	1.78	0.43	< 0.001

[a] IQR: interquartile range

4.3.5 Robustness

Figure 4–7 shows a high density scatter plot of the final TRE of registration experiments using the orthogonal-sweep acquisition for all vertebrae. Note that the randomization of the initial misalignment follows a Gaussian distribution, as was described in Subsection 4.3.2. It can be seen from the plot that the majority (82.7%) of all the registration runs have final TRE below the 2 mm threshold, which is the accuracy requirement recommended for spine surgery by experts in the field [125]. If 3 mm is used as a threshold to identify outliers, only

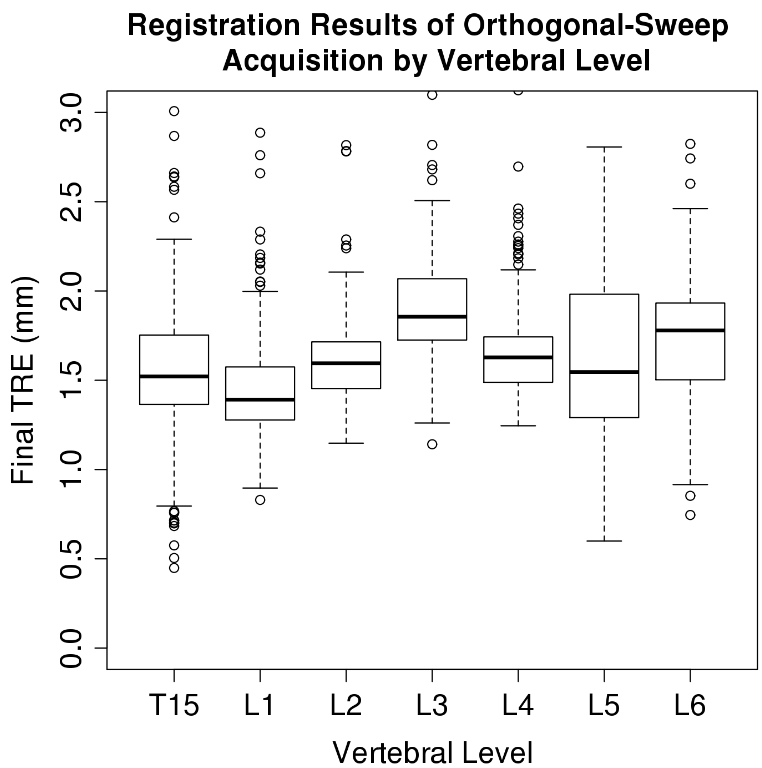

Figure 4–6: Boxplot of the final TRE by vertebral level for ultrasound-CT registration using the orthogonal-sweep acquistion.

5.7% of the total registration runs result in final TRE above this threshold. In addition, the registration accuracy stays relatively constant regardless of the initial misalignment, as shown by the linear fit through the final TREs. The linear fit is nearly horizontal with respect to increasing initial misalignment.

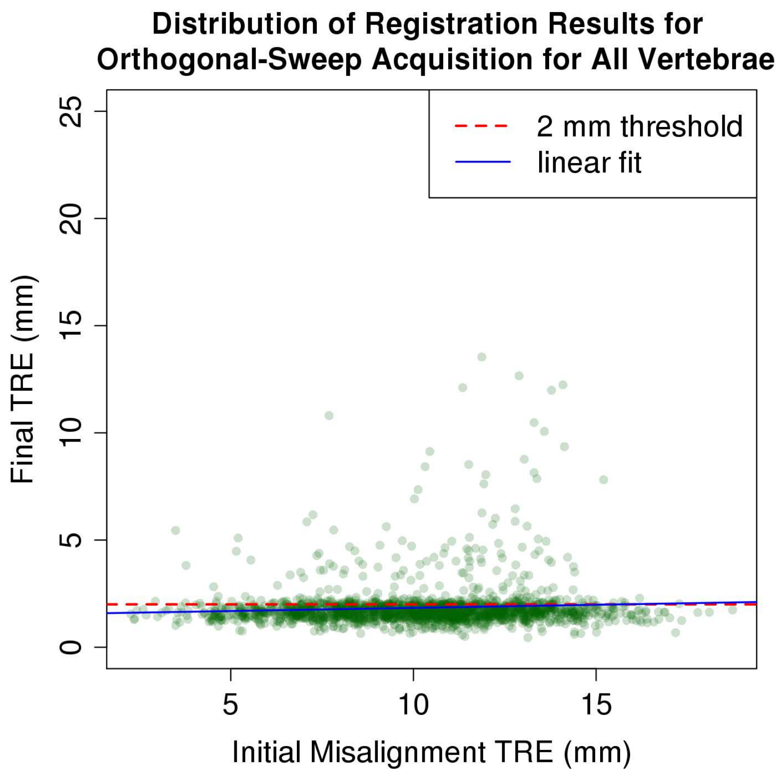

Figure 4–7: High density scatter plot of the final TRE of registration experiments using the orthogonal-sweep acquisition for all vertebrae and all porcine cadavers.

4.3.6 Validation of Initial Misalignment Simulation

A single landmark-based manual registration was performed on each vertebra of porcine cadaver 3 as examples of realistic initial misalignment. The ultrasound-CT registration technique was then applied on the images using these initial misalignments as the starting position to arrive at a final registration. The results are listed in Table 4–4. Note that the TREs of the initial misalignment from landmark registration are much less than the TRE limit (20 mm) used in the simulation of initial misalignment. In addition, both the individual translational and rotational components are also less than the limits of the simulation (10 mm and 10° respectively). The ultrasound-CT registration technique was able to achieve good final TRE values when starting from these landmark-based manual registrations. These results show that the simulated initial misalignments used in our validation experiments are as large or even larger than the realistic landmark registration based initial misalignments. Therefore, the simulated initial misalignments are sufficiently reliable to validate our registration technique.

Table 4–4: Example of realistic initial misalignments using landmark based registration

		T15	L1	L2	L3	L4	L5	L6
Landmark registration translational misalignment (mm)	X	0.42	-1.05	-0.71	-0.36	0.21	1.37	-1.35
	Y	-0.75	-0.10	-1.51	-0.68	-1.05	-1.97	-1.66
	Z	2.65	1.82	2.80	4.53	4.85	5.55	5.49
Landmark registration rotational misalignment (°)	X	-8.14	-8.95	-8.69	-8.10	-6.94	-6.18	-9.38
	Y	1.96	1.53	0.10	-0.22	0.72	0.99	-2.05
	Z	1.37	-3.34	1.79	-0.07	0.91	-1.21	1.51
Landmark registration **initial** misalignment TRE (mm)		3.05	3.80	3.25	5.52	5.92	6.70	7.10
Ultrasound-CT registration **final** TRE (mm)		**1.40**	**1.37**	**1.24**	**1.84**	**1.51**	**1.98**	**1.88**

4.4 Discussion

The main goal of the registration experiments presented here is to validate more extensively the ultrasound-CT registration technique previously developed in Chapter 3 [126]. In the previous results (Chapter 3), application of the registration technique on a single vertebra (L4) of one porcine cadaver resulted in TRE medians of 0.86-1.59 mm for different ultrasound sweeps. In the current experiments, conducted across multiple vertebrae and multiple subjects, the TRE medians are 1.65-2.31 mm for different sweeps and hence are larger than what was obtained previously from a single vertebra on a single subject ($p < 0.001$). This difference can partly be explained by the larger number of vertebrae and subjects involved. Indeed, the TRE ranges obtained in the current experiments are more representative of the true accuracy of the registration technique, because many more vertebral levels and subjects were used in the validation process.

The registration accuracy obtained in our experiments is better or comparable to that of other similar studies [100, 101, 114, 118, 138]. These are studies where the ultrasound-CT registration technique is applied for orthopedic surgery (not for soft tissue registration), is validated on cadavers, and the validation is with respect to a gold standard ground truth, which is generated with fiducials independent of the image registration technique. It is worth noting, however, that the TRE values only represent a combination of ultrasound calibration error and the inherent error of the registration technique, but do not consider the inaccuracy of the ground truth itself. In our experiments, we measured that the gold standard generation process itself varies with an error of 0.718 mm. In fact, this consideration should probably be taken into account in any validation study based on gold standard ground truth.

Analysis of the registration results by ultrasound sweep patterns revealed that the registration accuracy varies by the type of sweep employed. Notably, the orthogonal-sweep acquisition, which is a combination of two perpendicular sweep directions, results in better registration accuracy than the single-sweep acquisitions ($p < 0.001$). The accuracy and robustness of the registration using the orthogonal-sweep acquisition have also been shown to meet the requirements for spine IGS proposed by Cleary et al [125], as Fig. 4–7 demonstrates that the majority (82.7%) of the final TRE are below the 2 mm threshold regardless of the initial misalignment. In addition, Subsection 4.3.4 revealed that the registration accuracy varies by vertebral level. However, the same analysis indicates that although vertebrae far away from each other may result in different registration accuracy, neighbouring vertebrae tend to have statistically similar accuracy. The larger IQR of level L5 compared to the other vertebral levels is more likely due to a variability of the process of generating the gold standard rather than anatomical differences between L5 and the other levels.

One of the goals of performing ultrasound-CT registration is to reduce the surgical time by eliminating the time-consuming manual registration based on mapping vertebral surface points, which takes 10 to 15 min of intraoperative time per vertebra in a spinal fusion surgery using IGS [7, 131]. In our current registration procedure for each vertebra, the ultrasound acquisition typically takes 20-30 sec. It is followed by the reconstruction of ultrasound slices into an image volume, taking 5 min per vertebra on average on a 2 GHz linux-based system. At the same time as the reconstruction, a landmark-based manual registration is performed to obtain a starting position (initial misalignment) and typically takes 2 min. Following the completion of the reconstruction, the execution of our ultrasound-CT registration technique takes 2.5 min on average on the same processor. All these steps combined bring the total registration time to be 8 min per vertebra for the ultrasound-based spine IGS system, which is less than the 10-15 min taken by the surface-point-based manual registration. We are also working on optimizing the different steps of our registration technique to bring the total registration time to under 1 min in the future. One such optimization is the implementation of the slices-to-volume registration, which would eliminate the step of ultrasound reconstruction and save approximately 5 minutes. A second optimization may be to implement the registration on a graphic processing unit, thus reducing the remaining 3 minutes by a factor of 5 to 10.

4.5 Conclusions

We have validated our automated ultrasound-CT registration technique across three porcine cadavers for a total of 18 vertebrae, using fiducial-generated gold standard registrations as ground truth. We found that both the generation of gold standard and the simulation of initial misalignments are reliable for the current validation experiments. The validation results demonstrate that both the accuracy and the robustness of the registration technique satisfy the need of spinal fusion surgeries. In addition, we also found that the registration accuracy varies by the sweep pattern and the vertebral level, but neighbouring vertebrae tend to have statistically similar accuracy. The total registration time per vertebra is approximately 8 min, which needs to be reduced in the future by optimizing the different steps of the entire registration procedure. The registration technique would also need to be validated on human cadavers before applying it on patients.

CHAPTER 5
Ultrasound-CT Registration of Vertebrae without Reconstruction

Foreword

The ultrasound-CT registration technique presented previously has been extensively validated across multiple levels and cadaveric subjects. However, although the current technique is faster than the manual registration, it is still relatively time-intensive by requiring a total registration time of 8 min per vertebra. The most time consuming component of the current technique is to reconstruct ultrasound slices into a volume before the registration itself. Therefore, in this chapter, we introduce a modification to the existing technique by eliminating the step of reconstruction. This was achieved by directly registering a group of ultrasound slices to a single CT image volume. This slices-to-volume registration technique reduced the total registration time down to 4 min per vertebra. In addition, we also demonstrated that a trade-off between registration accuracy and registration speed could be established by changing the number of ultrasound slices used in each registration. The slices-to-volume registration also yields better accuracy because any data loss from the pixel interpolation during reconstruction is eliminated. Finally, the flexibility of the technique enables future improvement through more sophisticated slice selection strategy or the parallelization of computation on a group of image slices. This chapter has been published in the *International Journal of Computer Assisted Radiology and Surgery* [154].

Ultrasound-CT Registration of Vertebrae Without Reconstruction

C. X. B. Yan, B. Goulet, D. Tampieri, D. L. Collins

Int J Comput Assist Radiol Surg, 7(6):901-909, 2012

Abstract

Purpose: While robust and accurate, our previously developed volume-to-volume ultrasound-CT registration of vertebrae required that the 2D ultrasound slices be reconstructed into a 3D volume, a time-consuming step that increased the total registration time per vertebra. We have modified our registration technique to a slices-to-volume strategy to eliminate the ultrasound reconstruction step in order to make the total registration time more practical intraoperatively.

Methods: The slices-to-volume registration is achieved by performing backward scan line tracing on individual ultrasound slices as they are acquired, and then registering them as a group to the posterior vertebral surface extracted from the pre-operative CT image. The technique is validated using a lumbosacral Sawbones phantom and the lumbosacral section of three porcine cadavers.

Results: The slices-to-volume registration reduced the total registration time per vertebra from 8 min to 4 min. The registration accuracy and robustness of the slices-to-volume registration were found to be equal or superior to those of our previous volume-to-volume registration. In addition, a trade-off was found between registration accuracy and registration speed by changing the number of ultrasound slices used in the registration.

Conclusions: The slices-to-volume ultrasound-CT registration significantly reduces the total registration time per vertebra, making this automated technique more practical intraoperatively.

5.1 Introduction

In recent years, image-guided surgery (IGS) systems have been adopted to guide many surgeons in performing spinal fusion surgeries [127]. The IGS systems enable the surgeons to visualize both the surgical instruments and the patient anatomy together on the same screen, with the positions and orientations that reflect their true spatial relationship in real world. When the surgical targets cannot be seen directly with the naked eye, the surgeons are instead guided by what is displayed on the screen of the IGS system when operating. This technique increases the accuracy of the screw implantation in spine surgeries, leading to lower rate of complications and better postoperative function [16–18]. However, for the IGS systems to achieve these outcomes, an accurate spatial registration between the patient anatomy and preoperative image is essential. This registration has traditionally been performed manually through a time-consuming process of identifying anatomical landmarks and mapping out the posterior surface of the vertebrae [26]. This adds an additional 10-15 minutes of surgical time per vertebra, discouraging many from adopting IGS for spinal fusion surgeries.

The time-consuming manual registration has led to the introduction of tracked intraoperative ultrasound in IGS systems as a means to acquire patient bony anatomy in a non-invasive and automated manner. The ultrasound images can then be aligned to the preoperative CT images to achieve registration for femurs [94, 101, 114, 136, 137], pelvis [100–102, 114, 120, 136, 138–141, 155], or vertebrae [95, 96, 99, 103, 107, 109–112, 117, 118, 139, 142, 156]. We have previously developed an ultrasound-CT registration technique for spine IGS (Chapter 3 [126] and validated it on multiple porcine cadavers (Chapter 4 [153]), demonstrating good accuracy and robustness. The technique was able to reduce the total registration time down to 8 min per vertebra (instead of 10-15 min per vertebra in manual registration), while making the registration process more automated, accurate and robust. However, from a practical standpoint, a total registration time of 8 min per vertebra still takes too much intraoperative time and requires further reduction.

In this study, we introduce a slices-to-volume registration strategy that is a modification based on our existing ultrasound-CT volume-to-volume registration technique. Inspired by the work of Brooks et al [124], the slices-to-volume registration enables ultrasound slices to be directly registered to the CT volume without the need to be reconstructed first. This strategy yields better registration accuracy than a high-resolution ultrasound volume because any blurring or data loss that occurs as a result of pixel interpolation in the reconstruction step are eliminated. There is also no need to specify the resolution and griding of the ultrasound volume in advance. In addition, total registration time is further reduced by eliminating the time-consuming step of reconstructing an ultrasound volume with high resolution and accuracy. Finally, because the slices-to-volume registration enables us to become selective with which ultrasound slices to use, a minor goal of this study is to investigate whether it is possible to further reduce the execution time of the ultrasound-CT registration algorithm itself by using a smaller number of slices.

5.2 Methods

5.2.1 Imaging Subjects

The slices-to-volume registration technique was validated using the same ultrasound and CT images of the Sawbones phantom and the porcine cadavers as those previously acquired in Chapter 3 and 4 [126, 153]. By using the same input images as the previous experiments, the slices-to-volume registration technique can be directly compared to the original volume-to-volume registration technique. The Sawbones phantom is a radiopaque lumbosacral phantom (Sawbones Radiopaque Lumbar Phantom 1352-39) that simulates bone response to X-ray penetration, and it also has a foam cortical shell that simulates bone surfaces (Fig. 5–1a). Images were acquired for a single lumbar vertebra L4 of the Sawbones phantom for the experiments below. Additional data from the lumbosacral sections of three 60-kg porcine cadavers were also used for experiments (Fig. 5–1b). The image acquisition included lumbar vertebrae L3 to L6 of the first porcine cadaver, and T15 to L6 of the second and third porcine cadavers, totaling 18 vertebrae.

5.2.2 Coordinate Systems

The slices-to-volume registration technique involves the registration between two coordinate spaces, the *world space* and the *CT image space*. The *world space* is the physical space containing the patient and the surgical instruments. It is a space tracked by the optical camera (Polaris, Northern Digital Inc., Ontario, Canada). The camera is mounted on a stand 2-3 meters high and directed towards

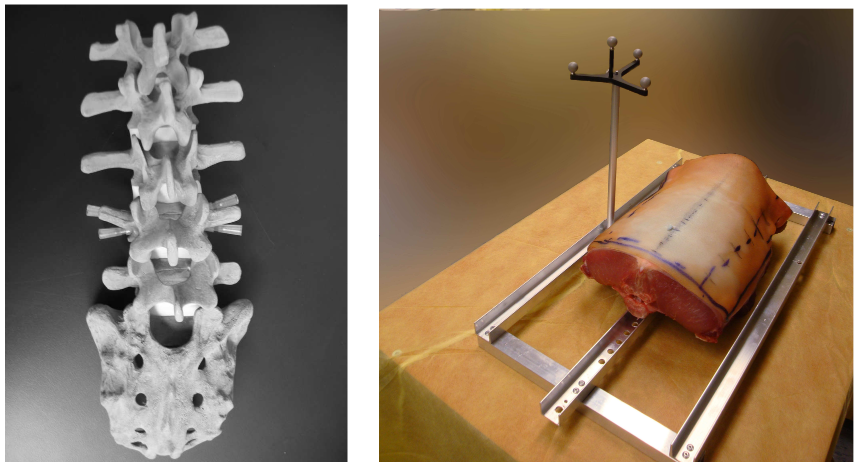

(a) (b)

Figure 5–1: (a) Sawbones Radiopaque Lumbar Phantom 1352-39 (b) The lumbosacral section of the porcine cadaver is rigidly fixed to the dynamic reference object (DRO, black object with four grey reflective spheres) through an aluminum frame.

the patient such that the camera's field of view is centered to the site of surgery. A dynamic reference object (DRO, an object with a reflective sphere at the extremity of each of its four arms for tracking) is mounted on the patient and its position and orientation are tracked by the camera. The *world space* is defined by using the position of the DRO as the origin of the coordinate system and by using the orientation of the DRO to define the axes of the coordinate system. With the *world space* defined, the position and the orientation of both the patient anatomy and the surgical instruments are described in the world space coordinates. When tracked ultrasound image slices are acquired from the patient, they are stored in world space coordinates. On the other hand, the *CT image space* is the local coordinate system within the preoperative CT image. The goal of the registration technique is to find an accurate transformation between the *world* *space* and the *CT image space* so that the patient and the surgical instruments in the real physical world can be aligned with the preoperative CT image. Such a transformation is obtained by registering the ultrasound images (in *world space*) to the CT image (in *CT image space*). A more complete description of such an IGS system is presented in Chapter 3 [126] for the interested readers.

5.2.3 Image Acquisitions

Both the Sawbones phantom and the porcine cadavers were imaged by the CT scanner (Picker International PQ6000) at the Montreal Neurological Institute and Hospital using the standard clinical preoperative spine neurosurgery protocol. The field of view was made wide enough to include all of the imaging subjects in their entirety. The imaging subjects were scanned from superior to inferior in axial slices with resolution of 0.35×0.35 mm^2 and slice thickness of 2.0 mm.

The same ultrasound scanner and settings were also used for both the Sawbones phantom and the porcine cadavers. The ultrasound scanner was a Philips-ATL HDI 5000 system with a multi-frequency phased array probe (4-7 MHz). The probe was tracked in space through four reflective spheres mounted on it (Fig. 5–2a) and it was calibrated to the world space coordinates for both the water medium and the surgical saline medium. When imaging the Sawbones phantom, the phantom was fixed on a base and immersed in a water-filled container, with the DRO fixed on the vertebra immediately superior to the current vertebra being scanned. For the imaging of the porcine cadavers, each cadaver was rigidly fixed on an aluminum frame that has a DRO installed on it (Fig. 5–1b). Then, a surgical cavity similar to that in an open-back surgery is created by incision and retraction. The skin, fat, fascia, muscles and ligaments were dissected and retracted away, as is done in open-back human surgery at our institution. Surgical saline is poured into the cavity to provide a medium for ultrasound imaging (Fig. 5–2b). For each vertebra, the orthogonal sweep acquisition was employed (Fig. 5–3), as it has been previously shown to be the best acquisition sweep (Chapter 4 [153]). A single vertebra is imaged and registered at a time.

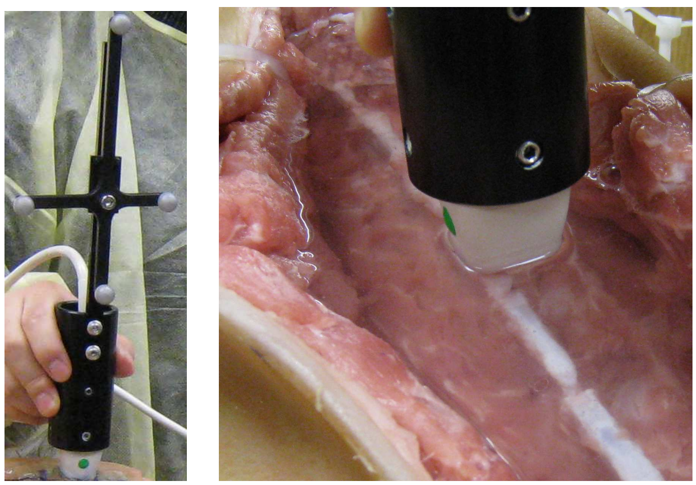

(a) (b)

Figure 5–2: (a) Ultrasound probe with four reflective spheres mounted for tracking purpose (b) Imaging the porcine cadaver through posterior/dorsal cavity filled with normal saline.

5.2.4 CT Image Preprocessing

The CT imaging of the patient is done preoperatively, and thus it can also be preprocessed for registration before the actual surgery to save intraoperative time. In the slices-to-volume registration, the CT image of the vertebrae is processed such that the posterior vertebral surface is extracted by forward scan line tracing

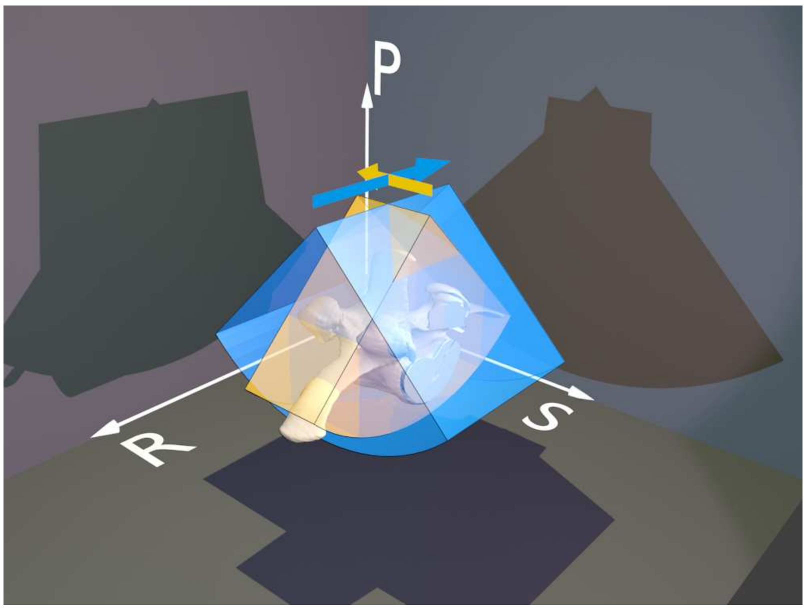

Figure 5–3: The orthogonal sweep consists of an axial sweep from superior to inferior (orange arrow) and a sagittal sweep from right to left (blue arrow). P: posterior, S: superior, R: right.

(see Chapter 3 [126]). In forward scan line tracing, an imaginary ultrasound probe projects scan lines that form a fan-shaped sector similar to the cross-section in a phased-array probe. The imaginary probe sweeps through the vertebrae in the CT image from superior to inferior (cranial-caudal for porcine cadaver) with axially-oriented slices. When the scan lines arrive at the vertebral bone surface, the surface is extracted based on the large intensity difference between the soft tissue and the bone. The preprocessed CT image is thus the posterior vertebral surface of the lumbosacral section.

5.2.5 Slices-to-Volume Registration

The main differences between slices-to-volume and volume-to-volume registration are in the steps of ultrasound image reconstruction, backward scan line tracing and registration lattice sampling. In volume-to-volume registration, the 2D ultrasound image slices first need to be reconstructed into a 3D volume. In our previous works, the ultrasound reconstruction used a pixel-based method [122] with a 3D kernel applied around each pixels of the ultrasound slices, filling the "holes" in between the ultrasound slices. The reconstruction time takes on average 5 min on a 2 GHz Linux-based system. Following reconstruction, the ultrasound volume undergoes backward scan line tracing to extract the posterior vertebral surface. The backward scan line tracing is similar to the forward scan line tracing described above (Subsection 5.2.4), with scan lines projecting from an imaginary probe in a fan-shaped sector. However, the difference is that in backward scan line tracing, the tracing does not start from the imaginary probe towards the posterior vertebral surface. Instead, the starting points are at the far ends of the scan lines and then they trace back towards the imaginary probe. When they encounter the posterior vertebral surface on their way, this surface is extracted. This exploits the acoustic shadow created by the bone surface in the ultrasound images. When the posterior vertebral surfaces are extracted from both the CT and ultrasound images, they are registered together by cross-correlation of intensity values using the optimization function:

$$\phi_{opt} = \arg\max_{\phi}[\mathbf{C}(CT, \mathbf{T}(US, \phi))] \tag{5.1}$$

where CT and US are the image volumes containing the posterior vertebral surfaces, $\mathbf{T}(US, \phi))$ is the rigid transformation that is applied to the ultrasound volume using the set of transformation parameters ϕ, and $\mathbf{C}$ is the intensity cross-correlation function defined as:

$$\mathbf{C}(CT, US) = \frac{\sum(CT(x_i) \cdot US(x_i))}{\sqrt{\sum CT(x_i)^2} \cdot \sqrt{\sum US(x_i)^2}} \tag{5.2}$$

where $CT(x_i)$ and $US(x_i)$ are respectively voxels that are sampled using a 3D cubic grid overlaid on the CT and ultrasound volumes. The final registration result obtained is the set of optimized transformation parameters ϕ_{opt} at which the cross-correlation is maximized.

In slices-to-volume registration, the reconstruction step is eliminated as the 2D ultrasound slices are directly input into the registration algorithm. In addition, instead of waiting for the volume to be reconstructed before extracting the posterior vertebral surface by backward scan line tracing, the ultrasound slices are preprocessed with backward scan line tracing as they are acquired. The preprocessed ultrasound slices are then registered to the CT volume using the optimization function:

$$\phi_{opt} = \arg\max_{\phi}[\frac{1}{N}\sum_{n=1}^{N}\mathbf{C_n}(CT, \mathbf{T_n}(US_n, \phi))] \tag{5.3}$$

where CT is still the image volume containing the posterior vertebral surface, US_n is the n$^{\text{th}}$ ultrasound slice, $\mathbf{T}(US_n, \phi))$ is the rigid transformation that is applied to the n$^{\text{th}}$ ultrasound slice using the set of transformation parameters ϕ, and $\mathbf{C_n}$ is the intensity cross-correlation function between the CT volume and the n$^{\text{th}}$ ultrasound slice. The cross-correlation function is still the same function as equation (5.2) except that the $US(x_i)$ are voxels sampled using a 2D rectangular grid overlaid on the n$^{\text{th}}$ ultrasound slice and $CT(x_i)$ is the voxel in the CT volume corresponding to $US(x_i)$. The cross-correlation for all N ultrasound slices are summed to arrive at an average cross-correlation, which is maximized by the optimization function to obtain the set of optimized transformation parameters ϕ_{opt}. Note that because the registration of a single vertebra can be modeled as a rigid registration, the relative spatial relationships between the ultrasound slices do not change during registration optimization. The ultrasound slices are thus registered as a group to the CT volume using the same set of transformation parameters ϕ. From a another viewpoint, this group of ultrasound slices can also be viewed as a sparse "ultrasound volume", with most of the volume being empty spaces between the scattered ultrasound slices. However, this sparse "ultrasound volume" differs from a real ultrasound volume in that the sampling is not a uniform 3D grid, but is instead concentrated in each of the ultrasound slices, whereas the empty spaces in between the slices are not sampled. The source code and a Linux binary of the slices-to-volume registration is available at “http://slices-to-volume-registration.googlecode.com/svn/” under the GPL3 license. Note that the freely available MINC libraries need to be preinstalled to build and execute this program.

5.2.6 Evaluation of Registration Accuracy and Robustness

The registration accuracy was assessed by comparing the registration transformation to a gold standard registration to compute a target registration error. A detailed description of the generation of gold standard registration and target registration error is beyond the scope of this article, but the interested reader is referred to Chapter 3 [126] for a complete description. In summary, the gold standard registration was computed from four pairs of world space and CT image space coordinates, which are the coordinates of a set of four imaging fiducials that were physically implanted on each vertebra. The registration accuracy was measured by the final target registration error (TRE), which is the root-mean-square distance between a set of sample targets that have been transformed by the slices-to-volume registration and those that have been transformed by the gold standard registration. The registration robustness is represented by the percentage of successful registrations (abbreviated as ”percent success”), where a registration is successful if its final TRE is below the 2 mm threshold, which was proposed by Cleary et al [125] for spine image-guided surgery. The registration speed is computed as the mean execution time of the registration program on a 2 GHz Linux-based system.

5.3 Validation Experiments

Three validation experiments were performed to assess the accuracy and robustness of the slices-to-volume registration, and to compare it with the volume-to-volume registration technique used previously (Chapter 3 [126]). Our goal is to demonstrate that the slices-to-volume method is as accurate as the volume-to-volume method, while being substantially more time efficient. In the first experiment, the slices-to-volume registration was performed on the same ultrasound slices and CT images of the Sawbones phantom as those used in Chapter 3 [126], with an average of 150 slices per ultrasound sweep. As in the previous experiments for the registration of the Sawbones phantom, a total of 300 registration experiments were performed with simulated new misalignments as the starting positions (see Chapter 3 [126]) to evaluate registration robustness.

In the second experiment, the slices-to-volume registration was performed on the same images as those used in the extensive validation with porcine cadavers (Chapter 4 [153]). However, because it was shown in the previous study (Chapter 4 [153]) that the ultrasound acquisition with double orthogonal sweeps yields the best accuracy and robustness over 10 ultrasound acquisition strategies, the slices-to-volume technique registered the orthogonal-sweep acquisitions of the 18 thoracolumbar vertebrae across three porcine cadavers, with an average of 115 slices per acquisition. As in the previous experiments, 100 registrations with simulated random initial misalignments were performed per vertebrae, totaling to 1,800 registration experiments.

The third experiment was designed to determine how the registration accuracy of the slices-to-volume technique depends on the number of slices used in the registration. To achieve this, the number of slices in each acquisition is reduced by a factor that increases progressively. The selected slices are evenly distributed throughout the acquisition. For example, if the number of slices is reduced by a factor of 5, then every fifth slice in the acquisition is selected for registration. Since the speed of the ultrasound sweeps is relatively constant throughout, this type of selection also results in a relatively even spatial distribution of slices within the range of the acquisition. The experiment was performed using the orthogonal-sweep acquisitions of all 18 vertebrae across three porcine cadavers, and the average numbers of slices selected at each reduction factor are shown in Table 5–1. For every vertebra and each reduction factor, 100 registrations runs with simulated random initial misalignments are performed, totaling to 12,600 registration experiments.

Table 5–1: Average number of slices selected at each reduction factor

Reduction factor	Average number of slices
1	570
2	285
5	115
10	58
20	30
50	13
100	7

5.4 Registration Results

The registration accuracy, robustness and execution speed of both the first (Sawbones phantom) and the second (porcine cadavers) validation experiments are summarized numerically in Table 5–2 and Table 5–3 respectively. The results of both the slices-to-volume and the volume-to-volume registration are shown next to each other for easy comparison. In Table 5–2, it can be seen that the registration accuracy and robustness of the slices-to-volume technique is similar to those of volume-to-volume technique for the Sawbones phantom, while the mean execution time is shorter for the slices-to-volume registration. Note that the execution time is for registration only, and does not include the 3D reconstruction time required for the volume-to-volume registration technique. Although the final TREs of the two techniques are statistically different ($p < 0.05$, Kruskal-Wallis test, see Fig. 5–4), the absolute difference of 0.01 mm between the medians of the final TREs is not practically important. On the other hand, Table 5–3 shows that the slices-to-volume technique achieves better final TRE ($p < 0.001$, Kruskal-Wallis test), percent success, and mean execution time than the volume-to-volume technique for registering porcine cadaver images.

The registration results of both the first and the second experiments are also plotted in the high density scatter plots of Fig. 5–5a and Fig. 5–5b. In both figures, the final TRE of the registrations are plotted against the initial misalignment TRE. Note the randomization of the initial misalignment follows a Gaussian distribution. The slices-to-volume registrations (blue) are plotted together with the volume-to-volume registrations (green) to visually compare

Table 5–2: Comparison of registration performance between volume-to-volume and slices-to-volume registration using Sawbones phantom images

Registration method	Final TRE (mm)		Percent success	Mean execution time (min:sec)
	median	IQR[a]		
Volume-to-volume	0.66	0.26	99.7%	2:23
Slices-to-volume	0.65	0.18	98.0%	2:00

[a] IQR: interquartile range

Table 5–3: Comparison of registration performance between volume-to-volume and slices-to-volume registration using porcine cadaver images

Registration method	Final TRE (mm)		Percent success	Mean execution time (min:sec)
	median	IQR		
Volume-to-volume	1.65	0.47	82.7%	2:44
Slices-to-volume	1.48	0.71	84.6%	1:56

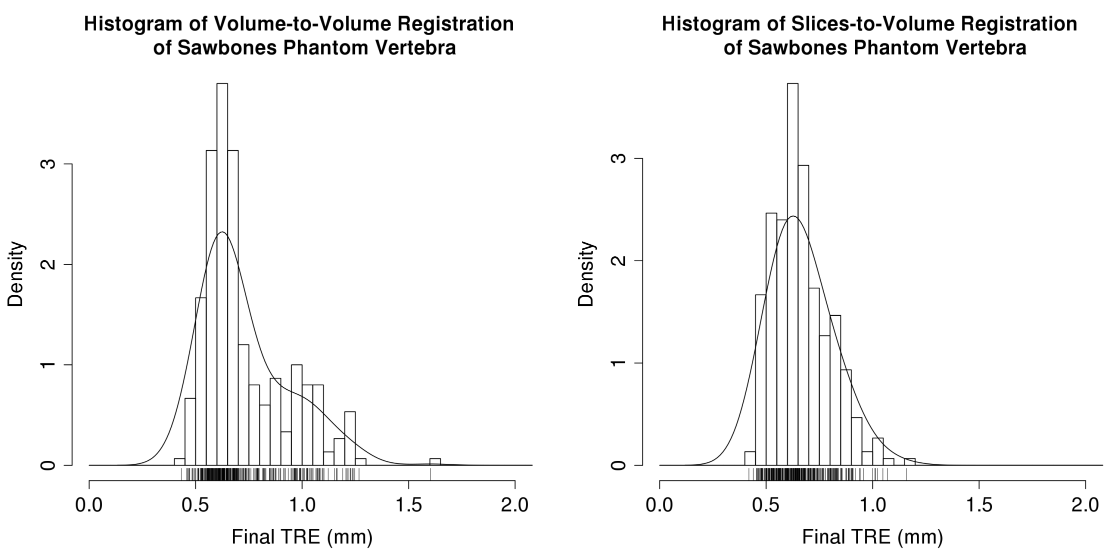

Figure 5–4: Final TRE histogram comparison of volume-to-volume registration and slices-to-volume registration for Sawbones phantom experiments.

the two techniques. It can be seen from Fig. 5–5a that for the registration of the Sawbones phantom images, the two techniques demonstrate very similar distribution and almost all registrations have final TREs under the 2 mm threshold with only a few exceptions. The slices-to-volume technique seems to be slightly more sensitive to higher initial misalignments (near 15 mm). For the registration of porcine cadaver images, Fig. 5–5b shows that both techniques yield final TREs that are mostly under the 2 mm threshold (with a success rate above 80% as shown in Tables 5–2 and 5–3). The slices-to-volume technique results in much less registration failure for initial misalignments lower than 15 mm, but results in more failures for initial misalignments above 15 mm.

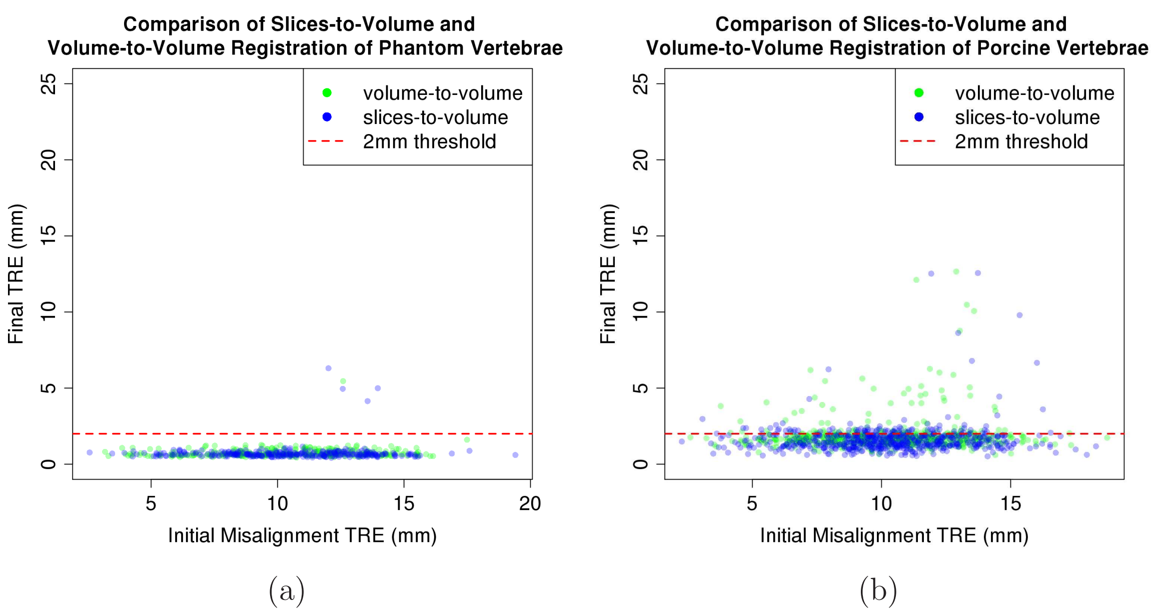

Figure 5–5: High density scatter plot where the final TREs of slices-to-volume registrations (blue) are overlaid on top of the final TREs of volume-to-volume registrations (green) for both (a) Sawbones phantom images and (b) porcine cadaver images.

Finally, the registration results of the third experiment are plotted in Fig. 5–6, which reveals the dependency of the registration accuracy and speed on the number of ultrasound slices used in the slices-to-volume registration. In the plot, it can be seen that the final TRE of registrations (green) decreases with increasing number of slices, indicating that higher accuracy can be achieved by inclusion of more slices in the registration. On the other hand, the mean execution time of the registration program (blue) increases with increasing number of slices, implying a negative correlation between the registration speed and the number of slices.

5.5 Discussion

In this study, we modified the original volume-to-volume ultrasound-CT registration technique to perform slices-to-volume registration, thus eliminating the ultrasound reconstruction step. With ultrasound reconstruction eliminated, the total registration time per vertebra is now the sum of ultrasound acquisition time, landmark-based manual registration time (to obtain a starting position) and the slices-to-volume registration time. It was determined from the experiments that mean execution time of slices-to-volume registration is almost 2 min. As the ultrasound acquisition typically takes 20-30 sec and landmark-based manual registration takes 1-2 min, the total registration time using the slices-to-volume registration technique is about 4 min per vertebra. This time is a significant reduction compared to the previous estimate of 8 min per vertebra using volume-to-volume registration (Chapter 4 [153]). An even larger reduction is the amount of time the surgeon has to spend waiting for the computer. Previously with volume-to-volume registration, the surgeon needed to wait 5-6 min (reconstruction

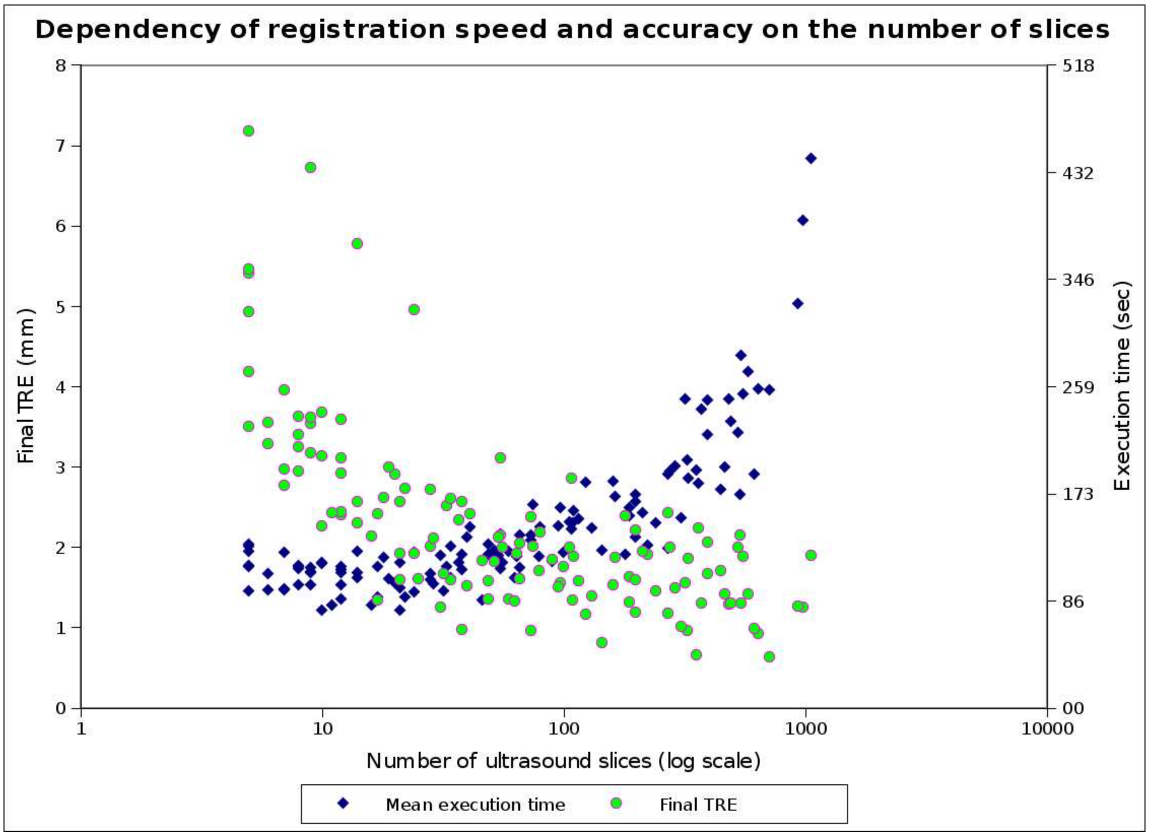

Figure 5–6: Scatter plot of both accuracy (final TRE, green) and speed (mean execution time, blue) of the registration with respect to the number of slices used in the registration. Note that each point in the graph corresponds to one registration experiment and that the number of slices is represented on a log scale.

plus registration time) before the final registration is available. Now with slices-to-volume registration, the surgeon only needs to wait for about 2 min of registration time before obtaining the final result, making the IGS system much more practical for intraoperative use.

The registration accuracy and robustness are also preserved in the slices-to-volume registration. The medians of the final TRE for slices-to-volume versus volume-to-volume registration are respectively 0.65 mm vs. 0.66 mm for Sawbones phantom, and 1.48 mm vs. 1.65 mm for porcine cadavers. The percent success rates are 98.0% vs. 99.7% for Sawbones phantom and 84.6% vs. 82.7% for porcine cadavers. Thus, both the accuracy and robustness of slices-to-volume registration are equal or better than those of volume-to-volume registration. The robustness of the slices-to-volume registration is also illustrated graphically in both Fig. 5–5a and Fig. 5–5b. Both figures show that the slices-to-volume technique results in less registration failure for initial misalignments lower than 15 mm, but results in more failures for initial misalignments above 15 mm, especially for porcine cadaver registrations. However, the range of initial misalignments that matter are usually under 10 mm, because practically speaking, the majority of the starting positions resulting from a quick landmark-based manual registration will have initial misalignments under 10 mm, as demonstrated previously in Chapter 4 [153]. Therefore, it is safe to conclude that the reduction in total registration time of slices-to-volume registration does not come at the expense of decrease in performance, as both the registration accuracy and robustness are well preserved compared to those of volume-to-volume registration, if not superior.

A minor goal of this study is to investigate the relationship between the number of slices used in the registration and the execution time of the registration algorithm. Figure 5–6 shows that the execution time is positively correlated with the number of slices used in the porcine cadaver registration, whereas the final TRE is inversely correlated with the number of slices. Therefore, there is a continuum of tradeoffs between registration accuracy and the execution time through the number of slices used. One can achieve a faster registration by sacrificing some accuracy or vice versa. It is up to the user of the registration technique to decide how to balance the two. However, the lower limit for final TRE for porcine cadaver registration is approximately 1.0 mm and the lower limit for execution time is 1 min.

It is possible to further speed up the execution of the slices-to-volume registration in the future by parallelizing the computation of the slices. In addition, because slices-to-volume registration enables the manipulation of registration input at the level of individual slices, it may be possible to further enhance the flexibility of the registration technique by allowing more slices to be acquired and added or artefactual slices to be removed if necessary.

5.6 Conclusions

We have developed and validated the slices-to-volume registration technique on both the Sawbones phantom and three porcine cadavers. We found that by eliminating the step of ultrasound reconstruction, the total registration time has been reduced from 8 min to 4 min and the waiting time from 6 min to 2 min. This reduction in time is achieved without sacrificing the performance of the registration, as it was shown that the accuracy and robustness of the slices-to-volume registration is at least as good as or even superior to those of the volume-to-volume registration. In addition, we also found that there is a tradeoff between the registration accuracy and the execution time of the slices-to-volume registration through the number of ultrasound slices used. The slices-to-volume registration can be rendered faster and more flexible in the future by parallelizing the computation of ultrasound slices and by allowing the addition or the removal of slices.

CHAPTER 6
Discussion and Conclusions

6.1 Summary and Discussion

The goal of this thesis was to develop an ultrasound-CT image registration technique of the vertebrae that would be practical for intraoperative application in image-guided spinal fusion surgery. This requires that the technique be automated, accurate, robust, reasonably fast and appropriately validated. More specifically, these requirements were detailed by Cleary et al [125] in the 2000 report based on the consensus from experts in the field. The registration accuracy should be 1-2 mm, the registration time should be under 5 minutes and the validation experiments should employ fiducial-based gold standard registration as the ground truth for assessing accuracy. Many of the current existing techniques have been reviewed in Section 2.4 and 2.5, and as was pointed out in Section 2.6, no existing study has satisfied all of these requirements together. In this thesis, I have developed an automated technique for ultrasound-CT registration of vertebrae, validated the technique extensively on multiple levels and subjects, demonstrated good accuracy and robustness, and optimized the registration algorithm to achieve a total registration time suitable for intraoperative use.

In Chapter 3, I proposed a new ultrasound-CT registration technique of the vertebrae. The technique first extracted vertebral bone surface from the ultrasound and CT image volumes. The surface extraction was through forward and backward tracing of scan lines of an imaginary phased-array ultrasound probe. Then, the extracted surfaces were registered together by cross-correlating their voxel intensities. The feasibility of the technique was demonstrated by preliminary registration experiments on a single lumbar vertebra in both a plastic phantom and a porcine cadaver.

In Chapter 4, I performed extensive validation of the registration technique developed in Chapter 3. I applied the technique on 18 vertebrae in 3 porcine cadavers, using 10 different ultrasound sweep patterns for each vertebra. For each unique combination of vertebra and sweep pattern, 100 registrations from 100 different simulated initial misalignment positions were executed, summing up to 18,000 registrations in total. I assessed the accuracy of each registration with respect to the gold standard registrations generated using the imaging fiducials implanted on each vertebra. The orthogonal-sweep pattern was found to yield the most accurate and robust registrations. The experiments have demonstrated that the registration technique yield registration accuracy and robustness that are better or comparable to the other state-of-the-art techniques that were also validated using fiducial-based gold standard registrations, as shown in Table 6–1.

In addition, I also studied the accuracy of the gold standard registration itself, as the process of generating the gold standard also introduced errors. It was found that the gold standard registration had a target registration error of

Table 6–1: Comparison of registration accuracy and robustness with other studies

Study	Anatomy	Mean TRE (mm)	% of TRE under 2 mm	% of TRE under 3 mm	% of TRE under 5 mm
Our technique	porcine cadaver, thoracolumbar	1.65	82.7%	94.3%	98.1%
Gill et al [118]	sheep cadaver, lumbar	0.6-2.26		87%	
Rasoulian et al [104]	sheep cadaver, lumbar	2.2		82%	
Penney et al [114]	human cadaver, pelvis and femurs	1.6			
Barratt et al [101]	human cadaver, pelvis and femurs	1.6			94.7%

0.718 mm. I also conducted experiments to investigate the range of the initial misalignments. I found that the initial misalignments obtained by landmark based manual registration are under 10 mm, which is lower than the upper limit (20 mm) of our simulated initial misalignments used in the registration experiments.

The focus of Chapter 5 was to modify the registration technique to eliminate the need for the reconstruction of ultrasound image slices into an image volume. Previously, the reconstruction was significantly prolonging the total registration time to 8 min per vertebra, whereas after eliminating the reconstruction, the total registration time was reduced down to 4 min per vertebra. The modified registration technique was able to achieve this reduction by directly registering the ultrasound image slices as a group to the CT image volume. This slices-to-volume registration technique not only significantly reduced the total registration time, but also demonstrated improved accuracy (median TRE 1.45 mm, 84.6% of TREs < 2 mm) and robustness compared to the original volume-to-volume registration (median TRE 1.65 mm, 82.7% of TREs < 2 mm). In addition, further experiments established that it is possible to trade-off registration accuracy for speed by using a smaller number of ultrasound image slices in the registration and vice versa.

The combination of the work presented in the Chapters 3 to 5 of this thesis has resulted in a registration technique that satisfies the requirements for intra-operative use. The technique has been validated using cadaveric studies with fiducial-based gold standard registration. It has an accuracy between 1-2 mm (median 1.45 mm); it is robust with 84.6% of registrations having TRE under 2 mm; and its total registration time is 4 min, less than the 5 min suggested by Cleary et al [125]. Therefore, we conclude that the registration technique we have developed in this doctoral thesis have met the goals set out at the thesis proposal.

6.2 Limitations and Future Work

6.2.1 Simultaneous Registration of Multiple Vertebrae

Reviewers of the manuscripts presented in this thesis have suggested the possibility of adapting the registration technique to register multiple vertebrae simultaneously. Currently, the technique in this thesis registers a single vertebra at a time, because the registration transformation needs to be updated for every individual vertebra before screw implantation on each level. The reason is that as the intervertebral discs and ligaments connecting neighbouring vertebrae are deformable, the relative position between the neighbouring vertebrae (hence spine curvature) could change with movement of patient spine. This curvature change is especially noted between the time when patient was imaged preoperatively in the supine position, to the time when patient was operated in the prone position. Therefore, a single rigid registration of multiple vertebrae is not appropriate, as the relative positions of neighouring vertebrae are not fixed (this was also explained in Section 3.2.1). Therefore, in the current technique, the preoperative CT image was cropped to each vertebral level before the registration of that level.

Early studies that registered multiple vertebrae simultaneously between ultrasound and CT images include Brendel et al [109, 110], Winter et al [157]. However, in these studies, the vertebrae were all registered rigidly as a single entity, without taking into considerations that deformations of the intervertebral structures could lead to changes in the relative positions of the neighbouring vertebrae. The authors of these studies pointed out this concern later and opted for registering a single vertebra at a time to address this issue [111, 112] (in their case, surface points of neighbouring vertebrae on the CT image were separated manually). Kadoury and Paragios [158] proposed in 2009 a technique to register multiple vertebrae from an articulated spine model in the upright position to a supine 3D intraoperative CT image of the spine. To allow intervertebral deformation in the registration process, they introduced Markov random fields (MRFs) to constrain the relationship between neighbouring vertebrae. These MRFs were included as smoothness terms in the optimization process. Gill et al [117, 118] proposed in the same year the use of a biomechanical model to constrain the alignment of multiple vertebrae during registration so that anatomically acceptable alignments were favoured. The energy between the vertebrae was modeled by spring equations and was added to the optimization process as a smoothness term. The weight of the term was user-defined through multiple trials to arrive at a weight that would yield the highest registration success rate. A similar biomechanical model simulating a grid of springs was also used by the same group in Rasoulian et al [104].

Simultaneous registration of multiple vertebrae is an effective technique when accurate representation of several neighouring vertebrae is needed, such as in image-guided spinal injection of local anesthetics. It is not as helpful in procedures where each vertebra needs to be updated individually before instrumentation, such as in pedicle screw implantation for spinal fusion. In these procedures, the registration needs to be updated just before screw implantation, because the mechanical force applied during the drilling and screw insertion of the neighbouring vertebra could change the intervertebral spatial relationship, and the dynamic reference object is also moved from one vertebra to the next as screw insertion proceeds to the next level. Nevertheless, it could be beneficial in the future to adapt the current registration technique for simultaneous registration of multiple vertebrae, as this would enable the technique to be applied to a wider range of image-guided spine interventions. This could be achieved through a piecewise rigid registration, where the preoperative CT image is cropped into multiple subvolumes, each containing a single vertebra. The subvolumes are then rigidly registered to the corresponding intraoperative ultrasound images and subsequently reconstructed back together for the final display of a CT image that has multiple vertebrae updated to their intraoperative positions and orientations.

The addition of a biomechanical model to constrain the vertebral alignment could help to improve registration accuracy if the model is accurate. However, in studies such as Kadoury and Paragios [158] and Gill et al [118], the accuracy of the model depends on how closely its parameters approximate the spine of the patient. The spring constant represented by a stiffness matrix may need to be optimized for each patient, especially for cases where prior pathologies exist. In addition, the weight assigned to the biomechanical model during the registration may also require adjustment by trial and error, as it is still uncertain with respect to how much constraint is most adequate for different settings of image acquisition and registration. Therefore, more investigation is needed in the future to design a biomechanical model that would be more flexible and adequate for a wide range of patient anatomy.

6.2.2 Intraoperative 3D Volumetric Ultrasound

Until recently, the majority of intraoperative ultrasound used were 2D ultrasound images. The most common method by which 3D ultrasound volumes were obtained is by reconstructing 2D ultrasound images acquired with a freehand tracked ultrasound probe, such as the method used in this thesis. However, the advent of volumetric 3D ultrasound technology has enabled true 3D ultrasound volumes to be acquired in a matter of seconds. The research community has started to use this technology in the detection and intervention of disease [107, 159–164]. Wein et al [159] registered intracardiac 3D volumetric ultrasound to the preoperative CT image to update in realtime the CT image position for the guidance of electrophysiology and interventional cardiology procedures. Ji et al

[160] stitched multiple 3D volumetric ultrasound of the brain acquired during neurosurgery by mutual information registration in order to expand the field of view of intraoperative ultrasound. Subsequently, Ji et al [161] registered the stitched intraoperative 3D ultrasound volumes to the preoperative MR images to provide patient-to-image registration for neuronavigation. Nam et al [162] registered 3D volumetric ultrasound of the liver to preoperative CT for image-guided liver intervention. Brounstein et al [107] and Hacihaliloglu et al [163, 164] extracted local phase bone features from 3D volumetric ultrasound of pelvic bones and registered them with the preoperative CT image to assist image-guided orthopedic surgery.

The advantages of 3D volumetric ultrasound over 2D freehand ultrasound are that the former has much faster acquisition time and does not require the extra step of reconstruction. In general, it takes less than 10 seconds to acquire an ultrasound volume with a 3D volumetric ultrasound probe. This short acquisition time enables near realtime registration and update of intraoperative images in time-sensitive applications such as cardiac intervention [159]. In addition, the elimination of the reconstruction step not only saves processing time, but also prevents the loss of information by interpolation. For this thesis, the registration technique developed could be easily adapted to use 3D volumetric ultrasound technology by performing volume-to-volume registration between ultrasound and CT images of the vertebrae. In fact, this technology effectively obviates the technique of registration without reconstruction developed in Chapter 5, because the 3D volumetric ultrasound directly acquires 3D image volumes.

Therefore, the technique of registration without reconstruction is suitable for the majority of 2D ultrasound probes currently in use, while the volume-to-volume registration technique could be easily applied to images acquired with 3D volumetric ultrasound probes.

6.2.3 Validation Experiments

Proper validation of the registration technique is an important prerequisite for a technique that is practical for intraoperative use. The clinical relevance of the validation is typically higher for animal and human cadavers than for plastic phantoms and simulated computer models, with the most relevant validation subjects being the patients themselves. In this thesis, validation experiments have been conducted on both plastic phantoms and porcine cadavers, demonstrating accurate and robust registration. Other animal cadaver experiments include Gill et al [118] and Rasoulian et al [104], which are two similar validation experiments on sheep cadavers for the registration of intraoperative ultrasound of vertebrae to preoperative CT. While it is much easier to procure fresh specimen of porcine cadavers, the porcine vertebrae still differ slightly from human anatomy, with larger transverse processes, shorter spinous processes, taller and narrower vertebral bodies, and larger pedicles. In this respect, human cadavers are anatomically more similar to live patients. Studies that have obtained intraoperative ultrasound of human cadaver vertebrae, femur and pelvis for registration validation include Barratt et al [101], Brendel et al [109], Penney et al [114]. On the other hand, given that it is difficult to procure fresh human cadavers that have not undergone preservative fixation or freezing, one may also argue that the slight anatomical differences of the vertebrae is outweighed by the fact that animal cadavers have unpreserved fresh soft tissue that are more clinically realistic.

Compared to cadaver validation, validation experiments performed on patients in actual surgical settings would have the highest clinical relevance. The main issue with patient validation is the lack of fiducial-based gold standard registration, because it would be unethical to implant imaging fiducials in patients only for research purposes. Without the gold standard registration, the accuracy measurement of the registration techniques is not as objective. Several clinical validation studies involving registration of intraoperative ultrasound of bony structures have employed a variety of methods to address this issue, some more effective than the others. For example, Amin et al [100] compared the registrations based on intraoperative ultrasound with the conventional surface-point-based registration, which is not the ground truth, but rather a registration achieved through the conventional manual method. Thus the comparison only demonstrates the relative error between two registration techniques and not the true accuracy. Similarly, Winter et al [111, 112] compared their registrations to a bronze standard reference registration, which is itself generated by the same registration technique, thus making the measurement the registration precision instead of accuracy. Perhaps the most effective assessment method that circumvents the need for imaging fiducials is that presented by Carrat et al [88]. In this study, registration accuracy was not assessed. Instead, the accuracy of the screw placement under the guidance of the registered image was assessed by measuring on the postoperative

CT the distance between the screw and anatomical landmarks of importance, which can be considered as gold standard ground truth.

Moving forward, there are three additional steps envisioned in the validation of the registration technique presented in this thesis. Firstly, the intraoperative ultrasound-based registration would be used to guide pedicle screw implantation in cadavers (preferably human) and the accuracy of the screw placements would be assessed by postoperative CT or dissection. Subsequently, the registration technique would be applied to a small number of real surgical cases of spinal fusion. The screw placement accuracy would be assessed by postoperative CT. Finally, a randomized controlled trial would investigate the screw placement accuracy, the screw placement operative time, and the postoperative functional status of the patients by comparing spinal fusions performed using the current registration technique with those performed using the conventional manual registration technique.

6.2.4 Parallel Computation

It was alluded in earlier chapters that the registration time could be further reduced by adapting the algorithm for parallel computation. This improvement combined with the faster acquisition by 3D volumetric ultrasound probe could make the intraoperative registration near realtime. Although realtime registration is not required for pedicle screw placement, the surgeons could always benefit from faster registration and shorter operative time. In addition, realtime registration could extend the technique's application to other procedures where timely update of preoperative image are advantageous, such as in image-guided biopsy of vertebral bones or vertebroplasty injections. A brief discussion is provided below on the possibility of adapting the current registration technique for parallel computation.

Parallel computation for medical image registration could be divided in two categories: parallel threads execution on multiple CPUs (central processing units) or data-parallel computing on programmable GPUs (graphics processing units). There have been numerous studies published in the past decade in both categories. The interested reader is referred to Shams et al [165] and Fluck et al [166] for a good review of the field. For both categories, memory access is an important issue for medical image registration, because the registration algorithm spends the majority of its execution time on performing simple computations (such as transformations and similarity measures) for a large amount of parallel data (voxels in medical images).

The execution on multiple CPUs could be further classified by their memory access architecture, such as symmetric multiprocessing where multiple CPUs share the same memory, or non-uniform memory access where each CPU has its own local memory that could be shared with other CPUs, or distributed computing on a cluster where data is distributed through a network of computers. While shared memory slows down memory access because of a bus that is shared, the distributed model also suffers from large overhead through the network interface. Therefore, the best architecture for our slices-to-volume registration would be multiprocessor with non-uniform memory access. In this architecture, each thread running on one of the CPUs works on an image subset (such as an ultrasound image slice) that is stored in its local memory. The result from multiple threads are combined to perform the overall optimization for registration.

Although multiprocessor architecture presents a reasonable solution for parallelization, the registration technique will likely gain the most improvement in speed from an implementation on programmable GPUs. Modern GPUs have highly parallel computational architecture with high memory throughput, performing at the order of teraflops at very affordable costs. The built-in hardware units of GPU for graphics rendering could also be used to accelerate the most time consuming components of image registration, namely, the transformation of images (requiring interpolation) and the computation of similarity metrics [165]. For the current thesis, the rigid transformation could be performed by the texture mapping unit of the GPU, while the similarity metric (normalized cross-correlation) could be computed by running a fragment program in the GPU's programmable rasterizer. It is usually difficult to predict the amount of performance gain with GPU acceleration before the implementation, but reducing the registration time by order(s) of magnitude would not be uncommon [165].

6.2.5 Future Directions

The text above discussed the limitations specific to the registration technique developed in this thesis and the works that remain to be completed in the future. However, some future directions could be identified in general for the field of intraoperative ultrasound registration for the image-guidance of orthopedic surgeries. One important area for improvement is that more clinical validations are needed. As we have reviewed in Section 2.4, many studies in this field have presented original registration techniques, but very few of them validated the technique clinically on patients. This is partly because some techniques have not been thoroughly validated on cadaver specimens first. It may also be because most orthopedic surgeons are reluctant to use surgical navigation due to the additional training requirement and lengthened operative time associated with image-guidance. In fact, the inconvenience and the time-intensiveness of patient-to-image registration are exactly what intraoperative ultrasound registration is trying to address by providing a faster and automated registration process. In addition, the registration time could be further reduced to near realtime with the future adoption of 3D volumetric ultrasound and the parallel computation on GPUs. In the not too distant future, a fast, accurate and simple to use registration technique based on intraoperative ultrasound will foster more interest in its clinical application and lead to more extensive clinical validations and wider clinical adoption.

6.3 Conclusions

The goal of this thesis was to develop a technique for ultrasound-CT registration of vertebrae that is automated, accurate, robust, reasonably fast and appropriately validated so that it is practical for intraoperative use in pedicle screw implantation. The intensity-based registration technique developed in this thesis registers extracted vertebral surfaces of ultrasound and CT images. This technique has been extensively validated on animal cadavers and it used fiducial-based gold standard registrations as ground truth. The experimental results have demonstrated that the technique is accurate, robust and can be executed within a time reasonable for intraoperative use. Further experiments on human cadavers and live patients will be necessary to apply this registration technique in clinical settings.

REFERENCES

[1] Rajaee SS, Bae HW, Kanim LE, Delamarter RB (2012) Spinal fusion in the united states: Analysis of trends from 1998 to 2008. Spine 37(1):67–76

[2] Fischgrund JS, Mackay M, Herkowitz HN, Brower R, Montgomery DM, Kurz LT (1997) Degenerative lumbar spondylolisthesis with spinal stenosis: A prospective, randomized study comparing decompressive laminectomy and arthrodesis with and without spinal instrumentation. Spine 22(24):2807–2812

[3] Hanley E (1995) The indications for lumbar spinal fusion with and without instrumentation. Spine 20(24 Suppl):143S–153S

[4] Schwab F, Nazarian D, Mahmud F, Michelsen C (1995) Effects of spinal instrumentation on fusion of the lumbosacral spine. Spine 20(18):2023–2028

[5] Deyo RA, Nachemson A, Mirza SK (2004) Spinal-fusion surgery-the case for restraint. New England Journal of Medicine 350(7):722–726

[6] Bono CM, Lee CK (2004) Critical analysis of trends in fusion for degenerative disc disease over the past 20 years: Influence of technique on fusion rate and clinical outcome. Spine 29(4):455–463

[7] Goulet B (2007) Lumbar pedicle screw insertion with preoperative CT-based navigation. Master's thesis, Université de Montréal

[8] Dickman CA, Fessler RG, MacMillan M, Haid RW (1992) Transpedicular screw-rod fixation of the lumbar spine: Operative technique and outcome in 104 cases. Journal of Neurosurgery 77(6):860–870

[9] Steinmann JC, Herkowitz HN, El-Kommos H, Wesolowski DP (1993) Spinal pedicle fixation. confirmation of an image-based technique for screw placement. Spine 18(13):1856–1861

[10] Suk S, Lee C, Kim W, Chung Y, Park Y (1995) Segmental pedicle screw fixation in the treatment of thoracic idiopathic scoliosis. Spine 20(12):1399–1405

[11] Abumi K, Shono Y, Ito M, Taneichi H, Kotani Y, Kaneda K (2000) Complications of pedicle screw fixation in reconstructive surgery of the cervical spine. Spine 25(8):962–969

[12] Esses S, Sachs B, Dreyzin V (1993) Complications associated with the technique of pedicle screw fixation. a selected survey of ABS members. Spine 18(15):2231–2239

[13] Merloz P, Tonetti J, Pittet L, Coulomb M, Lavallée S, Troccaz J, Cinquin P, Sautot P (1998) Computer-assisted spine surgery. Computer Aided Surgery 3(6):297–305

[14] Castro WHM, Halm H, Jerosch J, Malms J, Steinbeck J, Blasius S (1996) Accuracy of pedicle screw placement in lumbar vertebrae. Spine 21(11):1320–1324

[15] Gertzbein S, Robbins S (1990) Accuracy of pedicular screw placement in vivo. Spine 15(1):11–14

[16] Schulze CJ, Munzinger E, Weber U (1998) Clinical relevance of accuracy of pedicle screw placement: A computed tomographic-supported analysis. Spine 23(20):2215–2220

[17] Haberland N, Ebmeier K, Grunewald JP, Hliscs R, Kalff RL (2000) Incorporation of intraoperative computerized tomography in a newly developed spinal navigation technique. Computer Aided Surgery 5(1):18–27

[18] Laine T, Lund T, Ylikoski M, Lohikoski J, Schlenzka D (2000) Accuracy of pedicle screw insertion with and without computer assistance: A randomised controlled clinical study in 100 consecutive patients. European Spine Journal 9(3):235–240

[19] Scheufler KM, Franke J, Eckardt A, Dohmen H (2011) Accuracy of image-guided pedicle screw placement using intraoperative computed tomography-based navigation with automated referencing. part ii: Thoracolumbar spine. Neurosurgery 69(6):1307–1316

[20] Mercier L, Del Maestro R, Petrecca K, Kochanowska A, Drouin S, Yan CXB, Janke A, Chen S, Collins DL (2011) New prototype neuronavigation system based on preoperative imaging and intraoperative freehand ultrasound: system description and validation. International Journal of Computer Assisted Radiology and Surgery 6(4):507–522

[21] Laine T, Schlenzka D, Makitalo K, Tallroth K, Nolte LP, Visarius H (1997) Improved accuracy of pedicle screw insertion with computer-assisted surgery: A prospective clinical trial of 30 patients. Spine 22:1254–1258

[22] Arand M, Hartwig E, Kinzl L, Gebhard F (2002) Spinal navigation in tumor surgery of the thoracic spine: First clinical results. Clinical Orthopaedics and Related Research 399:211–218

[23] Tamura Y, Sugano N, Sasama T, Sato Y, Tamura S, Yonenobu K, Yoshikawa H, Ochi T (2005) Surface-based registration accuracy of CT-based image-guided spine surgery. European Spine Journal 14(3):291–297

[24] Nolte LP, Zamorano LJ, Jiang Z, Wang Q, Langlotz F, Berlemann U (1995) Image-guided insertion of transpedicular screws. a laboratory set-up. Spine 20(4):497–500

[25] Amiot L, Labelle H, DeGuise J, Sati M, Brodeur P, Rivard C (1995) Computer-assisted pedicle screw fixation. a feasibility study. Spine 20:1208–1212

[26] Glossop ND, Hu RW, Randle JA (1996) Computer-aided pedicle screw placement using frameless stereotaxis. Spine 21(17):2026–2034

[27] Kalfas IH, Kormos DW, Murphy MA, Mckenzie RL, Barnett GH, Bell GR, Steiner CP, Trimble MB, Weisenberger JP (1995) Application of frameless stereotaxy to pedicle screw fixation of the spine. Journal of Neurosurgery 83(4):641–647

[28] Foley KT, Smith MM (1997) Frameless stereotactic guidance of C1-2 transarticular screw placement: Clinical experience. In: 11th International Congress of Neurological Surgery, vol 99, p 360A

[29] Bloch O, Holly LT, Park J, Obasi C, Kim K, Johnson JP (2001) Effect of frameless stereotaxy on the accuracy of C1-2 transarticular screw placement.

Journal of Neurosurgery 95(1 Suppl):74–79

[30] Richter M, Mattes T, Cakir B (2004) Computer-assisted posterior instrumentation of the cervical and cervico-thoracic spine. European Spine Journal 13(1):50–59

[31] Lim MR, Girardi FP, Yoon SC, Huang RC, Cammisa FP (2005) Accuracy of computerized frameless stereotactic image-guided pedicle screw placement into previously fused lumbar spines. Spine 15(15):1793–1798

[32] Amiot LP, Lang K, Putzier M, Zippel H, Labelle H (2000) Comparative results between conventional and computer-assisted pedicle screw installation in the thoracic, lumbar, and sacral spine. Spine 25(5):606–614

[33] Nolte LP, Slomczykowski MA, Berlemann U, Strauss MJ, Hofstetter R, Schlenzka D, Laine T, Lund T (2000) A new approach to computer-aided spine surgery: fluoroscopy-based surgical navigation. European Spine Journal 9(7):S078–S088

[34] Fu TS, Chen LH, Wong CB, Lai PL, Tsai TT, Niu CC, Chen WJ (2004) Computer-assisted fluoroscopic navigation of pedicle screw insertion: An in vivo feasibility study. Acta Orthopaedica Scandinavica 75(6):730–735

[35] Rampersaud Y, Pik J, Salonen D, Farooq S (2005) Clinical accuracy of fluoroscopic computer-assisted pedicle screw fixation: a ct analysis. Spine 30(7):E183–190

[36] Lekovic GP, Potts EA, Karahalios DG, Hall G (2007) A comparison of two techniques in image-guided thoracic pedicle screw placement: a retrospective study of 37 patients and 277 pedicle screws. Journal of Neurosurgery Spine

7(4):393–398

[37] Ravi B, Zahrai, Rampersaud R (2011) Clinical accuracy of computer-assisted two-dimensional fluoroscopy for the percutaneous placement of lumbosacral pedicle screws. Spine 36(1):84–91

[38] Holly LT, Foley KT (2003) Three-dimensional fluoroscopy-guided percutaneous thoracolumbar pedicle screw placement. technical note. Journal of Neurosurgery 99(3 Suppl):324–329

[39] Geerling J, Gosling T, Gosling A, Ortega G, Kendoff D, Citak M, Krettek C, Hufner T (2008) Navigated pedicle screw placement: Experimental comparison between CT and 3D fluoroscopy-based techniques. Computer Aided Surgery 13(3):157–166

[40] Hott JS, Papadopoulos SM, Theodore N, Dickman CA, Sonntag VK (2004) Intraoperative iso-c c-arm navigation in cervical spinal surgery: Review of the first 52 cases. Spine 29(24):2856–2860

[41] Ito Y, Sugimoto Y, Tomioka M, Hasegawa Y, Nakago K, Yagata Y (2008) Clinical accuracy of 3D fluoroscopy-assisted cervical pedicle screw insertion. Journal of Neurosurgery Spine 9(5):450–453

[42] Acosta FL, Thompson TL, Campbell S, Weinstein PR, Ames CP (2005) Use of intraoperative isocentric C-arm 3D fluoroscopy for sextant percutaneous pedicle screw placement: case report and review of the literature. The Spine Journal 5(3):339–343

[43] Rajasekaran S, Vidyadhara S, Ramesh P, Shetty AP (2007) Randomized clinical study to compare the accuracy of navigated and non-navigated

thoracic pedicle screws in deformity correction surgeries. Spine 32(2):E56–E64

[44] Nakashima H, Sato K, Ando T, Inoh H, Nakamura H (2009) Comparison of the percutaneous screw placement precision of isocentric C-arm 3-dimensional fluoroscopy-navigated pedicle screw implantation and conventional fluoroscopy method with minimally invasive surgery. Spine 22(7):468–472

[45] Fraser J, Gebhard H, Irie D, Parikh K, Hartl R (2010) Iso-C/3-dimensional neuronavigation versus conventional fluoroscopy for minimally invasive pedicle screw placement in lumbar fusion. Minimally Invasive Neurosurgery 53(4):184–190

[46] Tian NF, Huang QS, Zhou P, Zhou Y, Wu RK, Lou Y, Xu HZ (2011) Pedicle screw insertion accuracy with different assisted methods: a systematic review and meta-analysis of comparative studies. European Spine Journal 20(6):846–859

[47] Ebmeier K, Giest K, Kalff R (2003) Intraoperative computerized tomography for improved accuracy of spinal navigation in pedicle screw placement of the thoracic spine. Acta Neurochirurgica 85:105–113

[48] Zausinger S, Scheder B, Uhl E, Heigl T, Morhard D, Tonn J (2009) Intraoperative computed tomography with integrated navigation system in spinal stabilizations. Spine 34(26):2919–2926

[49] Tormenti MJ, Kostov DB, Gardner PA, Kanter AS, Spiro RM, Okonkwo DO (2010) Intraoperative computed tomography image-guided navigation for

posterior thoracolumbar spinal instrumentation in spinal deformity surgery. Neurosurgical Focus 28(3):E11

[50] Metz LN, Burch S (2008) Computer-assisted surgical planning and image-guided surgical navigation in refractory adult scoliosis surgery: Case report and review of the literature. Spine 33(9):E287–E292

[51] Brennan RP, Smucker PY, Horn EM (2008) Minimally invasive image-guided direct repair of bilateral L-5 pars interarticularis defects. Neurosurgical Focus 25(2):E13

[52] Nottmeier EW, Seemer W, Young PM (2009) Placement of thoracolumbar pedicle screws using three-dimensional image guidance: experience in a large patient cohort. Journal of Neurosurgery Spine 10(1):33–39

[53] Sembrano JN, Polly DW, Gerald C, Ledonio T, Santos ERG (2012) Intraoperative3-dimensionalimaging (o-arm) for assessment of pedicle-screw position: Does it prevent unacceptable screw placement? International Journal of Spine Surgery 6(1):49–54

[54] Larson AN, Santos ERG, Polly DW, Ledonio CGT, Sembrano JN, Mielke CH, Guidera KJ (2012) Pediatric pedicle screw placement using intraoperative computed tomography and 3-dimensional image-guided navigation. Spine 37(3):E188–E194

[55] Silbermann J, Riese F, Allam Y, Reichert T, Koeppert H, Gutberlet M (2011) Computer tomography assessment of pedicle screw placement in lumbar and sacral spine: comparison between free-hand and O-arm based navigation techniques. European Spine Journal 20(6):875–881

[56] Ughwanogho E, Patel NM, Baldwin KD, Sampson NR, Flynn JM (2012) Computed tomography-guided navigation of thoracic pedicle screws for adolescent idiopathic scoliosis results in more accurate placement and less screw removal. Spine 37(8):E473–E478

[57] Costa F, Cardia A, Ortolina A, Fabio G, Zerbi A, Fornari M (2011) Spinal navigation: Standard preoperative versus intraoperative computed tomography data set acquisition for computer-guidance system: Radiological and clinical study in 100 consecutive patients. Spine 36(24):2094–2098

[58] Black P, Alexander E, Martin C, Moriarty T, Nabavi A, Wong T, Schwartz R, Jolesz F (1999) Craniotomy for tumor treatment in an intraoperative magnetic resonance imaging unit. Neurosurgery 45(3):423–31

[59] Kremer P, Tronnier V, Steiner HH, Metzner R, Ebinger F, Rating D, Hartmann M, Seitz A, Unterberg A, Wirtz CR (2006) Intraoperative mri for interventional neurosurgical procedures and tumor resection control in children. Childs Nervous System 22(7):674–678

[60] Muragaki Y, Iseki H, Maruyama T, Kawamata T, Yamane F, Nakamura R, Kubo O, Takakura K, Hori T (2006) Usefulness of intraoperative magnetic resonance imaging for glioma surgery. Acta Neurochirurgica 98:67–75

[61] Foroglou N, Zamani A, Black P (2009) Intra-operative MRI (iop-mr) for brain tumour surgery. British Journal of Neurosurgery 23(1):14–22

[62] Senft C, Bink A, Franz K, Vatter H, Gasser T, Seifert V (2011) Intraoperative MRI guidance and extent of resection in glioma surgery: arandomised, controlledtrial. The Lancet Oncology 12(11):997–1003

[63] Kubben PL, ter Meulen KJ, Schijns OE, ter Laak-Poort MP, van Overbeeke JJ, van Santbrink H (2011) Intraoperativemri-guidedresection of glioblastoma multiforme: asystematicreview. The Lancet Oncology 12(11):1062–1070

[64] Makary M, Chiocca EA, Erminy N, Antor M, Bergese SD, Abdel-Rasoul M, Fernandez S, Dzwonczyk R (2011) Clinical and economic outcomes of low-field intraoperative mri-guided tumor resection neurosurgery. Journal of Magnetic Resonance Imaging 34(5):1022–1030

[65] Unsgaard G, Ommedal S, Muller T, Gronningsaeter A, Nagelhus H, Toril A (2002) Neuronavigation by intraoperative three-dimensional ultrasound: Initial experience during brain tumor resection. Neurosurgery 50(4):804–812

[66] Gerganov V, A AS, Akbarian A, Samii LSM, Fahlbusch R (2009) Reliability of intraoperative high-resolution 2D ultrasound as an alternative to high-field strength mr imaging for tumor resection control: a prospective comparative study. Journal of Neurosurgery 111(3):512–519

[67] Solheim O, Selbekk T, Lindseth F, Unsgaard G (2009) Navigated resection of giant intracranial meningiomas based on intraoperative 3D ultrasound. Acta Neurochirurgica 151(9):1143–1151

[68] Gerganov VM, Samii A, Giordano M, Samii M, Fahlbusch R (2011) Two-dimensional high-end ultrasound imaging compared to intraoperative MRI during resection of low-grade gliomas. Journal of Clinical Neuroscience 18(5):669–673

[69] Unsgaard G, Solheim O, Lindseth F, Selbekk T (2011) Intra-operative imaging with 3D ultrasound in neurosurgery. Acta Neurochirurgica 109:181–186

[70] Conlon R, Jacobs M, Dasgupta D, Lodge JA (2003) The value of intra-operativeultrasound during hepatic resection compared with improved preoperative magnetic resonance imaging. European Journal of Ultrasound 16(3):211–216

[71] Beller S, Hunerbein M, Eulenstein S, Lange T, Schlag PM (2007) Feasibility of navigated resection of liver tumors using multiplanar visualization of intraoperative 3-dimensional ultrasound data. Annals of Surgery 246(2):288–294

[72] Ngo C, Pollet AG, Laperrelle J, Ackerman G, Gomme S, Thibault F, Fourchotte V, Salmon RJ (2007) Intraoperative ultrasound localization of nonpalpable breast cancers. Annals of Surgical Oncology 14(9):2485–2489

[73] Barentsz MW, van Dalen T, Gobardhan PD, Bongers V, Perre CI, Pijnappel RM, van den Bosch MAAJ, Verkooijen HM (2012) Intraoperative ultrasound guidance for excision of non-palpable invasive breast cancer: a hospital-based series and an overview of the literature. Breast Cancer Research and Treatment 135(1):209–219

[74] Shin LK, Brant-Zawadzki G, Kamaya A, Jeffrey RB (2009) Intraoperative ultrasound of the pancreas. Ultrasound Quarterly 25(1):39–48

[75] Chung BI, Lee UJ, Kamoi K, Canes DA, Aron M, Gill IS (2011) Laparoscopic partial nephrectomy for completely intraparenchymal tumors. The

Journal of Urology 186(6):2182–2187

[76] Cooper PR, Epstein F (1985) Radical resection of intramedullary spinal cord tumors in adults: Recent experience in 29 patients. Journal of Neurosurgery 63(4):492–499

[77] Zhou H, Miller D, Schulte DM, Benes L, Bozinov O, Sure U, Bertalanffy H (2011) Intraoperativeultrasound assistance in treatment of intradural spinal tumours. Clinical Neurology and Neurosurgery 113(7):531–537

[78] Degreif J, Wenda K (1998) Ultrasound-guided spinal fracture repositioning. Surgical Endoscopy 12(2):164–169

[79] Lerch K, Volk M, Heers G, Baer W, Nerlich M (2002) Ultrasound-guideddecompression of the spinalcanal in traumaticstenosis. Ultrasound in Medicine & Biology 28(1):27–32

[80] Gupta S, Takhtani D, Gulati M, Khandelwal N, Gupta D, Rajwanshi A, Gupta S, Suri S (1999) Sonographically guided fine-needle aspiration biopsy of lytic lesions of the spine: Technique and indications. Journal of Clinical Ultrasound 27(3):123–129

[81] Bonsanto MM, Metzner R, Aschoff A, Tronnier V, Kunze S, Wirtz CR (2005) 3D ultrasound navigation in syrinx surgery - a feasibility study. Acta Neurochirurgica 147(5):533–541

[82] Arzola C, Davies S, Rofaeel A, Carvalho JCA (2007) Ultrasound using the transverse approach to the lumbar spine provides reliable landmarks for labor epidurals. Anesthesia and Analgesia 104(5):1188–1192

[83] Galiano K, Obwegeser AA, Bale R, Harlander C, Schatzer R, Schocke M, Gruber H (2007) Ultrasound-guided and ct-navigation-assisted periradicular and facet joint injections in the lumbar and cervical spine: A new teaching tool to recognize the sonoanatomic pattern. Regional Anesthesia and Pain Medicine 32:254–257

[84] Weber P, Schlegel J, Meiche J, Peter L, Harland U (2001) A system for ultrasound based intraoperative navigation in spine surgery. In: 2001 IEEE Ultrasonics Symposium, vol 2, pp 1361–1364

[85] Bucholz RD, Yeh DD, Trobaugh J, McDurmont LL, Sturm CD, Baumann C, Henderson JM, Levy A, Kessman P (1997) The correction of stereotactic inaccuracy caused by brain shift using an intraoperative ultrasound device. In: CVRMed-MRCAS97, vol 1205, pp 459–466

[86] Keles GE, Lamborn KR, Berger MS (2003) Coregistration accuracy and detection of brain shift using intraoperative sononavigation during resection of hemispheric tumors. Neurosurgery 53(3):556–564

[87] Letteboer M (2005) Brain shift estimation in image-guided neurosurgery using 3-D ultrasound. IEEE Transactions On Biomedical Engineering 52(2):268–276

[88] Carrat L, Tonetti J, Merloz P, Troccaza J (2000) Percutaneous computer assisted iliosacral screwing: Clinical validation. In: Delp SL, DiGioia A, Jaramaz B (eds) MICCAI 2000, Springer, vol LNCS 1935, pp 1229–1237

[89] Tonetti J, Carrat L, Blendea S, Merloz P, Troccaz J, Lavallée S, Chirossel JP (2001) Clinical results of percutaneous pelvic surgery. computer assisted

surgery using ultrasound compared to standard fluoroscopy. Computer Aided Surgery 6:204–211

[90] Hu Y, Ahmed HU, Taylor Z, Allen C, Emberton M, Hawkes D, Barratt D (2012) Mr to ultrasound registration for image-guided prostate interventions. Medical Image Analysis 16(3):687–703

[91] Wein W, Brunke S, Khamene A, Callstrom MR, Navab N (2008) Automatic CT-ultrasound registration for diagnostic imaging and image-guided intervention. Medical Image Analysis 12(5):577–585

[92] Mercier L, LangøT, Lindseth F, Collins DL (2005) A review of calibration techniques for freehand 3-D ultrasound systems. Ultrasound in Medicine & Biology 31(4):449–471, 0301-5629 Journal Article

[93] Ault T, Siegel MW (1994) Frameless patient registration using ultrasonic imaging. In: Proceedings of First International Symposium on Medical Robotics and Computer-Assisted Surgery, pp 74–82

[94] Ault T, Siegel MW (1995) Frameless patient registration using ultrasonic imaging: A preliminary study. Journal of Image Guided Surgery 1(2):94–102

[95] Lavallée S, Troccaz J, Sautot P, Mazier B, Cinquin P, Merloz P, Chirossel JP (1996) Computer-Assisted Spinal Surgery Using Anatomy-Based Registration, MA: MIT Press, pp 425–449

[96] Herring JL, Dawant BM, Maurer Jr CR, Muratore DM, Galloway RL, Fitzpatrick JM (1998) Surface-based registration of CT images to physical space for image-guided surgery of the spine: A sensitivity study. IEEE Transactions On Medical Imaging 17(5):743–752

[97] Lorensen WE, Cline HE (1987) Marching cubes: A high resolution 3d surface construction algorithm. Computer Graphics 21(4):163–169

[98] Besl PJ, McKay ND (1992) A method for registration of 3D shapes. IEEE Transactions On Parern Analysis And Machine Intelligence 14(2):239–256

[99] Muratore DM, Russ JH, Dawant BM, Galloway Jr RL (2002) Three-dimensional image registration of phantom vertebrae for image-guided surgery: A preliminary study. Computer Aided Surgery 7:342–352

[100] Amin DV, Kanade T, Anthony M DiGioia III BJ (2003) Ultrasound registration of the bone surface for surgical navigation. Computer Aided Surgery 8:1–16

[101] Barratt DC, Penney GP, Chan CSK, Slomczykowski M, Carter TJ, Edwards PJ, Hawkes DJ (2006) Self-calibrating 3D-ultrasound-based bone registration for minimally invasive orthopedic surgery. IEEE Transactions On Medical Imaging 25(3):312–323

[102] Moghari MH, Abolmaesumi P (2007) Point-based rigid-body registration using an unscented kalman filter. IEEE Transactions On Medical Imaging 26(12):1708–1728

[103] Rasoulian A, Mousavi P, Moghari MH, Foroughi P, Abolmaesumi P (2010) Group-wise feature-based registration of CT and ultrasound images of spine. In: Miga MI, Wong KH (eds) Proceedings of SPIE, SPIE, vol 7625, p 76250R

[104] Rasoulian A, Abolmaesumi P, Mousavi P (2012) Feature-based multibody rigid registration of CT and ultrasound images of lumbar spine. Medical

Physics 39(6):3154–3166

[105] Foroughi P, Boctor E, Swartz M, Taylor R, Fichtinger G (2007) Ultrasound bone segmentation using dynamic programming. In: Ultrasonics Symposium, 2007. IEEE, pp 2523–2526

[106] Yushkevich PA, Piven J, Hazlett HC, Smith RG, Ho S, Gee JC, Gerig G (2006) User-guided 3d active contour segmentation of anatomical structures: Significantly improved efficiency and reliability. Neuroimage 31(3):1116–1128

[107] Brounstein A, Hacihaliloglu I, Guy P, Hodgson A, Abugharbieh R (2011) Towards real-time 3D US to CT bone image registration using phase and curvature feature based GMM matching. In: Fichtinger G, Martel A, Peters T (eds) MICCAI 2011, vol 6891, pp 235–242

[108] Hacihaliloglu I, Abugharbieh R, Hodgson A, Rohling R (2008) Bone segmentation and fracture detection in ultrasound using 3d local phase features. In: Metaxas D, Axel L, Fichtinger G, Szekely G (eds) MICCAI 2008, Springer, vol 5241, pp 287–295

[109] Brendel B, Winter S, Rick A, Stockheim M, Ermert H (2002) Registration of 3D CT and ultrasound datasets of the spine using bone structures. Computer Aided Surgery 7:146–155

[110] Brendel B, Siepermanna J, Winter S, Ermert H (2005) In vivo evaluation and in vitro accuracy measurements for an ultrasound-CT registration algorithm. In: International Congress Series - CARS 2005, vol 1281, pp 583–588

[111] Winter S, Brendel B, Pechlivanis I, Schmieder K, Igel C (2008) Registration of CT and intraoperative 3-D ultrasound images of the spine using evolutionary and gradient-based methods. IEEE Transactions on Evolutionary Computation 12(3):284–296

[112] Winter S, Pechlivanis I, Dekomien C, Igel C, Schmieder K (2009) Toward registration of 3D ultrasound and CT images of the spine in clinical praxis: Design and evaluation of a data acquisition protocol. Ultrasound in Medicine & Biology 35(11):1773–1782

[113] Penney GP, Barratt DC, Chan CSK, Slomczykowski M, Carter TJ, Edwards PJ, Hawkes DJ (2005) Cadaver validation of intensity-based ultrasound to CT registration. In: Duncan J, Gerig G (eds) MICCAI 2005, Springer, vol LNCS 3750, pp 1000–1007

[114] Penney GP, Barratt DC, Chan CSK, Slomczykowski M, Carter TJ, Edwards PJ, Hawkes DJ (2006) Cadaver validation of intensity-based ultrasound to CT registration. Medical Image Analysis 10(3):385–395

[115] Wein W, Röper B, Navab N (2007) Integrating diagnostic b-mode ultrasonography into ct-based radiation treatment planning. IEEE Transactions On Medical Imaging 26(6):866–879

[116] Gill S, Mousavi P, Fichtinger G, Pichora D, Abolmaesumi P (2009) Groupwise registration of ultrasound to CT images of human vertebrae. In: Miga MI, Wong KH (eds) Proceedings of SPIE, SPIE, vol 7261, p 72611O

[117] Gill S, Mousavi P, Fichtinger G, Chen E, Boisvert J, Pichora D, Abolmaesumi P (2009) Biomechanically constrained groupwise US to CT registration

of the lumbar spine. In: Yang GZ, Hawkes D, Rueckert D (eds) MICCAI 2009, Springer, vol LNCS 5761, pp 803–810

[118] Gill S, Abolmaesumi P, Fichtinger G, Boisvert J, Pichora D, Borshneck D, Mousavi P (2012) Biomechanically constrained groupwise ultrasound to CT registration of the lumbar spine. Medical Image Analysis 16(3):662–674

[119] Khallaghi S, Mousavi P, Borschneck D, Fichtinger G, Abolmaesumi P (2011) Biomechanically constrained groupwise statistical shape model to ultrasound registration of the lumbar spine. In: Taylor R, Yang GZ (eds) IPCAI 2011, Springer, Lecture Notes in Computer Science, vol 6689, pp 47–54

[120] Ghanavati S, Mousavi P, Fichtinger G, Foroughi P, Abolmaesumi P (2010) Multi-slice to volume registration of ultrasound data to a statistical atlas of human pelvis. In: Miga MI, Wong KH (eds) Proceedings of SPIE, SPIE, vol 7625, p 76250O

[121] Ghanavati S, Mousavi P, Fichtinger G, Foroughi P, Abolmaesumi P (2011) Phantom validation for ultrasound to statistical shape model registration of human pelvis. In: Wong KH, III DRH (eds) Proceedings of SPIE, SPIE, vol 7964, p 79642U

[122] Solberg OV, Lindseth F, Torp H, Blake RE, Hernes TAN (2007) Freehand 3D ultrasound reconstruction algorithms–a review. Ultrasound in Medicine & Biology 33(7):991–1009

[123] Blackall JM, Rueckert D, Maurer Jr CR, Penney GP, Hill DLG, Hawkes DJ (2000) An image registration approach to automated calibration for freehand 3D ultrasound. In: Delp SL, DiGioia A, Jaramaz B (eds) MICCAI 2000,

Springer, vol LNCS 1935, pp 462–471

[124] Brooks R, Collins DL, Morandi X, Arbel T (2008) Deformable ultrasound registration without reconstruction. In: Metaxas D, Davies B, Axel L (eds) MICCAI 2008, Springer, vol LNCS 5242, pp 1023–1031

[125] Cleary K, Anderson J, Brazaitis M, Devey G, DiGioia A, Freedman M, Grönemeyer D, Lathan C, Lemke H, Long D, Mun SK, Taylor R (2000) Final report of the technical requirements for image-guided spine procedures workshop. Computer Aided Surgery 5(3):180–215

[126] Yan CXB, Goulet B, Pelletier J, Chen SJS, Tampieri D, Collins DL (2011) Towards accurate, robust and practical ultrasound-CT registration of vertebrae for image-guided spine surgery. International Journal of Computer Assisted Radiology and Surgery 6(4):523–537

[127] Holly LT, Foley KT (2007) Image guidance in spine surgery. Orthopedic Clinics of North America 38:451–461

[128] Kim KD, Johnson JP, Block O, Masciopinto JE (2001) Computer-assisted thoracic pedicle screw placement: An in vitro feasibility study. Spine 26(4):360–364

[129] Youkilis AS, Quint DJ, McGillicuddy JE, Papadopoulos SM (2001) Stereotactic navigation for placement of pedicle screws in the thoracic spine. Neurosurgery 48(4):771–779

[130] Bolger C, Wigfield C, Melkent T, Smith K (1999) Frameless stereotaxy and anterior cervical surgery. Computer Aided Surgery 4(6):322–327

[131] Kalfas IH (2009) Image-guided spinal navigation: Principles and clinical applications. In: Ozgur B, Benzel E, Garfin S (eds) Minimally Invasive Spine Surgery, Springer New York, pp 7–22

[132] Peters TM (2006) Image-guidance for surgical procedures. Physics in Medicine and Biology 51:R505–R540

[133] Villavicencio AT, Burneikiene S, Bulsara KR, Thramann JJ (2005) Utility of computerized isocentric fluoroscopy for minimally invasive spinal surgical techniques. Journal of Spinal Disorders & Techniques 18(4):369–375

[134] Gering DT, Nabavi A, Kikinis R, Hata N, O'Donnell LJ, Grimson WEL, Jolesz FA, Black PM, III WMW (2001) An integrated visualization system for surgical planning and guidance using image fusion and an open MR. Journal of Magnetic Resonance Imaging 13(6):967 – 975

[135] Rampersaud YR, Foley KT, Shen AC, Williams S, Solomito M (2000) Radiation exposure to the spine surgeon during fluoroscopically assisted pedicle screw insertion. Spine 25(20):2637–2645

[136] Barratt DC, Chan CS, Edwards PJ, Penney GP, Slomczykowski M, Carter TJ, Hawkes DJ (2008) Instantiation and registration of statistical shape models of the femur and pelvis using 3D ultrasound imaging. Medical Image Analysis 12(3):358–374

[137] Mozes A, Chang TC, Arata L, Zhao W (2010) Three-dimensional A-mode ultrasound calibration and registration for robotic orthopaedic knee surgery. The International Journal of Medical Robotics and Computer Assisted Surgery 6(1):91–101

[138] Tonetti J, Carrat L, Kvallek S, Pittet L, Merloz P, Chirossel JP (1998) Percutaneous iliosacral screw placement using image guided techniques. Clinical Orthopaedics and Related Research 354:103–110

[139] Ionescu G, Lavallée S, Demongeot J (1999) Automated registration of ultrasound with CT images: Application to computer assisted prostate radiotherapy and orthopedics. In: Taylor C, Colchester A (eds) MICCAI 1999, Springer, vol LNCS 1679, pp 768–778

[140] Foroughi P, Song D, Chintalapani G, Taylor RH, Fichtinger G (2008) Localization of pelvic anatomical coordinate system using US/atlas registration for total hip replacement. In: Metaxas D, Davies B, Axel L (eds) MICCAI 2008, Springer, vol LNCS 5242, pp 871–879

[141] Oszwald M, Citak M, Kendoff D, Kowal J, Amstutz C, Kirchhoff T, Nolte L, Krettek C, Hüfner T (2008) Accuracy of navigated surgery of the pelvis after surface matching with an A-mode ultrasound probe. Journal of Orthopaedic Research 26(6):860–864

[142] Peterhans M, Talib H, Linguraru MG, Styner M, Ballester MAG (2008) A method for frame-by-frame US to CT registration in a joint calibration and registration framework. In: IEEE ISBI 2008, pp 1131–1134

[143] Gill S (2009) Biomechanically constrained ultrasound to computed tomography registration of the lumbar spine. Master's thesis, Queen's University

[144] Glossop N, Hu R (1997) Assessment of vertebral body motion during spine surgery. Spine 22(8):903–909

[145] Hellier P, Coupé P, Morandi X, Collins DL (2010) An automatic geometrical and statistical method to detect acoustic shadows in intraoperative ultrasound brain images. Medical Image Analysis 14(2):195–204

[146] Jain AK, Taylor RH (2004) Understanding bone responses in B-mode ultrasound images and automatic bone surface extraction using a bayesian probabilistic framework. In: Walker WF, Emelianov SY (eds) Proceedings of SPIE: Medical Imaging 2004: Ultrasonic Imaging and Signal Processing, SPIE, vol 5373, pp 131–142

[147] Nelder JA, Mead R (1965) A simplex method for function minimization. The Computer Journal 7(4):308–313

[148] Press WH, Flannery BP, Teukolsky SA, Vetterling WT (1988) Numerical Recipes in C. Cambridge University Press

[149] Olsson DM, Nelson LS (1975) The nelder-mead simplex procedure for function minimization. Technometrics 17(1):45–51

[150] Comeau RM, Sadikot AF, Fenster A, Peters TM (2000) Intraoperative ultrasound for guidance and tissue shift correction in image-guided neurosurgery. Medical Physics 27(4):787–800

[151] Dath R, Ebinesan AD, Porter KM, Miles AW (2007) Anatomical measurements of porcine lumbar vertebrae. Clinical Biomechanics 22(5):607–613

[152] Horn BK (1987) Closed-form solution of absolute orientation using unit quaternions. Journal of the Optical Society of America A 4(4):629–642

[153] Yan CXB, Goulet B, Chen SJS, Tampieri D, Collins DL (2012) Validation of automated ultrasound-CT registration of vertebrae. International Journal of

Computer Assisted Radiology and Surgery 7(4):601–610

[154] Yan CXB, Goulet B, Tampieri D, Collins DL (2012) Ultrasound-CT registration of vertebrae without reconstruction. International Journal of Computer Assisted Radiology and Surgery 7(6):901–909

[155] Tonetti J, Carrat L, Blendea S, Troccaz J, Merloz P, Lavallée S, Chirossel JP (2001) Clinical validation of computer assisted pelvic surgery using ultrasound, a percutaneous safe technique with low radiation exposure. Studies in Health Technologies and Informatics 81:515–520

[156] Lang A, Mousavi P, Gill S, Fichtinger G, Abolmaesumi P (2012) Multimodal registration of speckle-tracked freehand 3D ultrasound to CT in the lumbar spine. Medical Image Analysis 16(3):675–686

[157] Winter S, Brendel B, Igel C (2005) Registration of bone structures in 3D ultrasound and CT data: Comparison of different optimization strategies. In: International Congress Series - CARS 2005, vol 1281, pp 242–247

[158] Kadoury S, Paragios N (2009) Surface/volume-based articulated 3D spine inference through Markov random fields. In: Yang GZ, Hawkes D, Rueckert D (eds) MICCAI 2009, vol LNCS 5762, pp 92–99

[159] Wein W, Camus E, John M, Diallo M, Duong C, Al-Ahmad A, Fahrig R, Khamene A, Xu C (2009) Towards guidance of electrophysiological procedures with real-time 3D intracardiac echocardiography fusion to C-arm CT. In: Yang GZ, Hawkes D, Rueckert D (eds) MICCAI2009, vol LNCS 5761, pp 9–16

[160] Ji S, Roberts DW, Hartov A, Paulsen KD (2009) Combining multiple true 3D ultrasound image volumes through re-registration and rasterization. In: Yang GZ, Hawkes D, Rueckert D (eds) MICCAI2009, vol LNCS 5761, pp 795–802

[161] Ji S, Roberts DW, Hartov A, Paulsen KD (2012) Intraoperative patient registration using volumetric true 3D ultrasound without fiducials. Medical Physics 39:7540–7552

[162] Nam WH, Kang DG, Lee D, Lee JY, Ra JB (2012) Automatic registration between 3D intra-operative ultrasound and pre-operative ct images of the liver based on robust edge matching. Physics in Medicine and Biology 57(1):69–91

[163] Hacihaliloglu I, Abugharbieh R, Hodgson AJ, Rohling RN, Guy P (2012) Automatic bone localization and fracture detection from volumetric ultrasound images using 3-D local phase features. Ultrasound in Medicine & Biology 38(1):128–144

[164] Hacihaliloglu I, Wilson DR, Gilbart M, Hunt MA, Abolmaesumi P (2012) Non-iterative partial view 3D ultrasound to CT registration in ultrasound-guided computer-assisted orthopedic surgery. International Journal of Computer Assisted Radiology and Surgery pp DOI:10.1007/s11,548–012–0747–9

[165] Shams R, Sadeghi P, Kennedy R, Hartley R (2010) A survey of medical image registration on multicore and the GPU. IEEE Signal Processing Magazine 27(2):50–60

[166] Fluck O, Vetter C, Wein W, Kamen A, Preim B, Westermann R (2011) A survey of medical image registration on graphics hardware. Computer Methods and Programs in Biomedicine 104(3):e45–e57

List of Abbreviations

CT	Computed Tomography
CPU	Central processing unit
DRO	Dynamic reference object
FRE	Fiducial registration error
GPU	Graphics processing unit
IGS	Image-guided surgery
MRI	Magnetic resonance imaging
TRE	Target registration error